On the thermo-hydro-mechanical behaviour of Argillaceous hard soils - weak rocks

Saeed Tourchi

ABSTRACT

Analysis and interpretation of the thermo-hydro-mechanical (THM) behaviour of argillaceous rocks is still among the most challenging of problems in geomechanical engineering. The comprehensive review of this wide variety of this class of materials has shown how different geotechnical parameters play various roles in the assessment of deep geological repository of high- and intermediate-level long-lived radioactive waste. After considering the wide variety of this class of materials, some common behaviour features are sought concerning compressibility, structure development, brittleness and progressive failure, anisotropy, effects of discontinuities, hydraulic properties. A comprehensive literature review on laboratory experimental results of the temperature effect on thermal, hydrolic and mechanical behaviour of argillaceous rocks is also caried out. Those features are examined in the context of appropriate behaviour frameworks developed for this type of materials. Two themes are then selected for special consideration: brittleness and progressive failure and the response of argillaceous weak rocks to deep underground excavations and in situ heating tests. For the second topic, particular attention is given to field results obtained in deep underground laboratories for nuclear waste disposal. The paper concludes with a summary of the main points.

Keywords: clays, argillites, compressibility, swelling, anisotropy, discontinuities, permeability, hydromechanical coupling, strength, brittleness, progressive failure, underground excavations in situ testing; radioactive waste; temperature effects; Coupled THM processes.

Preprint submitted to EarthArXiv (non peer-reviewed).

1. Introduction

In the middle of the increasing concern regarding carbon emissions and global warming, non-fossil fuel alternatives are gaining increasing attention, in particular to nuclear power. With an increasing interest in nuclear energy, radioactive waste will grow simultaneously. Three main strategies were developed for the management of spent nuclear fuel: reprocessing, storage, and direct disposal. Nowadays, deep geological disposal is accepted internationally as the safe and most feasible disposal method of high-level radioactive waste (HLW) (IAEA 2003). The principle of geological disposal of radioactive waste is to place carefully prepared and packaged waste in excavated tunnels in geological formations such as salt, hard rock, or clay (Kim et al. 2011). Several countries, including France, the United States, Germany, Sweden, Finland and Canada, have built underground research laboratories (URLs) to carry out related research of geological disposal. URLs are a crucial tool to integrate the various hydrologic, thermal, mechanical, chemical and biological phenomena and coupled processes in a realistic geological setting. Repository construction foresees the excavation of a network of tunnels in a suitable rock formation located within a few hundred meters below the ground level (Gens et al. 2009a, b).

Argillaceous rocks and stiff clay formations have great potential as possible geological host medium for radioactive waste. The host rock will be subjected to simultaneous thermal, hydraulic and mechanical (THM) phenomena resulting from the heat-emitting nature of the high-level radioactive waste (HLW) and the highly confined isolation system conditions. The THM processes will control the evolution and long-term response of the whole isolation system; therefore, a good understanding of the main THM phenomena is required to achieve a safe design of HLW repositories.

The behaviour of the argillaceous geomaterials, under thermal loading, has to be considered in the framework of THM couplings as the various THM phenomena interact. Olivella and Gens have developed conceptual and mathematical models for coupled THM processes since the early 1990s.

Beginning with thermal phenomena, it may be claimed that heat conduction is in most instances, the primary mechanism for heat transport. The heat conduction reacts to temperature gradients, T. Nevertheless, due to the movement of the three phases: solid, liquid and gas, additional heat transfer will also be undertaken by advection. The endogenous residual heat from phase changes can also have serious thermal effects. As for hydraulic phenomena, two of the main ones are, of course, liquid and gas advective fluxes. The term hydraulic is used in a generic way here, including both the flow of liquid and gas. In the absence of gravitational or osmotic potential gradients, liquid and gas pressures regulate

advective flows in a unique way. Consider that the pressures of liquid and gas are now used instead of water and air. This is in line with the assumption that more than one species may be present at each phase Advective flows are subject to phases. Non-advective (diffusion) flows are potentially significant, as more than one species may be present in the fluid phases. The most important of these is the diffusion of water vapor in the gas phase, especially in nonisothermal conditions. The conventional conceptual interpretation of this phenomenon is the binary diffusion one. There is another mol of air (considered as a single species) diffusing in the opposite direction for each mol of water vapour diffusing in one direction. Consequently, the total contribution to advective flow is zero. Vapor diffusion is controlled by concentration (or partial pressure) of vapour gradients. Essentially the same considerations can be made for the dissolved air diffusion in the liquid phase, although it is usually much less relevant in practice. Eventually, in addition to the usual stress/strain relationship, the mechanical behaviour of unsaturated porous media will be associated with additional contributions from changes in suction (matric and sometimes osmotic) and temperature changes. Most of the above-mentioned phenomena are in fact strongly coupled, and they must be perceived as parts of a single integrated system.

To assess the hydro-mechanical effects of the thermal transient on the host material in a deep repository, various in situ heating tests have been performed at several underground laboratories (Gens 2011). The CACTUS, ATLAS, and CERBERUS tests (Picard et al. 1994; Bernier and Neerdael 1996; de Bruyn and Labat 2002; François et al. 2009a) were performed in the Boom clay at the HADES underground research facility in Mol, Belgium. The HE-D test was carried out in the Mont Terri laboratory in Northern Switzerland, which was constructed in Opalinus clay. And the TER, TED and ALC1604 heating tests were performed in Bure at the Meuse-Haute Marne laboratory located in Eastern France (Garitte et al. 2014), which was constructed in the Callovo–Oxfordian claystone.

This paper deals with the thermo-hydro-mechanical (THM) behaviour of argillaceous hard soils-weak rocks, i.e. geological materials where fine-grained particles predominate (Hawkins, 2000). They have been widely distributed in nature and are estimated to represent up to 50% (Pettijohn 1957) in the world's sedimentary rock mass and to surface in about one-third (Franklin and Gruspier 1983). Although weak metamorphic argillaceous rocks obviously exist (e.g. (Kavvadas 1999), this work mainly focuses on sediments and sedimentary rocks. In accordance with the deep geological disposal application, materials ranging from hard soils to weak rocks are considered although no precise limits for those categories have ever been uniformly defined. Thus Hawkins (Hawkins 2000b) suggests a lower

threshold for undrained shear strength of very stiff soils of 160 kPa and upper unconfined compression strength for weak rocks of 10 MPa. There have also been many other attempts for the definition of hard soils-weak rock not only with respect to strength but, also, in terms of porosity and compressibility (Clayton 1997).

Specifically, three argillaceous geomaterials receive special attention, Boom clay, Opalinus clay and Callovo-Oxfordian (COx) claystone in this work as they correspond to the materials being investigated in three underground laboratories in the context of deep geological disposal of high-level radioactive waste. The laboratories are the HADES Underground Research Facility (Mol, Belgium) in Boom clay (Bastiaens and Bernier 2006), the Mont Terri underground laboratory (St. Ursanne, Switzerland) in Opalinus clay (Thury and Bossart 1999) and he Meuse-Haute Marne underground laboratory (Bure, France) in Callovo-Oxfordian claystone (Delay et al. 2007). These argillaceous materials are investigated at both the small and large scale through laboratory and in situ experiments.

The tremendous interest in these materials lies in the fact that hard argillaceous geomaterials are very desirable as potential host media for high-level radioactive waste. They provide advantageous features such as low permeability, a degree of self-healing capability when damaged, substantial retardation properties for solute transport, and no unpredictable economic value. The probable need to support the excavated openings, and exposure to chemical behaviour and desaturation caused by ventilation are possible shortcomings (Gens et al. 2007a). High-level radioactive waste is strongly heat emitting; so thermal properties assessment is also one of the priorities of those investigations (Gens et al. 2009c); (Gens 2010).

Table 1 presents some general properties for three materials, Boom clay, Opalinus clay and Callovo-Oxfordian (COx) claystone. They should be viewed only as reference values; the variability and anisotropy of the materials cannot be fully collected in the Table and parameter values outside the ranges given certainly occur. Opalinus clay and COx claystone are obviously part of the indurated mudrock class that tends towards the rock end of hard soils–the weak spectrum of rocks. On the other hand, Boom clay is considerably weaker and is closer to the range soil area. Thus, the materials emphasized cover a large proportion of the geological span considered, providing information on a useful range of geotechnical characteristics and behaviour. Nonetheless, very low permeability is prominent to all of them.

Table 1: Some reference properties for the host materials of the three underground laboratories (modified from (Gens 2013).

	COx claystone	Opalinus clay	Boom clay
Dry density (g/cm3)	2.21-2.33	2.22-2.33	1.61-1.78
Calcite content (%)	23 - 42	6 - 22	0 - 3
Porosity (%)	11-16	11-14	35-40
Water content (%)	<6.5	4 - 8	20-30
Clay content (%)	50-65	45-55	40-70
Liquid limit (%)	21-25	21-25	55-80
Plasticity index (%)	11-19	13-17	32-51
Young's modulus (GPa)	3.6-8.5	4-10	0.2-0.4
UCS (MPa)	10-16	8-22	2-2.8
Permeability (m/s)	$0.7\text{-}5\times10^{-13}$	$0.5\text{-}5\times10^{-13}$	$2\text{-}5\times10^{-12}$
Geological stage	Callovo-Oxfordian	Aalenian	Rupelian
(millions of years)	156-164	171-176	28.4-33.9

This paper is organized as follows. The behaviour under compressive loading is examined first in the context of behaviour frameworks developed for this type of materials. A discussion on some additional aspects of mechanical behaviour like brittleness and progressive failure and material anisotropy follows. Hydraulic behaviour and hydromechanical coupling are considered next. Afterwards, the thermal behaviour is reviewed in order to examine more closely the behaviour of argillaceous rocks under thermal loading. Finally, an overview of in situ heating tests based on Belgian, Swiss, and French disposal programs, discusses the outstanding research issues in disposal from the aspect of geotechnical engineering, such as brittleness and progressive failure, the response of argillaceous weak rocks to deep underground excavations and coupled thermo-hydro- mechanical (THM) response of this sedimentary clays.

2. On mechanical behaviour

2.1 Gravitational compaction and structure development

By constructing general behaviour frameworks of argillaceous materials, the overall behaviour can be perceived in an integrated and structured manner, underlining common behaviours patterns that can be identified in inexplicably quite different materials. The usual starting point in these developments is the paper by Skempton (Skempton 1969) on the consolidation of clays by gravitational compaction in which he plotted a series of in situ consolidation curves for a wide range of argillaceous materials and accordingly a dependency of the sedimentation consolidation curves (SCCs) slope with the plasticity of

the material was identified. Later (Burland 1990)) normalized the same type of data for normally consolidated soils using void ratio rather than water content and they observed that data plots very close to a single line, the sedimentation compression line (SCL), which lies above the intrinsic consolidation line (ICL).

A soil structure, which is a characteristic of most natural materials, is the ability of natural clays to lie right to the possible stress states of the reconstituted material (Gens 2013). It is worth noting that both fabric and antepartum bonding are the product of the soil structure. The framework was extended to include materials with different sensitivities by (Cotecchia and Chandler 2000); higher sensitivity corresponded with more cemented materials. The impact of natural soil and rock structure was considered by (Leroueil and Vaughan 1991) with a unified approach later in 1991. They also identified a structured soil's ability to lie on a stress state outside the space allowed for the unstructured reconstituted soil and drew attention to the effects of structural degradation when a natural soil is stressed beyond the yield point. Those factors can be outlined in the Figure 1 where the oedometer consolidation lines for a structured and a destructured soil are given.

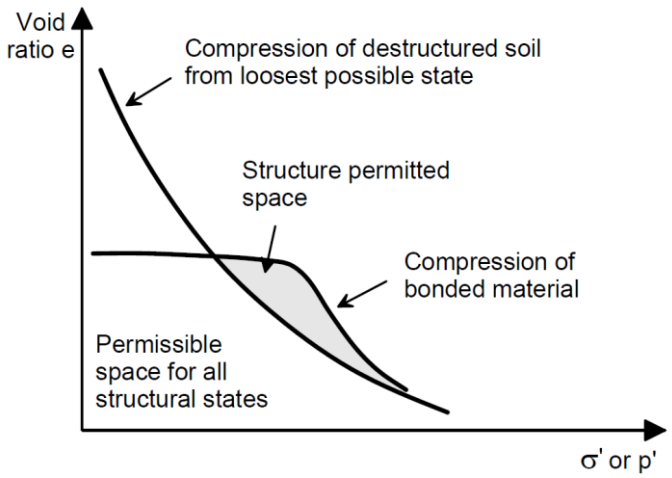

Figure 1. The comparison of structured and destructured compression in the oedometer test (Lemueil and Vaughan 1990).

The outcomes of a one-dimensional Boom clay compression test provide a good example for this type of behaviour. Figure 2 shows one-dimensional compression test results on Boom clay sample. The intrinsic compression line (ICL) corresponds to the reconstituted material, whereas the sedimentation compression line (SCL) is obtained as the best-fit regression line of the field $e-\log\left(\sigma_v'\right)$ relationship for several argillaceous materials (see (Burland 1990), for more details). The yield point lies beyond the

ICL, and in situ vertical stress as shown in the figure. However, when loaded after yielding, the compression curve tends to converge to the ICL as the load is increased.

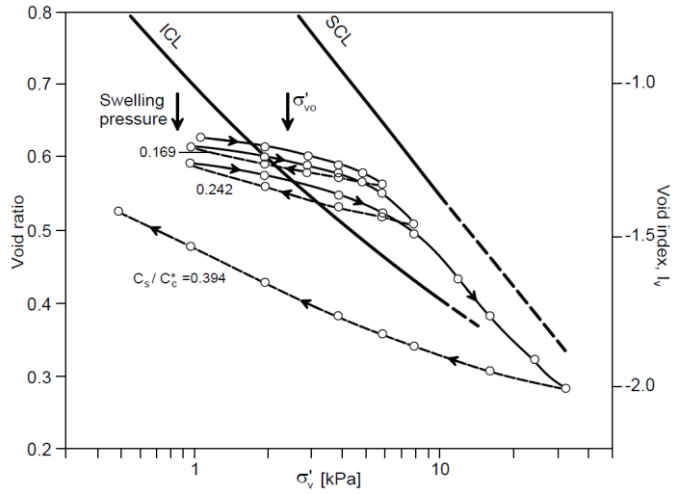

Figure 2. One dimensional compression behaviour of Boom clay (Burland 1990); (Horseman et al. 1987).

After loading beyond the yield point, the structures can also be degraded due to compression from the slope of the swelling line. Figure 3 provides a remarkable example of experimental results achieved in a high-pressure oedometer test on the Panama Canal's Culebra shale. The Degradation (line with black symbols) takes place during compression. Then the material (line with white symbols) is unloaded and experiences enormous swelling, which ends in a void proportion higher than the original.

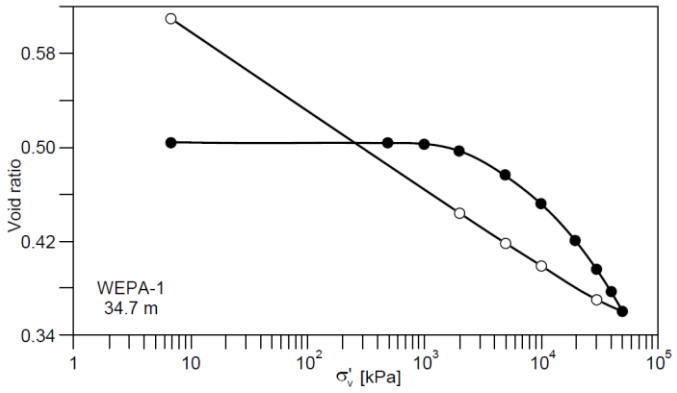

Figure 3. High-pressure oedometer test on Culebra shale ((Banks et al. 1975) referenced in Gens, 2013).

Interestingly, there are very few cases of consolidation lines going beyond sedimentation compression lines of natural clays (SCC). Test results on samples of clays from France extracted from large depths are shown in Figure 4. As Figure 4 shows, the consolidation curves go beyond the intrinsic consolidation curve but, again, they do not cross the corresponding sedimentation consolidation curves. Therefore, it seems either the development of post-sedimentary structures is rare or that the swelling / weathering and/or sample removal effects have been overcome by such additional structures.

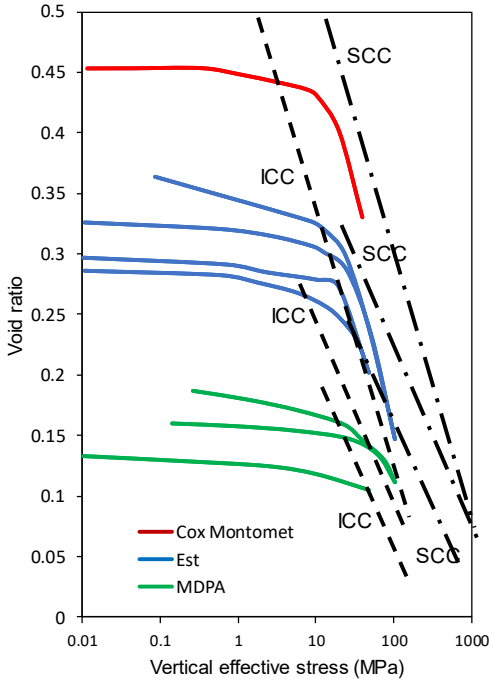

Figure 4. Oedometer compression curves for three argillaceous rocks from France (modified from (Heitz and Hicher 2002).

Another important observation is that, after loading, some materials do not converge onto the intrinsic consolidation line because there is a stable structure configuration that allows stable void ratios above the intrinsic consolidation line. The behaviours of Vallericca clay, shown in Figure 23, is an example. (Coop and Cotecchia 1995) have obtained a similar result by testing normally consolidated clays from Sibari, Italy.

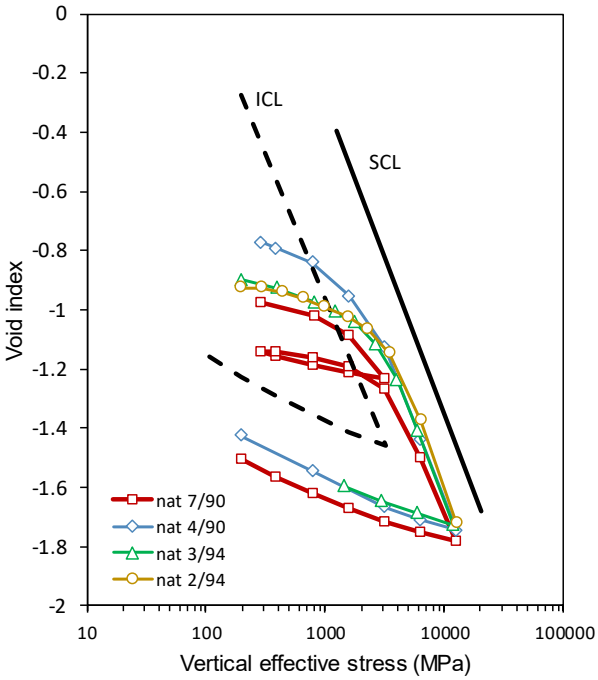

Figure 5. One-dimensional compression data for Vallericca clay (modified from (Amorosi and Rampello 2007).

To summarize, the observation of compression lines of natural materials and their relationship with the ICL provides a unifying framework, on the basis of the work described in (Burland 1990)(Cotecchia and Chandler 2000)(Leroueil and Vaughan 1991), for a readily measurable assessment of the effects of gravitational compaction and structure (fabric and bonding).

2.2 Brittleness and progressive failure

Argillaceous rocks generally fail quasi-brittle under deviatoric loading. Ductile behaviours are also possible to observe if the samples are tested at very high effective confining stresses (e.g. Ohtsuki et al. 1981), but brittle failure predominates in conventional geotechnical situations. (Skempton 1964)) put forward one of the first descriptions of this kind of behaviour on the basis of slow drained tests carried out on a stiff clayey material in the direct shear box apparatus (Figure 6). He identified a first stage, characterized by resistance increases to a maximum value, defined the peak strength.

After this point a strain softening process begins to develop. It consists of a decrease in strength until a limit state reaches, where the strength will no longer decrease during further displacement application. This lowest-bound constant strength is known as residual strength and was early identified using the ring shear apparatus by (Tiedemann 1937) and (Hvorslev 1937). As shown in Figure 6, the intercept of cohesion vanishes, and the friction angle decreases slightly as the force envelope moves from peak to residual. The reduction of the friction angle may vary from 1° or 2° to 10°, depending on the materials. It should be noted that, during the process, water content increases, evidencing the material's tendency to dilate during shearing.

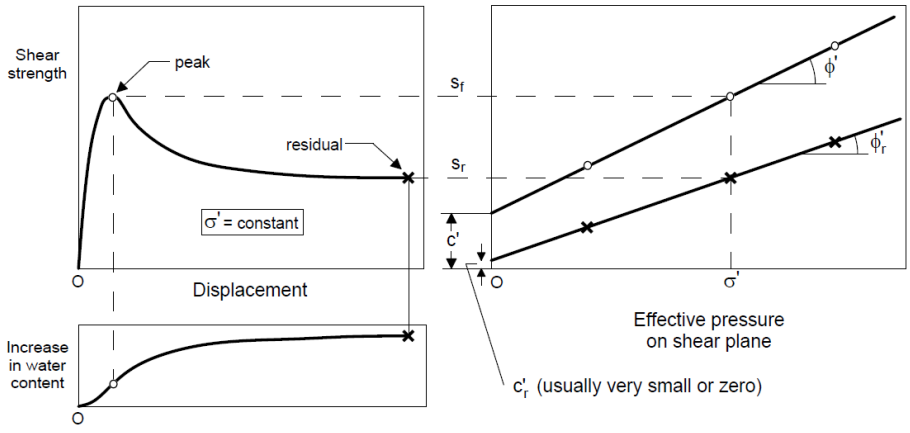

Figure 6. Shear characteristics of stiff clayey materials (Skempton, 1964).

Later, these phenomenological features were used to distinguish the softening process between two different stages (Figure 7). The first stage occurs just after the peak, characterized by a high rate of

strength loss associated with interparticle bond degradation and breakage ((Burland 1990); (Simpson 1979)). The second stage follows the first and is characterized by a gentler reduction in strength until the residual value, generally attributed to a gradual realignment of clay particles along the failure plane (Gens, 2013). Fully softened strength is often known as the strength between both stages (((Terzaghi et al. 1996); (Mesri and Shahien 2003); (Skempton 1970) or post-rupture strength (Burland 1990).

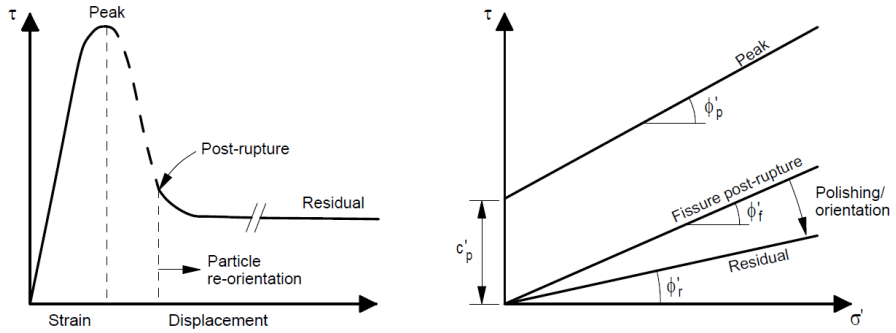

Figure 7. Conceptual scheme for the strength of argillaceous hard soils and weak rocks (Jardine et al. 2004a).

Argillaceous rocks are not an exception regarding this type of behaviour. As an example, Figure 8 and Figure 9 show typical stress-strain curves of Kimmeridge Bay Shale and COx claystone under triaxial loading presented by Nygård et al. (2006) and (Belmokhtar et al. 2018) respectively. In Figure 8, the peak, fully softened, and residual strengths can be clearly identified in curves M2 and M3. It seems moreover that strain reachable in triaxial tests are not large enough to reach the residual strength for high confining pressures (M4 and M5), while post-peak curve could not be experimentally followed at low confining pressures (curve M1), probably because the large dilatancy experienced by the sample at this level of stress leads to the loss of control of the test.

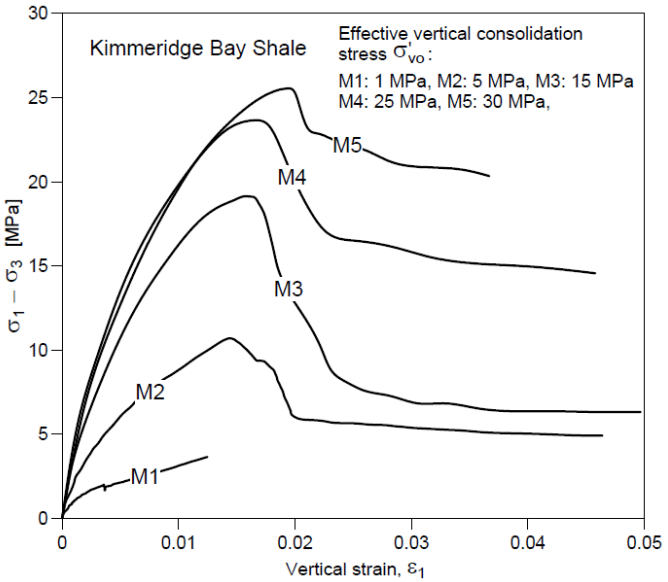

Figure 8. Stress-strain behaviour of Kimmeridge Bay Shale under triaxial loading (Nygård et al. 2006).

Figure 9a presents stress–strain curves in drained triaxial compression tests with different confining stresses performed by (Hu et al. 2014) on COx claystone sample. The loading procedure was conventional and composed of two stages: setup of confining stress and application of deviatoric stress under drained condition. Six values of confining stress are used such as 2, 5, 10, 15, 20 and 40 MPa. As shown in this figure, the mechanical response of claystone is strongly dependent upon confining stress.

Under low confining stress, there exists some nonlinear phase at the beginning of deviatoric loading. This nonlinear phase is attributed to the progressive closure of initial bedding planes and microcracks in the axial direction. With the increase in confining stress, such a nonlinear phase disappears because the initial microcracks are almost closed during the application of confining stress. Also, under low confining stress, the sample failure is marked by sharp peak stress, due to the coalescence of cracks leading to splitting of sample. Under higher confining stress, this peak stress state is much less pronounced and even disappears (confining stress of 40 MPa). The failure of sample is generally associated with the onset of shear enhanced compaction bands. There is a clear transition from brittle to ductile behaviour with confining stress increase. However, for all confining stress, after a more and less marked linear stress strain phase, we observe nonlinear responses of material before and after peak stress. These nonlinear inelastic strains are directly related to the nucleation and growth of microcracks and mainly generated by frictional sliding along cracks surfaces.

There is a clear transition from volumetric compressibility to dilatancy for almost all the confining stress considered (Hu et al. 2014)(Belmokhtar et al. 2018) However, this transition occurs much earlier under low confining stress than higher one. Physically, this volumetric dilatancy in brittle rocks under compressive stresses may be related to the normal opening of microcracks generated by frictional sliding along rough crack surfaces. This is similar to the published experimental data on dilatant effects on clayey rocks (Naumann et al. 2007); (Zhu and Wong 1997).

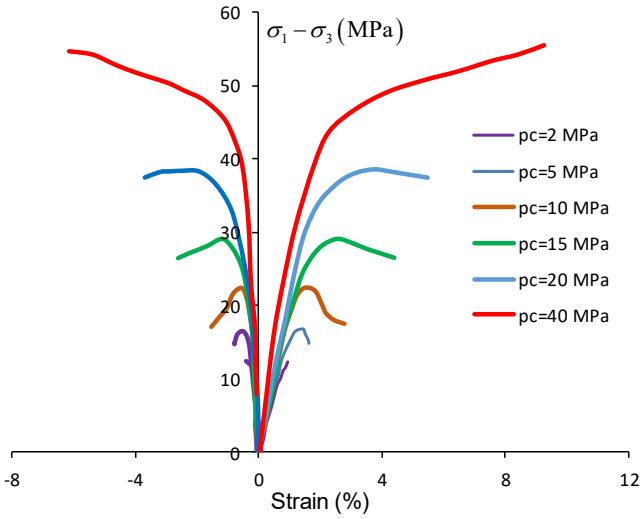

Figure 9. Stress–strain curves in drained triaxial compression tests with different confining stresses (Hu et al. 2014).

The post-peak response is governed by the creation of a shear plane with an inclination of about 65° with respect to horizontal, as shown in Figure 10. These results are comparable to other ones obtained in claystones by Naumann et al. (2007), Zhang et al. (2007), Hu et al. (2014) and Menaceur et al. (2015).

Figure 10. Sheared specimen (EST51338b), with shear plane inclined at an angle of 65° from horizontal (Belmokhtar et al. 2018).

The values of shear strength are plotted together in a q – p′ diagram together with the results of Hu et al., (2014) on small specimens and Menaceur et al. (2015) in the hollow cylinder apparatus (Figure 11). One observes a good overall comparability of the drained shear strength data obtained on various devices, with parallel curves that provide the same value of friction angle of 21°. Shear strength values are also well related with respect to the specimen's porosities, with the largest strength at lower porosity of 13% (Hu et al. 2014; Menaceur et al. 2015) and smallest one at the highest porosity of 17% (Menaceur et al. 2015).

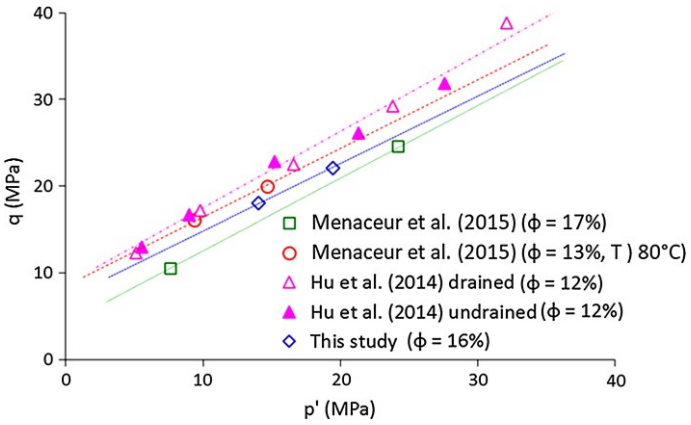

Figure 11. Comparison of the shear envelopes with data of shear tests determined with different devices on saturated specimens of the Callovo-Oxfordian claystone(Belmokhtar et al. 2018).

2.3 Material Anisotropy

It has long been recognised that geomaterials may exhibit anisotropic behaviour ((Donath 1964); (Ladd and Varallyay 1965); (McLamore and Gray 1967)), whose origin has been related to different sources such as deposition processes (Oda and Nakayama, 1989), tectonic processes (Amadei 1996), loading history (Li and Yu 2009) and fabric (Anandarajah 2000), among others. In argillaceous rocks, it is essentially related to the process of sedimentation and compaction, which results in an oriented structure controlled by bedding planes and fissility. As a consequence, two main directions of anisotropy (parallel and orthogonal to the bedding plane) are generally identified and modelled in the framework of transverse isotropy (or cross- anisotropy). The degree of anisotropy has been often related to the compaction process, due to both porosity reduction and smectite-to-illite transformation with diagenesis (Vernik and Liu 1997), although micro-cracks and kerogen content may also play a role ((Carcione 2000); (Vernik and Liu 1997).

It has been well described in (Mánica 2018) that anisotropy can be generally observed in properties such as stiffness, strength or permeability. Stiffness anisotropy in argillaceous rocks has been usually assessed indirectly through its seismic velocity anisotropy (Vernik and Liu 1997). Anisotropy can be inferred from field seismic measurements by considering the non-hyperbolic moveout of wave reflection (Alkhalifah 1997), or in laboratory through multi- (Hornby 1998) or single-core methods (Wang 2002b, a). Direct stiffness measurements have also been reported (Niandou et al. 1997); (Valès et al. 2004). In general, measurements indicate a marked tendency for higher stiffness (or wave velocities) in the direction parallel to the bedding planes than perpendicular thereto. In Figure 12, (Sayers 2013) collected data of various shales from the literature where the relationship between the Young's moduli perpendicular and parallel to bedding is shown, and where the mentioned tendency is clearly identified.

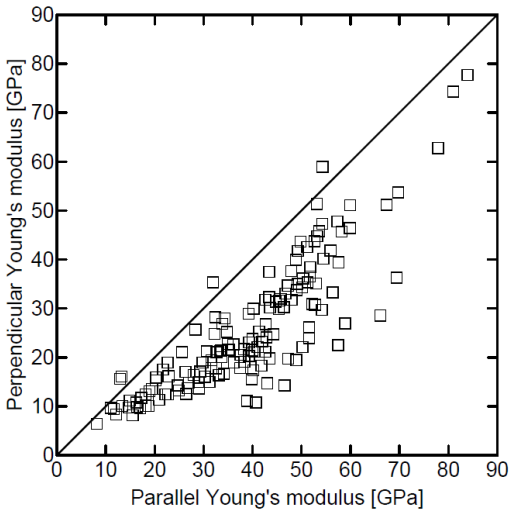

Figure 12. Perpendicular versus parallel Young's modulus of various shales (modified from Sayers, 2013).

Data on the strength anisotropy of argillaceous rocks are scarce, although this issue is currently gaining increasing attention, especially in relation with hydraulic fracturing issues. Anisotropy is usually assessed by conventional methods for strength determination (e.g. uniaxial compression or triaxial compression test) on samples trimmed with different bedding orientations (Cho et al. 2012); (Niandou et al. 1997)(Valès et al. 2004)). Figure 13 shows typical strength distributions in shale rocks, where the minimum strength is generally obtained for intermediate orientations between the loading and the bedding planes.

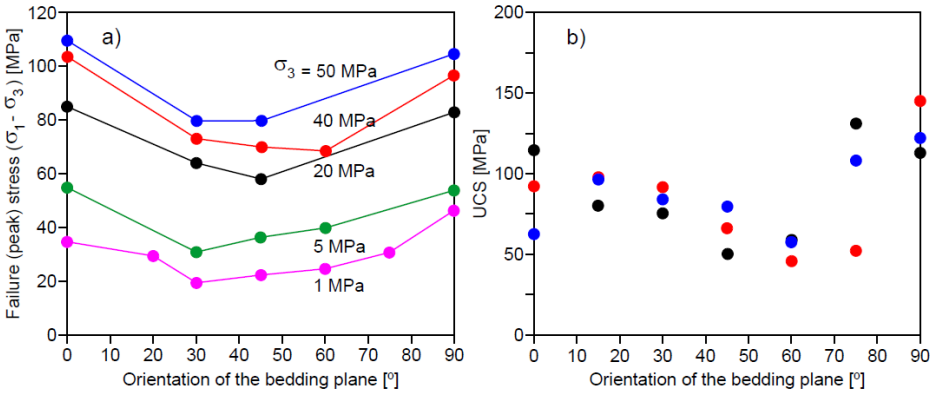

Figure 13. Strength variations (a) under triaxial loading of Tournemire shale (Niandou et al., 1997) and (b) under uniaxial loading of Boryeong shale (Cho et al., 2012).

3. On hydraulic behaviour

3.1 Permeability

Very low permeability of argillaceous materials implies that the precise determination of permeability is often difficult and requires the use of transient methods (Figure 14).

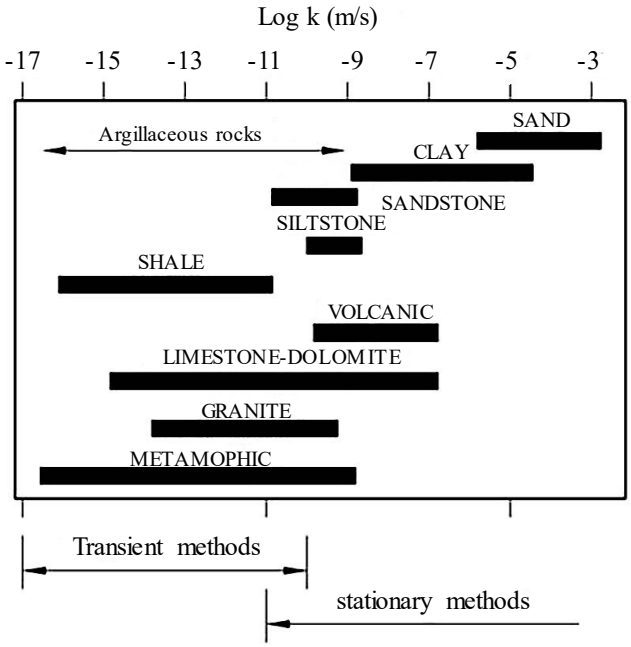

Figure 14. Range of permeabilities measured under a confining pressure of 10 MPa indicating the type of determination method (Brace 1980).

Permeability ranges for argillaceous materials as a function of porosity are given in Figure 15. Looking at the figure, permeabilities lie well within the same range and the plot extends to very low porosity values. However, what is most evident in Figure 15 is not the predicted reduction of permeability with porosity, but the broad range of values for a given porosity (Gens 2013), this implies that the permeability predicted by using the porosity is a rough estimation and what matters is pore size (more precisely the largest interconnected pore entry magnitude that is related to pore (and grain) size distribution). It is also perhaps worth mentioning due to the possible effect of the presence of thin more granular layers values is bound to be higher in the case of field measurements.

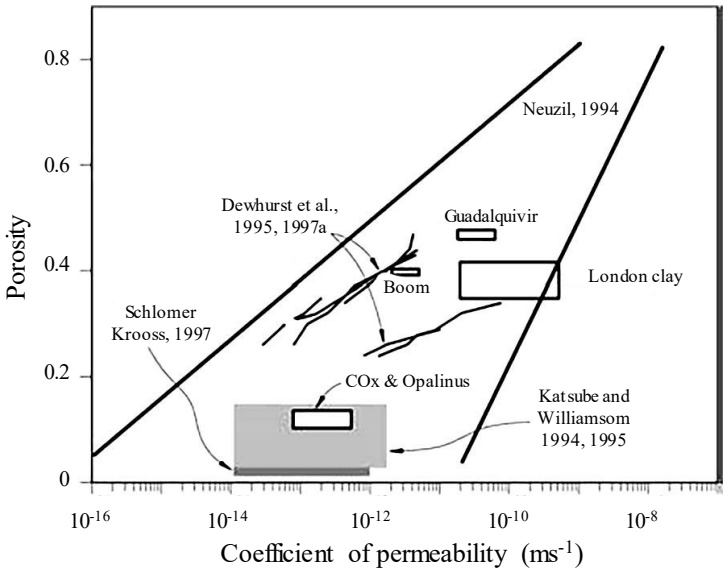

Figure 15. Range of porosity-permeability data for argillaceous materials (modified from (Neuzil 1994).

The microstructural features of sedimentary materials may also result in anisotropy of permeability. In general, observations show that the permeability measured parallel to bedding is higher than the one measured perpendicular thereto (Bhandari et al. 2015); (Kwon et al. 2004). An example is shown in Figure 16 where tests on COx claystone specimens cut parallel and perpendicular to bedding exhibit about one order of magnitude difference in permeability (Zhang and Rothfuchs 2004a). Bonding may affect permeability contrastingly. On the one hand, bonding tends to reduce porosity, thus reducing permeability. Strong bonding, on the other hand, can keep fissures open even during swelling, increasing bulk permeability.

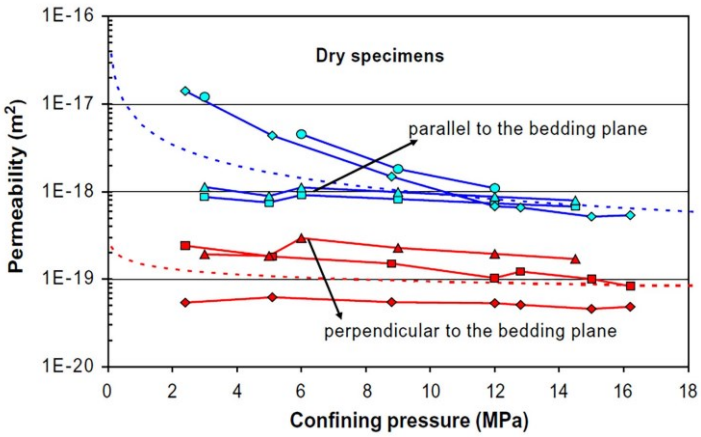

Figure 16. Dependence of intrinsic gas permeability on confining pressure for COx claystone specimens cut parallel and perpendicular to the bedding planes (Zhang and Rothfuchs 2004a).

Figure 17 shows the reduction of transmissivity (directly related to permeability) in Opalinus clay measured in a saturated zone damaged by an excavation in the Mont Terri laboratory. This

transmissivity reduction implies a quite significant capacity for self-sealing even in strongly bonded materials such as Opalinus clay.

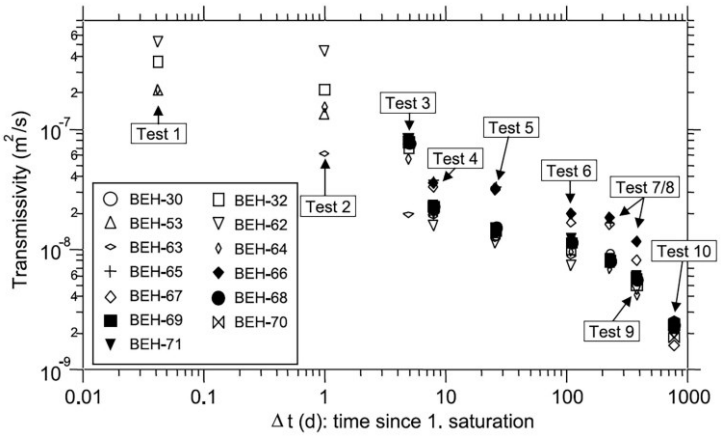

Figure 17. Time evolution of transmissivity measured in a saturated excavation damaged zone in Opalinus clay (Bossart et al. 2004).

3.2 Hydromechanical coupling: Biot's coefficient

Due to low porosity of argillaceous materials Terzaghi's principle of effective stress is not assured (Jardine et al. 2004b). Biot's poromechanical theory could be convenient framework considering cases (Biot and Willis 1957)(Coussy 2004). In the simple case of poroelasticity, effective stress becomes:

$$\sigma'_{ij} = \sigma_{ij} - bu\delta_{ij} \qquad b = 1 - K_d / K_s \tag{1}$$

Where σ'_{ij} are the effective stresses, σ_{ij} the total stresses, *u* the pore pressure, δ_{ij} Kronecker's delta, K_d the drained volumetric modulus of the skeleton , K_s the volumetric modulus of the solid phase and *b* Biot's coefficient which is a key property for the porous medium in the context of poroelastic theory.

There has been a sustained effort to determine Biot's coefficient of the COx claystone by a number of researchers using both oedometer and isotropic triaxial tests as summarised by (Mohajerani 2011)) (Figure 18). A large proportion of the range of results obtained arises may arises from testing procedures and difficulties and more research is needed in this area.

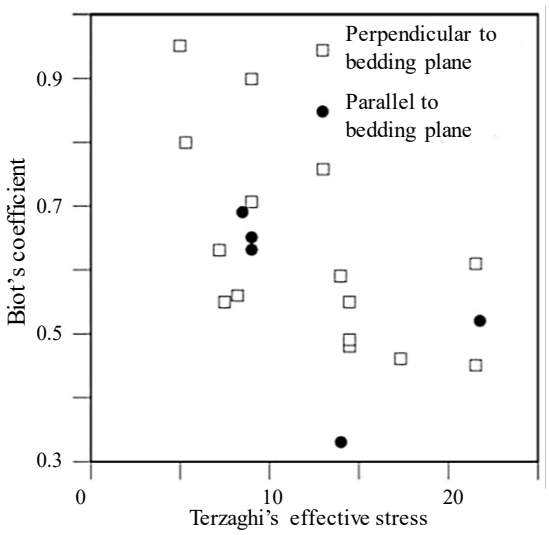

Figure 18. Measured Biot's coefficient for COx claystone as a function of stress level (Salager 2008).

4. On thermal behaviour

6.1 Elastic response

Early attempts to describe the elastic behaviour of argillaceous rocks at elevated temperatures assumed that the elastic properties of these material are temperature independent. Menaceur et al., (2015) performed a series of triaxial tests have been conducted on COx claystone specimens along various thermo-hydro-mechanical paths in fully saturated and drained conditions by using the hollow cylinder

device. All the values obtained at 25°C and 80°C are plotted together in

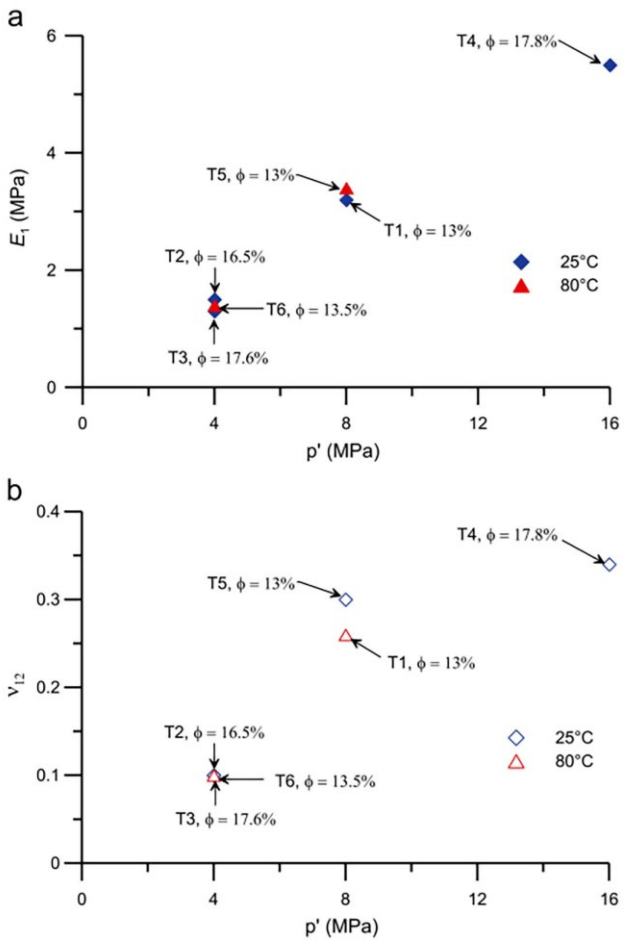

Figure 19 that clearly shows that there is no effect of temperature on the elastic properties determined here (Young's modulus E_1 and Poisson coefficient v_{12}). Similar comparison has been drawn in Mohajerani et al., (2014) from isotropic compression tests, showing no effect of temperature (80°C) on the elastic compression parameters.

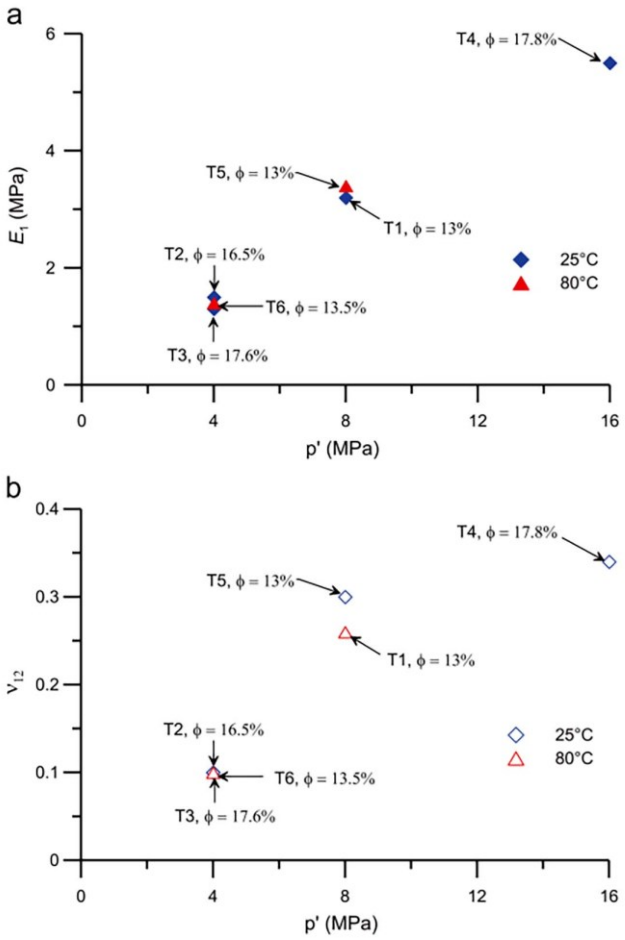

Figure 19. Elastic parameters, (a) Young's modulus, (b) Poisson coefficient (Menaceur et al., 2015).

Considering that lateral decompression tests (LD) correspond more closely to the stress paths in the surrounding rocks of an underground cavity during excavation than the conventional triaxial compression tests (CTC), Liu et al., (2019) were investigated elastic properties of the claystone by conducting unloading–reloading cycles during the LD tests under five different values of temperature from 20 to 90 °C which are the representative temperature range for the host claystone specified in the French radioactive waste disposal project for the investigation of thermal effects. Four unloading–reloading cycles have been performed during the differential stress phase in each LD test. The four elastic moduli, such as defined in Eq. (1.2), are calculated from the stress–strain curves in each loading-reloading cycle.

$$\mathrm{M}_{11}=\frac{\Delta\sigma_1}{\Delta\varepsilon_1},\ \mathrm{M}_{31}=\frac{\Delta\sigma_3}{\Delta\varepsilon_1},\ \mathrm{M}_{13}=\frac{\Delta\sigma_1}{\Delta\varepsilon_3},\ \mathrm{M}_{33}=\frac{\Delta\sigma_3}{\Delta\varepsilon_3} \tag{2}$$

The variations of these moduli as functions of the relative normalized axial strain are plotted in Figure 20a–d. From Figure 20a, the modulus M_{11} varies in the range of [3,6] GPa depending on the values of

temperature and axial strain. It seems that the temperature has no significant effect on the values of the modulus M11 except that there is an important degradation at T = 90 ◦C . The values of the modulus M_{31} are presented in Figure 20b and evolve within the range of [− 3.3, − 1.5] GPa, which are about a half of the values of the corresponding modulus M_{11} (absolute values). The variation characteristics of M_{31} are practically the same as those of M_{11} . One can see that the two moduli related to the axial strain (M_{11} and M_{31}) show a significant degradation when the normalized axial strain is higher than 0.6. The thermal effect on these moduli becomes significant only when the temperature reaches 90 °C.

In Figure 20c, the values of the modulus M_{13} are given and included in the range of [− 17, − 10] GPa. For the two axial moduli related to the axial strain, the thermal effect is negligible except for the case of T = 90 ◦C for which an obvious degradation of the modulus is observed and amplified by the applied axial strain. As a difference with the modulus M_{11} , the modulus M_{13} exhibits a continuous decrease during nearly the whole loading process. The decrease is enhanced when the normalized axial strain is higher than 0.6. The values of the modulus M_{33} presented in Figure 20d vary within the range of [5, 7.5] GPa, which are also about a half of the values of the corresponding M_{13} (in absolute values). The variations of M_{33} with the axial strain are similar to those of M_{13} .

As a conclusion, the two moduli related to the lateral strain (M_{13} and M_{33}) exhibit an earlier and larger degradation (mechanical damage) induced by the shear stress loading than the moduli related to the axial strain (M_{11} and M_{31}), but the thermal degradation effect is also evident only when the temperature reaches 90°C. The difference of mechanical damage rate between the axial and lateral directions suggests that the COx claystone can exhibit an induced anisotropy by mechanical loading.

The effect of temperature increase on the elastic properties of the COx claystone is not yet clearly demonstrated. Further tests are needed to verify the existence of a potential critical temperature from which there is a significant decrease of elastic modulus for the COx claystone.

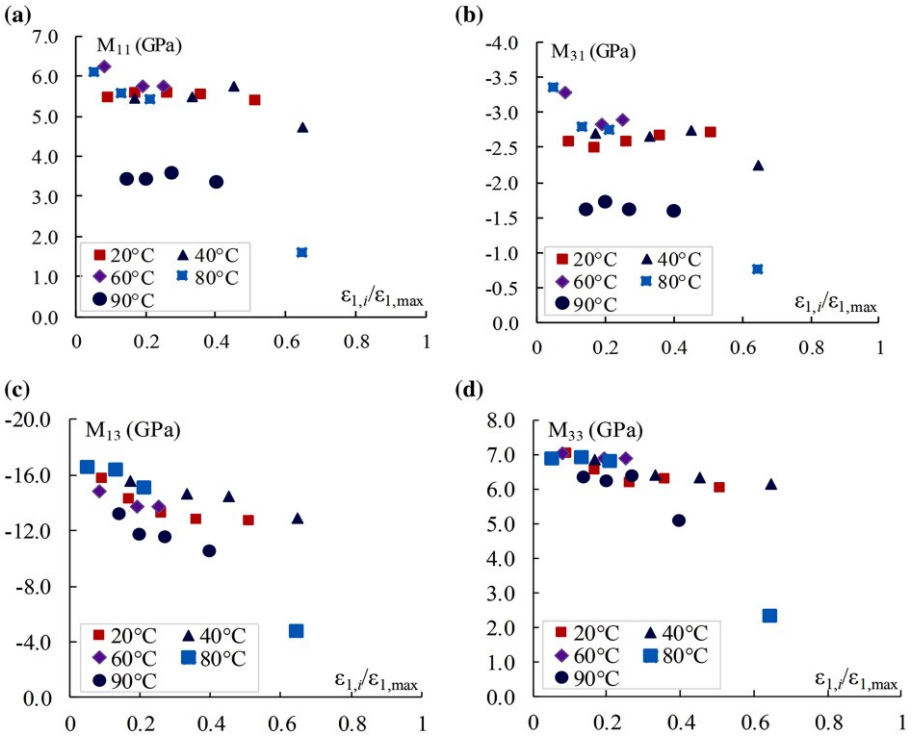

Figure 20. Unloading moduli variation during LD tests under different temperatures (Liu et al., 2019).

6.2 Volume change behaviour

Comprehensive experimental data on the thermal effects on volume change behaviour of argillaceous hard soils-weak rocks is scarce in the scientific literature (Campanella and Mitchell 1968); (Plum and Esrig 1969); (Habibagahi 1976); (Demars and Charles 1982); (Houston et al. 1985); (Eriksson 1989); (Hueckel and Borsetto 1990); (Towhata et al. 1993); (Boudali et al. 1994); (Tanaka 1995); (Crilly 1996); (Fox and Edil 1996); (Delage et al. 2000); (Graham et al. 2001)). (Campanella and Mitchell 1968) performed a series of isotropic consolidation tests on a saturated remoulded illite at different temperatures using triaxial equipment. The experimental results revealed that the compressibility index was independent of temperature, but the preconsolidation pressure reduced with increasing temperature. The variation of the compressibility index with temperature was also investigated by (Plum and Esrig 1969). They carried out one-dimensional consolidation tests on illite and Newfield clay and showed that the compressibility index of the material varied with temperature. This was in contrast with the observations of Campanella and Mitchell (1968). Nevertheless, the changes in the compressibility indices with temperature were insignificant at high stresses. Later, (Eriksson 1989) and (Boudali et al. 1994)) repeated (Plum and Esrig 1969) tests and showed that temperature had no effect on the compressibility indices. Similar results were also reported by Graham et al (2001) for isotropic consolidation. The decrease in the preconsolidation pressure by temperature, which was first observed

by Campanella and Mitchell (1968), was further investigated and confirmed by (Habibagahi 1973), Eriksson (1989), Boudali et al (1994), and Graham et al (2001). This effect causes the entire compression curve to move towards smaller effective stresses with increasing temperature. Some investigators have also shown that with an increasing temperature, the soil becomes more compressible in unloading-reloading regions (e.g. Eriksson, 1989; Tanaka, 1995). However, results to the contrary have been reported by Campanella and Mitchell (1968) and Crilly (1996).

The pioneering work of (Hueckel and Borsetto 1990)) on Boom Clay samples demonstrated that the volume changes of natural clays under constant isotropic effective stress depended on the overconsolidation ratio (OCR), independently of the applied stress. A thermo-plastic contraction is observed in normally consolidated clays and an elasto (expansion) plastic (contraction) response is observed in overconsolidated clays, depending on the OCR. This has been confirmed in Boom Clay by (Sultan et al. 2002) as shown in Figure 21 that presents the results of drained thermal tests run on samples at various OCRs in which the temperature elevation was very slowly applied (1 ◦C/h) to ensure fully drained conditions. In the overconsolidated regime, Figure 21 also shows that the temperature of the expansion-contraction transition increases with the OCR as accounted for in the thermomechanical model of (Cui et al. 2000).

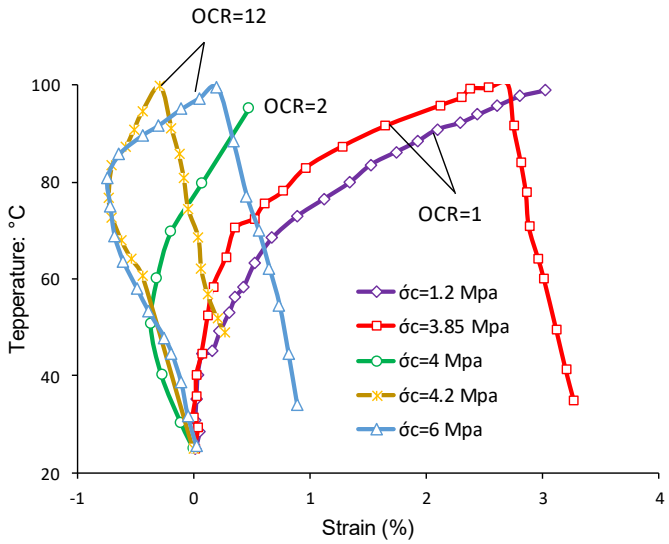

Figure 21. Thermoelastoplastic response of Boom Clay (modified after (Sultan et al. 2002).

Whereas the thermoelastic expansion can be easily interpreted in terms of thermal dilation of the solid phase (see thermal dilation coefficients in Table 2), the plastic contraction is more difficult to interpret. It seems that the role of water adsorbed along the clay particles plays an important role. There would be two modes of separating the adsorbed water from the (plastic) clay particles along which they are

bonded: either by compression and squeezing out (effect of preconsolidation) or by heating, given that in general temperature reduces the physico-chemical interactions between molecules (consider for instance the effects of temperature on the Brownian movement and the changes in properties of gases when submitted to temperature elevation)(Delage 2013).

Table 2. Thermal expansion and compressibility coefficients of some typical minerals present in clays and claystones.

Mineral	Thermal expansion coefficient ($°C^{-1}$), α_s	Reference	Solid compressibility (GPa^{-1}), c_s	Reference
Clay	3.4×10^{-5}	(McTigue 1986)	0.02	(Skempton 1954); (McTigue 1986)
Quartz	3.34×10^{-5}	(Palciauskas and Domenico 1982)	0.0265	(Bass 1995)
Calcite	1.38×10^{-5}	(Fei 1995)	0.0136	(Bass 1995)
Felspar	1.11×10^{-5}	(Fei 1995)	0.0145	(Bass 1995)
Water	27 × 10–5	(Spang 2002)	0.447	(Spang 2002)

The response of a specimen of Opalinus clay to a drained thermal cycle between 25°C and 80°C under in situ mean stress conditions is presented in Figure 22. The figure shows that the first temperature elevation phase is characterized by a linear thermo-elastic expansion that is typical of overconsolidated samples between 25°C and 65°C, followed by a plastic contraction between 65°C and the maximum temperature applied, i.e. 83°C. The subsequent cooling phase is characterized by a thermo-elastic contraction with a slope approximately parallel to that of the first heating phase, confirming the reversible nature of the response. The thermal irreversible contraction observed during the first heating phase is comparable to that observed in normally consolidated plastic clays (e.g. (Baldi et al. 1988) and (Delage et al. 2000). In fine grained soils, this phenomenon is understood as a thermal consolidation of the sample which corresponds to the rearrangement of the grains after a critical temperature.

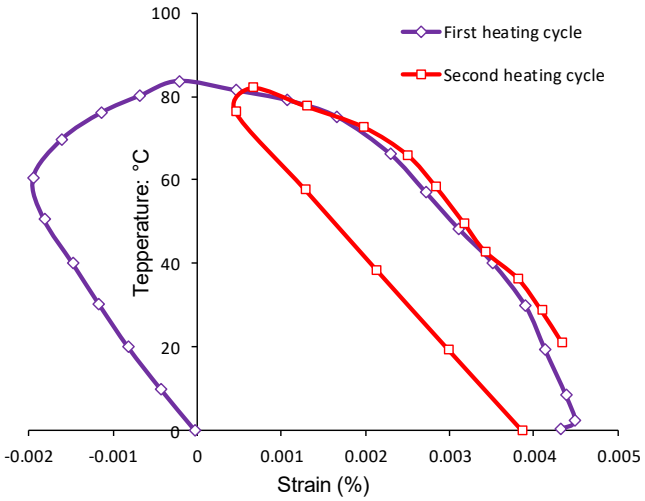

Figure 22. Drained thermal volume changes of Opalinus clay under in situ mean stress conditions (Monfared et al. 2012).

It is interesting to relate this first temperature threshold to the maximum temperature previously experienced by the Opalinus clay. From geological arguments the maximum burial depth of the Opalinus clay at Mont Terri is 1350 m. Assuming a geothermal gradient of about 0.03 °C/m, the value of 65°C appears as a plausible maximum temperature experienced by the material before our test. The observed behaviour is typical of thermal hardening, with an elastic thermal expansion observed below the maximum supported temperature, followed by a plastic contraction at yielding once the maximum temperature is attained.

In the COx claystone, a contracting behaviour has been observed when heating the sample under in situ stress, comparable to the response of normally consolidated clays (Mohajerani et al. 2014). It seems that the claystone has kept the memory of its maximum supported temperature like overconsolidated soils conserve the memory of the maximum supported load. Thermal volumetric behaviour of COx claystone characterized by the strong post-sedimentation diagenetic bonds which has an important role as compared to plastic clays like Boom and Opalinus. Indeed, most numerical predictions of the behaviour of claystones around waste disposal systems consider a thermo-elastic response (Gens et al. 2007a). Actually, this trend is not in agreement with the in-situ measurements of thermally induced pore pressure that appeared to be correctly modelled under a thermoelastic (dilating) hypothesis.

The contracting behaviour of the COx claystone by temperature, which was already evidenced by Mohajerani et al., (2014), was further investigated and confirmed by (Menaceur et al. 2015a). They were performed two drained heating tests to investigate the thermal volumetric response of the COx claystone. They confirmed the contracting behaviour already evidenced Mohajerani et al., (2014), but

with smaller contraction coefficient. A possible reason of the significantly smaller contraction observed here could come from the differences in origin and in porosity between the specimens. More porous samples have larger clay content and clay content is the driving force of thermal contraction, given that the grains of quartz and calcite contained in the clay matrix simultaneously expand, probably resulting in some thermal damage at the interface between the grains and the clay matrix.

Later, (Zhang et al. 2017) was determined thermal expansion behaviour of the claystones by heating and cooling the samples under different isostatic stresses and undrained conditions which was consistent with the in situ observations during heating experiments. Figure 23 shows the strain evolution measured on a COx claystone sample during a heating/cooling cycle under sequentially lowered confining stress. The sample with a high initial saturation degree was heated by stepwise increasing temperature from 23°C to 68°C and then cooled down to the ambient temperature. The data show that (a) each temperature increases generated expansion in all directions; (b) the expansion did not change much with time at each constant temperature below 47°C and then a gradual contraction reversely occurred at higher temperatures; and (c) cooling down yielded contraction and then was followed by a swelling process as shown in Figure 23.

The sedimentary clay rocks commonly exhibit thermal anisotropy with bedding structure. Figure 24 illustrates the thermal expansion anisotropy of an Opalinus sample without confining load. The expansion coefficient of $\alpha_{\perp}$ =1.6×10^{-6} ºC^{-1} measured in direction perpendicular to the bedding planes is about one order of magnitude higher than that of $\alpha_{\parallel}$ = 1.5×10^{-6} ºC^{-1} parallel to the bedding planes. The thermal anisotropy observed may not be so significant when the claystone is subjected to confining stress such as the lithostatic stress in the rock mass, which hinders opening of microfissures lying in the bedding planes.

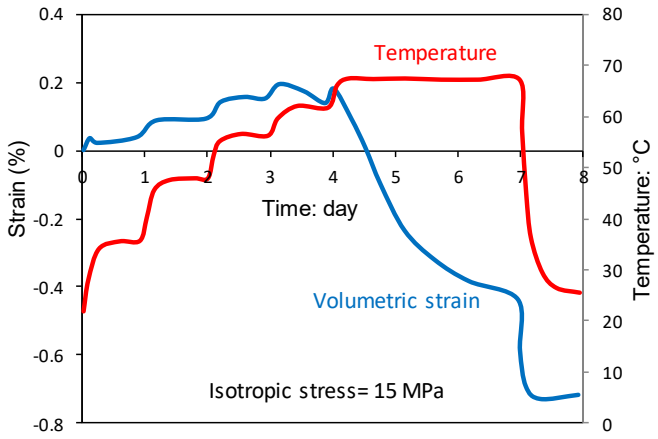

Figure 23. Thermal expansion and contraction of a COx claystone sample during heating and cooling under different isostatic stresses (modified after (Zhang et al. 2017).

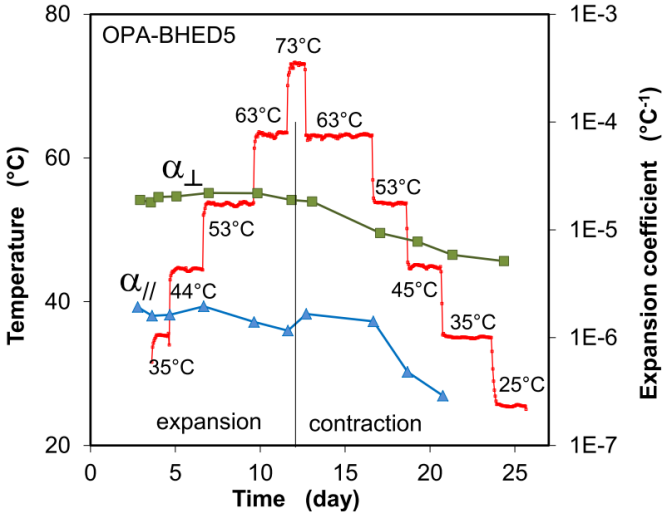

Figure 24. Anisotropy of thermal expansion of an Opalinus sample without confining load (Zhang et al. 2017).

6.3 Temperature influence on the strength

6.3.1 Effect of temperature on the preconsolidation pressure

The key thermal effects in argillaceous materials are those that lead to irreversible changes, particularly irreversible deformation. To address the irreversible strain in thermal conditions, the classical notion of the elasticity domain in the elasto-plastic context must be revised. The main new feature is the strong sensitivity of the plastic limit to temperature. However, other prominent thermomechanical characteristics of soils like a substantial thermoplastic contraction in normally and slightly overconsolidated soils, as opposed to the thermoelastic expansion of heavily overconsolidated these geomaterials need to be considered in this context. Several authors have studied the effect of temperature on the preconsolidation stress (e.g. (Tidfors and Sällfors 1989); (Eriksson 1989); (Belanteur

et al. 1997); Bouladi et al. 1994; (Akagi and Komiya 1995); (Sultan et al. 2002) (Figure 25). The results of these studies confirm a decrease in preconsolidation stress with the increase in temperature.

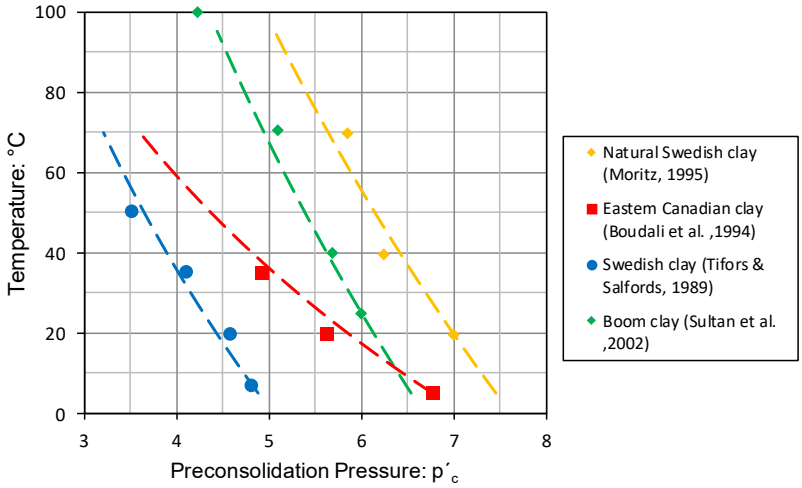

Figure 25. Decrease in the preconsolidation of Boom clay with temperature.

6.3.2 Effect of temperature on the compression index and swelling index

(Campanella and Mitchell 1968) presented the first works on the effect of temperature on the compression index and swelling index of clays. They carried out isotropic compression tests on three illite samples at three different temperatures (24.7-37.7-51.4°C). Their results show that these indices are not affected by temperature, Figure 26. According to (Cui et al. 2004) this conclusion seems correct when the stress level is relatively low (less than 1 MPa); on the other hand, with stronger constraints, (Sultan 1997) have shown that the compression index at different temperatures converges to a value when the total stress increases, which has also been shown by (Tanaka 1995).

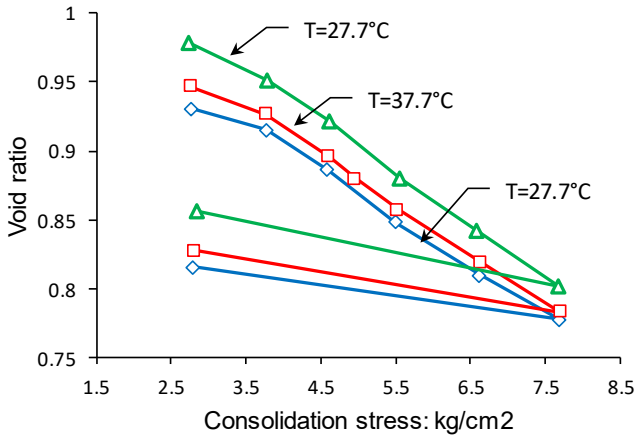

Figure 26. Isotropic compression of three samples of illites at three temperature levels, according to (Modified after (Campanella and Mitchell 1968)

6.3.3 Effect of temperature on shear strength

A conflicting report of temperature, causing strength increases or decreases were reported in literature. (Hueckel et al. 2009) have concluded that there is no unique a priori answer to the question, at least in the temperature range 4°C<T<120°C. Nevertheless, it has also been shown that the strength dependency on temperature is material-specific and the evolution of both the yield and failure behaviour is critically dependent on the history of thermomechanical loading, in particular the stress and drainage state in which the heating is done, which was suggested earlier by (Kuntiwattanakul et al. 1995) as well. Experimental studies of the triaxial strength of argillaceous materials show that remoulded kaolin clay and natural Boom Clay exhibit temperature dependence of their internal friction, whereas this is not the case for largely smectitic or illitic clays (Hueckel and Borsetto 1990); (Hueckel and Baldi 1991); (Cekerevac and Laloui 2004). Interestingly, the effects of the thermal variation of internal friction depend heavily on the history of heating and loading. In particular, the state of stress at which heating is performed, including the soil overconsolidation ratio, impacts on the ensuing variation of strength (Hueckel et al. 2009). Figure 24 shows the friction angle evolution with temperature for different argillaceous materials. For a material such as kaolin, the effect of temperature is significant. (Despax 1976) and (Robinet et al. 1996) observed a significant decrease in the friction angle for kaolin while the results of (Cekerevac and Laloui 2004) on this material show an increase in the friction angle.

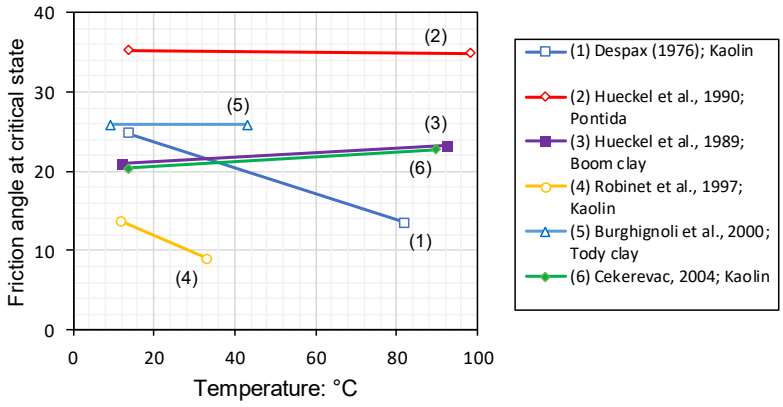

Figure 27. Effect of temperature on the friction angle of argillaceous materials.

In 1999, De Bruyn performed several series of CIU triaxial tests at different temperatures on Boom clay samples taken around the CERBERUS in situ experiment. Considering that these samples were submitted for the excavation of the Test Drift and for the drilling of the experiment itself, it is observed that heating to about 90°C has led to a significant loss (30%) of cohesion (in five years) and eventually

lead to decrease in shear strength. This strength reduction was later confirmed by (Hueckel et al. 2009) which is discussed above.

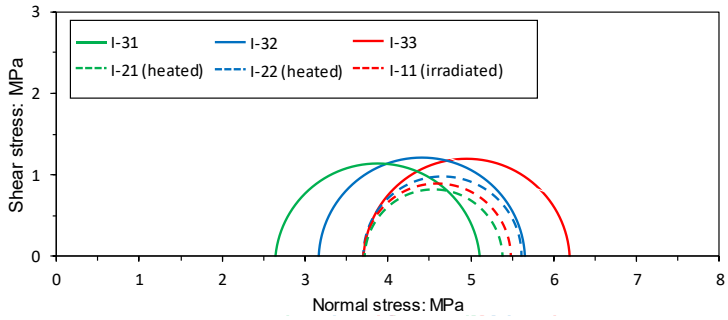

Figure 28. CIU tests on samples taken around CERBERUS in situ experiment (Bruyn 1999).

Undrained triaxial shearing tests under constant 3 MPa confining stress on Opalinus clay specimens with bedding planes inclined of 30–40° were run at various temperatures from 20 to 115°C by (Zhang et al. 2007a). The specimens had an initial degree of saturation of 88%. They observed in such conditions a more ductile behaviour at elevated temperature with a clear decrease in strength due to temperature elevation. Figure 29 shows the undrained short-term compression behaviour of the saturated Opalinus clays at temperatures between 20°C and 116°C and at lateral stresses around 3MPa. The axial load was parallel to the bedding planes. It is obvious that the Opalinus clays became more plastic at the elevated temperatures. The weakness is probably caused by thermally-induced pore pressure increase and the corresponding decrease in effective confining stress on one hand and by thermally-induced reduction of the inherent cohesion and friction resistance of the bound pore water between solid particles on the other hand. Correspondingly, the effective confining stress must reduce down to zero. Therefore, the strengths obtained at high temperatures of 70°C-116°C are lower than that at 20°C, as compared in Figure 30 with the average strength envelope for the direction parallel to the bedding planes (Bock 2001). The strength at 116°C is as low as the uniaxial strength at 20°C.

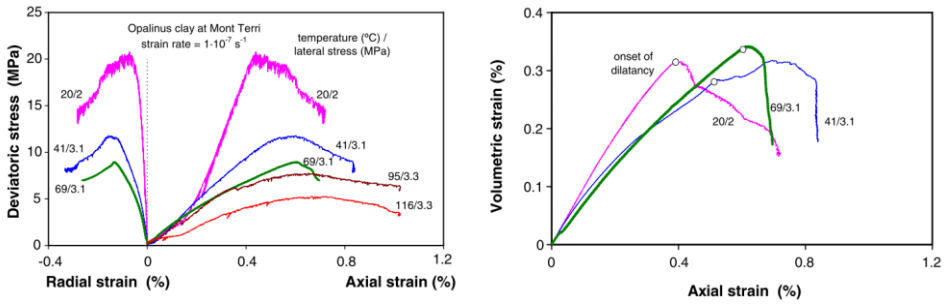

Figure 29. Compression behaviour of the Opalinus clay at elevated temperatures and under undrained conditions (Zhang et al. 2007a).

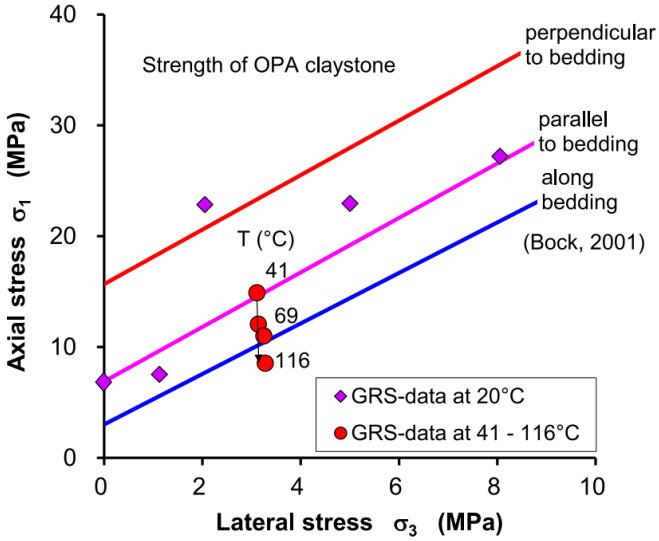

Figure 30. Comparison of the strengths obtained at high and ambient temperatures for the Opalinus clay (Zhang et al. 2017).

More recently, (Zhang et al. 2014), conducted triaxial micro-compression tests on unsaturated triaxial specimens submitted to a relative humidity of around 74%. They observed little sensitivity with respect to temperature in the stress-strain curves obtained between 20°C and 95°C under a confining stress of 15 MPa (around twice the in-situ effective stress), whereas a decrease in peak stress (with small sensitivity in the elastic regime) was observed under a confining stress of 5 MPa (smaller than the in-situ stress).

(Masri et al. 2014) conducted a series of what they called “pseudo-drained” triaxial shear tests on Tournemire claystone at temperatures between 20°C and 250°C under three confining pressures (5, 10 and 20 MPa). Their observations are comparable to that made by Zhang et al. (2007) on Opalinus clay, with significantly more ductile behaviour observed at elevated temperature and peak stress decreasing from 90 MPa at 20°C down to 40 MPa at 250°C.

While substantial progress has been made in understanding the principal effects of elevated temperature in Boom clay and Opalinus clay, the failure conditions of COx claystone at elevated temperatures remain less well understood. In fact, there is a somewhat confusing view of the experimental evidence concerning the thermal dependence of shear strength in COx claystone.

(Bauer et al. 1997) and later (Andra 2005) were reported that the temperature influence on the strength of the COx claystone is not so significant in undrained condition. Moreover, in contrast to the undrained thermal tests heating a claystone in drained condition, increasing the inner friction resistance between solid particles against shearing and hence strengthening the rock. As shown in Figure 31 strength envelopes at different temperatures are close to each other, indicating an insignificant influence of

temperature on the strength. Nevertheless, the strength reached by the drained heating tests at T = 90ºC-150 ºC (upper part in Figure 31) are much higher than the undrained thermal strength.

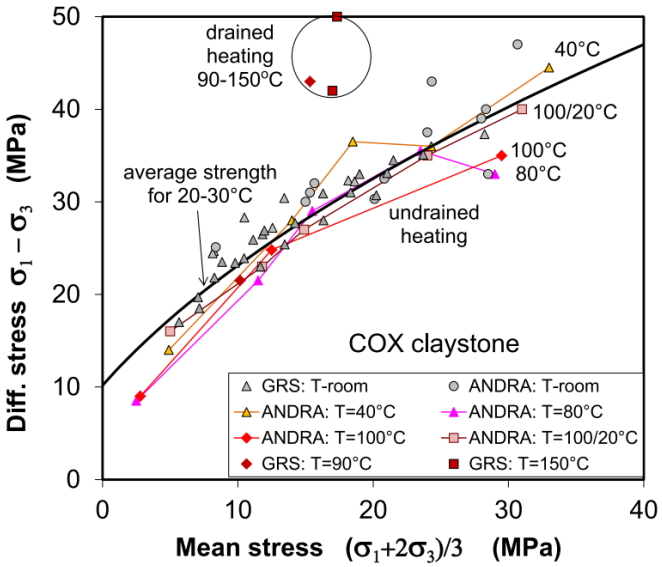

Figure 31. Comparison of drained and undrained thermal strengths of the COx claystone (Zhang 2018).

Previous works indicate that there is a *suspicion* of shear strength change in COx claystone with elevated temperature representing a contrast behaviour with the Boom clay and Opalinus clay strength evolution with temperature.

However, due to obvious experimental difficulties, these results are based on tests that have not been conducted under fully saturated and drained conditions. In this regard, and to overcome this shortcoming, (Menaceur et al. 2015a) were performed two drained heating tests under fully saturated conditions with well adapted devices and procedures. The preliminary results evidenced a more ductile response and slightly smaller shear strengths of the COx claystone at elevated temperature, in agreement with the available published data on argillaceous material like the Boom clay and Opalinus clay.

Figure 32 shows the values of peak strength as a function of effective mean stress for all of the tests carried out here, together with the data obtained in (Hu et al. 2014) at 25°C under fully saturated conditions. All tests at 25°C are aligned along parallel lines that define a friction angle of 21° equal to that proposed in (Hu et al. 2014). As shown in the figure there is a decrease in cohesion that makes the more porous specimen weaker with the cohesion of 1.94 MPa at 17% compared to 4.2 MPa at 13%. The two points obtained at a porosity of 13% at a temperature of 80°C are located slightly below the points at the same porosity and 25°C, indicating a slight reduction in shear strength due to temperature.

The slight difference observed is actually in the range of the dispersion observed when testing COx specimens.

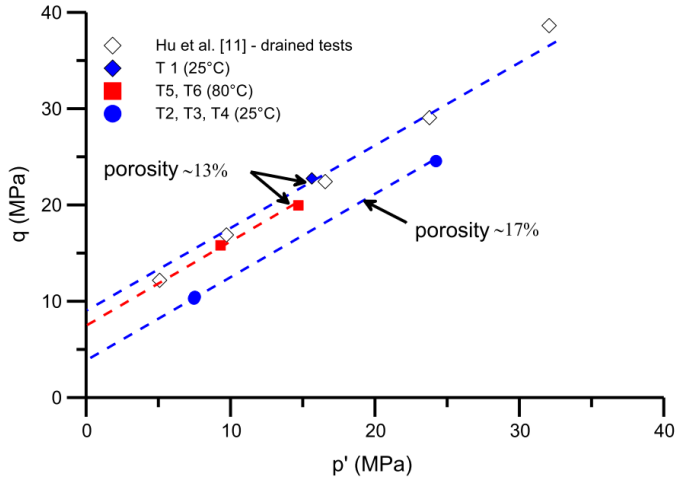

Figure 32. Shear strength of all tests carried out in the plan q–p' ((Menaceur et al. 2015a)).

The decrease in the COx claystone strength by temperature, which was first observed by (Menaceur et al. 2015a), was further investigated and confirmed by (Liu et al. 2019). They were designed and performed a series of lateral decompression (LD) tests, based on a theoretical analysis of stress evolution in surrounding rocks of an underground cavity during excavation, to investigate the thermomechanical behaviour of the COx claystone. A number of unloading–reloading cycles were included in each LD test. Furthermore, to evaluate the effect of temperature on mechanical strength and elastic properties of the COx claystone, the LD tests are performed under five different values of temperature from 20 to 90°C. The shear strength as well as failure pattern in the LD tests were analysed. The COx claystone showed a shear failure in the LD tests, and the failure was characterized by the creation of a localized macro-crack and of a damaged zone with many micro-cracks around the macro-crack.

The temperature increase induced a degradation of the shear strength of the COx claystone. An obvious mechanical damage of elastic properties was observed in the COx claystone during the shear stress loading in the LD tests. This damage was more important in the lateral direction than the axial one, leading to an induced anisotropy of the material. As shown in Figure 33, with the increase of temperature, the irreversible strain during the nonlinear phase before the peak stress is significantly enhanced. Therefore, it seems that the temperature increase induces a more ductile behaviour in the COx claystone.

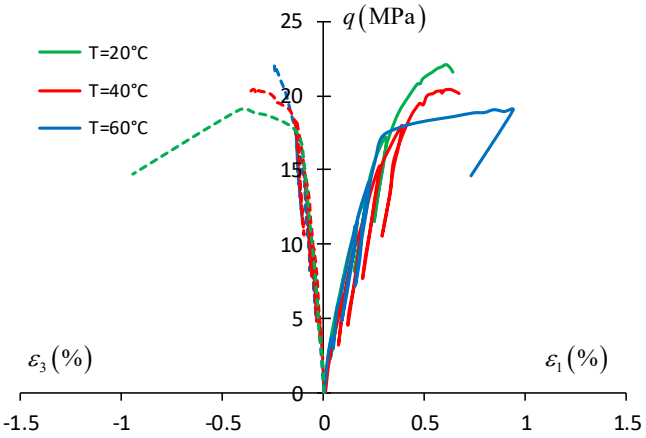

Figure 33. Experimental results of LD test under T = 20, 40 and 60°C (modified after (Liu et al. 2019).

Moreover, the values of differential stress, radial stress, and axial and lateral strain at the peak state are calculated and presented in Figure 34 for the LD tests under the different values of temperature. It is observed that the peak differential stress decreases with the increase of temperature.

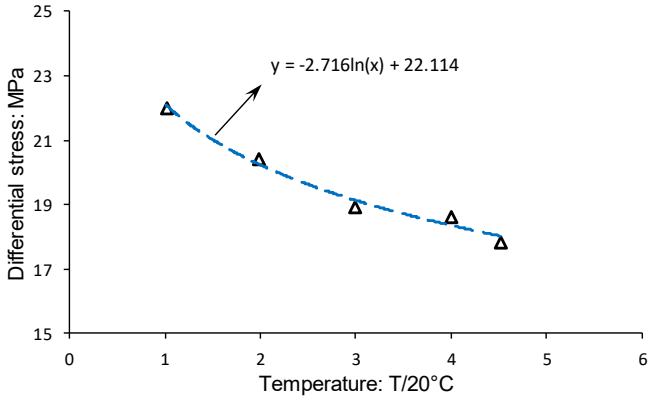

Figure 34. Thermal effect on peak stress in LD tests: Differential stresses at peak strength (modified after Liu et al. 2019).

6.4 Thermal pressurization

In argillaceous rocks, the main hydraulic phenomenon associated with thermal effects is the generation of pore pressure due to changes of temperature. When argillaceous rocks are subjected to a temperature increase, the pore pressure will also increase due to the fact that the thermal expansion of the water is larger than that of the porous skeleton itself. However, the low permeability of argillaceous rocks ensures that the resulting excess pore pressure does not dissipate rapidly. By looking at Table 2, it can be observed that the water expansion coefficient is almost one order of magnitude higher than that of the minerals, and that the coefficient of quartz and clay are comparable and larger than that of calcite or feldspar. Given that the structure of claystones is generally characterized by a clay matrix containing grains (of quartz, calcite and feldspar), one can suspect some significant differential

expansions in the solid phase at clay-calcite interfaces (the most frequent) and also at clay- feldspar interfaces. (Ghabezloo and Sulem 2010) gathered some values of the thermal pressurization coefficient ($\Lambda = \Delta p / \Delta t$; MPa/ºC) measured in various soils and rocks and presented in Table 3. The table has been completed by their own values on the Rothbach sandstone, by a value on Boom Clay recently obtained by (Lima et al. 2010) and by a value on the Opalinus claystone deduced from the data of (Muñoz et al. 2009).

Table 3. Thermal expansion coefficients of various soils and rocks.

Mineral	Thermal expansion coefficient (MPa/ºC $^{-1}$)	Reference
Clay	0.01	(Campanella and Mitchell 1968)
Boom Clay	0.06	(Vardoulakis 2002)
	0.019	(Lima et al. 2010)
Opalinus claystone	0.1	(Muñoz et al. 2009)
Sandstone	0.05	(Campanella and Mitchell 1968)
Kayenta sandstone	0.59	(Palciauskas and Domenico 1982)
Rothbach sandstone	From 0.25 to 0.025	(Ghabezloo and Sulem 2010)
Clayey fault gouge	0.1	(Sulem et al. 2004)(Sulem et al. 2007)
Intact rock at great depth	1.5	(Lachenbruch 1980)
Mature fault at 7000 m depth	Intact fault wall: 0.92; Damaged fault wall: 0.31	(Rice 2006)

Some large values have been obtained in rocks, but the values in clays are between 0.01 MPa/ºC and 0.1 MPa/ºC. Quite different values are given for clays, in particular in Boom Clay, comparing the data of (Vardoulakis 2002) that were obtained from experimental data of (Sultan 1997) and of (Lima et al. 2010). Later (Delage 2013) showed that the thermally induced pore pressure did not depend only on the mineral composition and porosity of the rock, but on the stress state, the range of temperature variation and the previously induced damage. The pressure dependency of the compressibility of both rock and water and the temperature dependency of the pore water compressibility appeared to play an important role, as shown by (Ghabezloo and Sulem 2010) who provided values between 0.25 MPa/ºC and 0.025 MPa/ºC at temperatures between 20°C and 70°C for the Rothbach sandstone.

Figure 35 shows the thermally induced excess pore water pressures observed on COx during heating and cooling in a temperature range of 30°C - 120°C. The slightly desaturated samples were firstly resaturated at the temperature of 30°C for about 10d. The subsequent undrained load generated high pore pressures of 11-12 MPa at sample. The following undrained heating from 30°C to 60°C resulted in a large increase in pore pressure from 1 MPa to 12 MPa at COx sample. The thermally induced excess

pore water pressures remained over time, except for P_{out} at COx sample. However, as unexpected, further heating up to 80°C, 100°C and 120°C did not produce higher pore pressures. This might result from the possible escape of the thermally mobilized pore water through the insolation boundary, which might not resist such high temperatures. The release of the pore water and the resulting dissipation of the pore pressure led to gradual compaction of the porous medium.

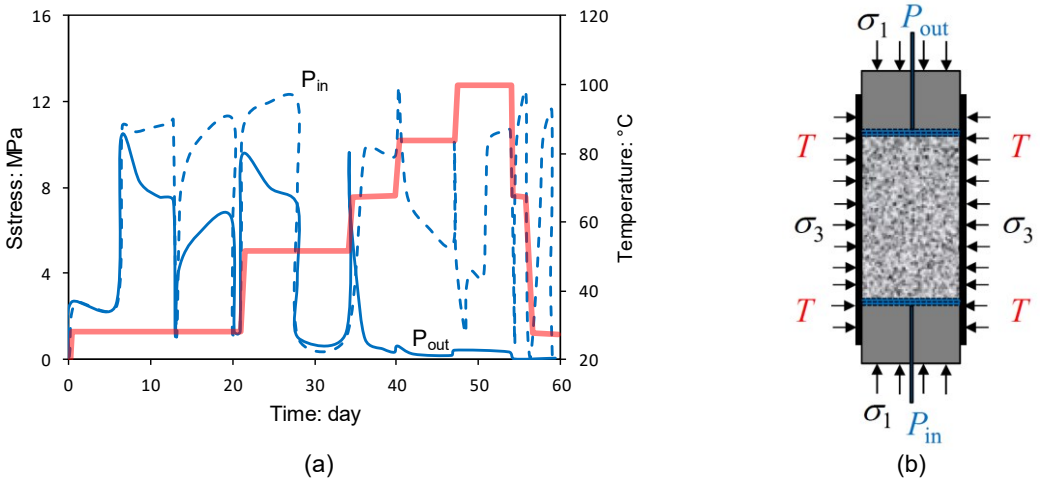

Figure 35. (a) Thermally induced excess pore water pressures of COx claystone (b) THM load conditions of thermal experiments on normal-sized samples. σ_1 is external axial stress; σ_3 is external radial stress; P_{in} is water back pressure at inlet; P_{out} is water back-pressure at outlet. (modified after (Zhang et al. 2017).

The data shown in Figure 36 show the response in pore pressure obtained in a COx sample along a ramp of stepwise progressive temperature elevation between 25°C and 70°C. Compared with thermal response of dummy metal sample, the first peak of temperature corresponds to the instantaneous response of the water contained in the permeable porous elements in COx sample. Afterwards some time has to be waited to get equilibrium between the pore water and that present in the porous elements, leading to the drainage of pore water from the specimen to the porous elements.

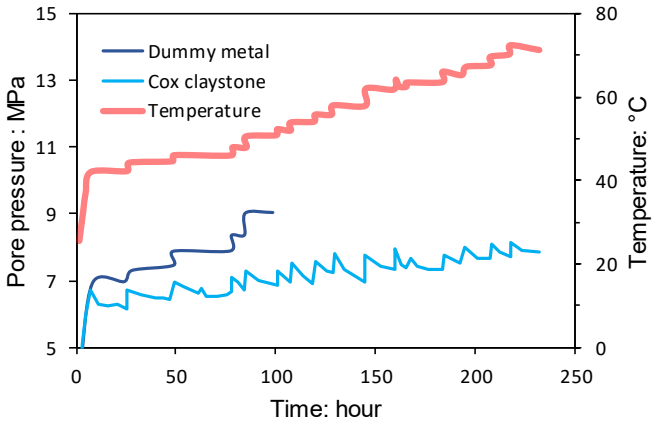

Figure 36. Comparison between thermally induced excess pore water pressures with a COx claystone and a dummy metal sample (Modified after (Mohajerani et al. 2012).

6.5 Effect of temperature on permeability

The effect of temperature on the permeability of argillaceous materials has been studied by different authors. Among others, (Habibagahi 1976) studied this effect on a mixture of illite (70%) and chlorite (20%). He showed that the hydraulic conductivity of material increases with temperature, Figure 37a. This increase in hydraulic conductivity can be explained by the decrease in the viscosity of water with temperature. If we reinterpret Habibagahi's data in terms of intrinsic permeability and void index (Figure 37b) we observe that permeability is almost insensitive to temperature change. The same trend is observed by (Morin and Silva 1984), (Towhata et al. 1993), (Khemissa 1998) on different clays.

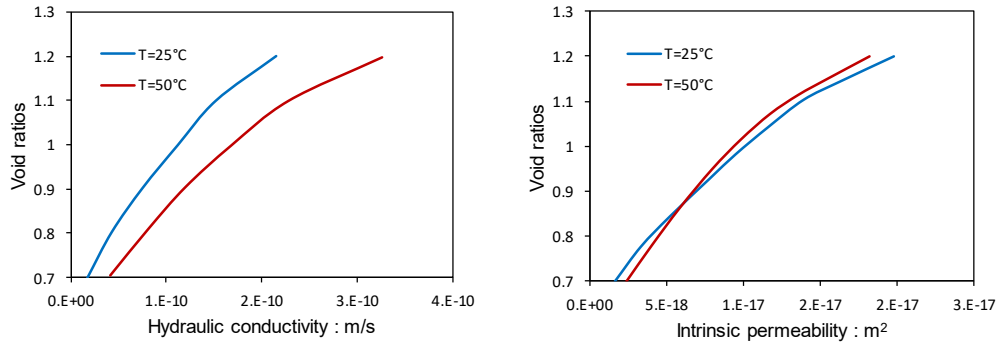

Figure 37. Effect of temperature on the permeability of an illite clay chlorite mixture (a) Hydraulic conductivity (b) Intrinsic permeability (modified from (Habibagahi 1976).

Later in 2000, Delage studied the effect of temperature on the permeability of Boom clay (Delage et al. 2000). They found a linear relationship between porosity and permeability which is independent of temperature, as shown in Figure 38.

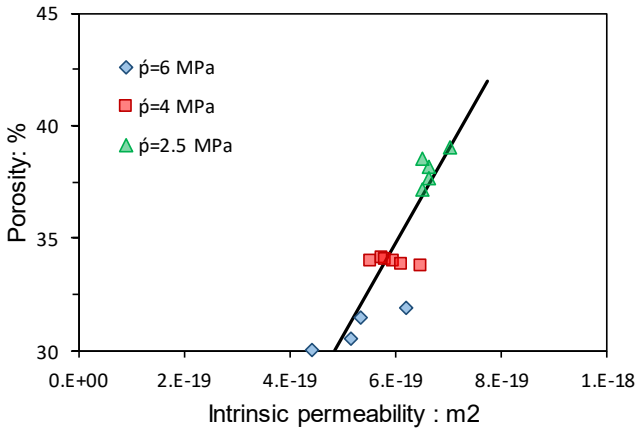

Figure 38. Insensitivity of the permeability-porosity relationship of Boom clay with temperature (modified after (Delage et al. 2000).

Recently (Menaceur et al. 2015b) were performed steady-state radial permeability tests on the COx claystone. They have reported that the permeability is not totally independent of temperature, unlike

what was previously observed on the Boom clay (Delage et al., 2000), with here a slight increase with temperature. Note that these tests also showed an enhancement of swelling with temperature, with around twice more swelling at 80°C compared to 25°C under the same stress conditions.

6.6 Self-sealing and temperature effects

Thermal impact on the self-sealing capacity of damaged claystone is one of the most concerns in the assessment of the long- term safety of HLW repositories. This was examined by measuring water permeability of fractured claystones in various thermal conditions.

Thermal effects on the self-sealing behaviour of argillaceous materials have been investigated within the TIMODAZ project (Yu et al. 2014). Within the framework of this project (Monfared et al. 2012) performed series of hollow cylinder triaxial tests to investigate the effect of the temperature increase on the hydro-mechanical properties of sheared Boom clay samples. One of the main interests of the hollow cylinder test is that it allows performing permeability tests that do account for the shear plane network affecting a sheared sample. The system was then applied to the investigation of the combined effects of shear discontinuities and temperature on the permeability of a Boom Clay specimen. They observed excellent self-sealing properties of the Boom Clay, faster diffusion at elevated temperature and a very minor impact of temperature on intrinsic permeability.

Figure 39 shows pore pressure dissipation obtained in various conditions (after sample resaturation under in situ stress conditions, after shearing, after heating the sheared sample and after cooling). The slower diffusion observed after shearing compared to the initial state confirms the excellent self-sealing properties of the Boom Clay as shown in Figure 39. However, they have reported slight decrease in intrinsic permeability which is due to a decrease in porosity that results from the increase in mean effective pressure occurring during shearing. The faster diffusion observed at elevated temperature (Figure 39) in the sheared sample is due to the decrease in viscosity of water with temperature. Indeed, the permeability values obtained from the experiment, show that the intrinsic permeability is not significantly affected.

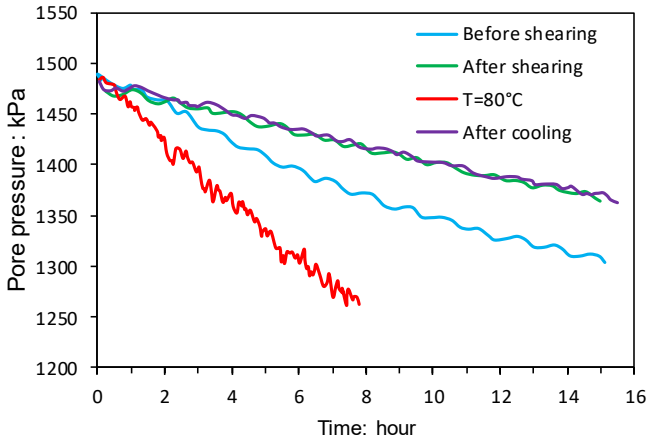

Figure 39. Experimental data and model results for pore pressure dissipation, external wall transducer (modified after (Monfared et al. 2012).

These data, along with other data obtained in the Opalinus clay (conducted by Monfared et al., 2012), show that the self-sealing properties of both the Boom Clay and the Opalinus clay are not affected by temperature elevation. This important result obtained within the TIMODAZ project is quite important in terms of performance assessment (Yu et al., 2014).

Thermal impact on the sealing of fractures was also investigated by heating cracked COx and Opalinus samples under constant confining stress and water injection pressure by (Zhang 2011). A test was performed on an axially-cracked COx claystone sample under an axial stress of 2.5 MPa and a radial stress of 2.0 MPa. The synthetic water was introduced into the fractured sample at inlet pressure of 0.5 MPa while the outlet was kept atmospheric. The sample was heated stepwise from 27°C to 40, 60, 75, 90°C and then cooled down to 60°C and 30°C, whereby radial strain normal to the fracture planes and water permeability in axial direction parallel to the fractures were measured. Figure 40 shows the evolution of the normal strain and the water permeability. Each rapid temperature rise caused a fast expansion of the fractured sample. After a short-term compaction and water injection at 27°C, the fractured sample expanded gradually with time but the intrinsic permeability decreased due to the effect of swelling and slaking of clay matrix between fractures as mentioned before. At elevated temperature of 40°C, the dilation continued while the permeability increased slightly. Over 60°C, the swelling disappeared, and the permeability varied slightly. In contrast to the heating effects, cooling down to 60°C and 30°C led to a compaction of the fractures and a drop-in permeability down.

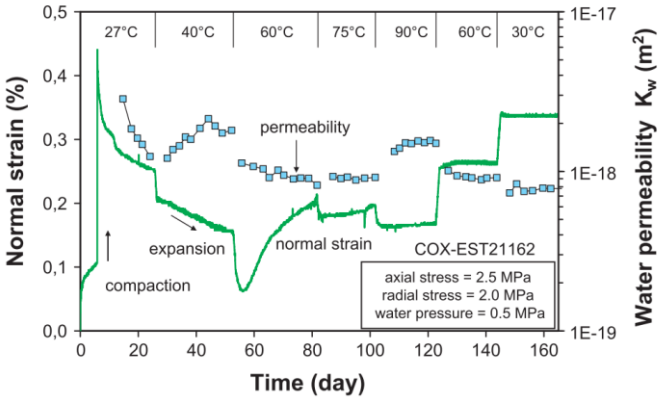

Figure 40. Evolution of normal strain and permeability parallel to fractures during water flowing under different temperatures ((Zhang 2011).

Long-term measurements of water permeability were performed on cracked COx and Opalinus samples at temperatures between 20°C and 90°C.

The synthetic water was injected into the fractured. The results are summarized in Figure 41. Again, the water-induced effect on the hydraulic sealing of fractures is evident during the first stage at 20°C. The permeability decreased at Opalinus and COx sample. Subsequently, the rates of permeability reduction, however, are less affected by the temperature increase up to 60°C. Further heating up to 90°C and cooling down to 60°C had no effect on the permeability which had been obtained. The second cooling-down phase to 20°C, however, induced a slight decrease in permeability for the Opalinus and COx samples.

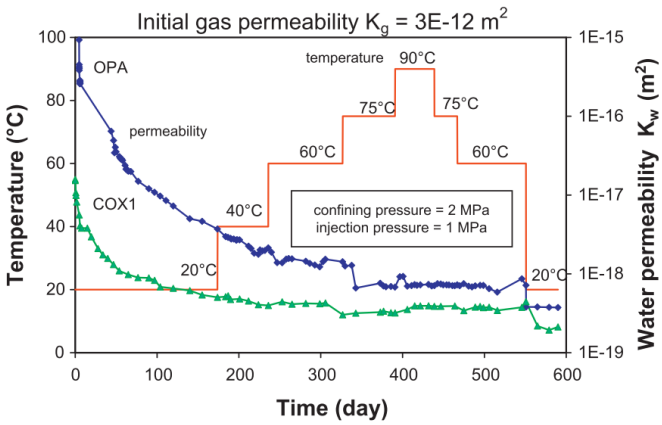

Figure 41. Long-term measurements of water permeability on fractured COx and Opalinus samples at different temperatures ((Zhang 2011).

Figure 42 depicts the last data of water permeability within each phase as function of applied temperature. It is obvious that the water permeability of the fractured claystones decreases more or less with increasing temperature and drops down further after cooling. So, an important conclusion can be drawn. thermal loading up to the maximum temperature of 90°C designed for repositories in clay rocks

has no negative effects on the sealing process of fractures in the EDZ. However, because the hydraulic conductivity depends both on the structure of fractures and pores in the material and the thermally induced changes in viscosity and density of the pore water, the relatively constant intrinsic permeability suggests an enhanced hydraulic conductivity during heating due to the decrease of water viscosity.

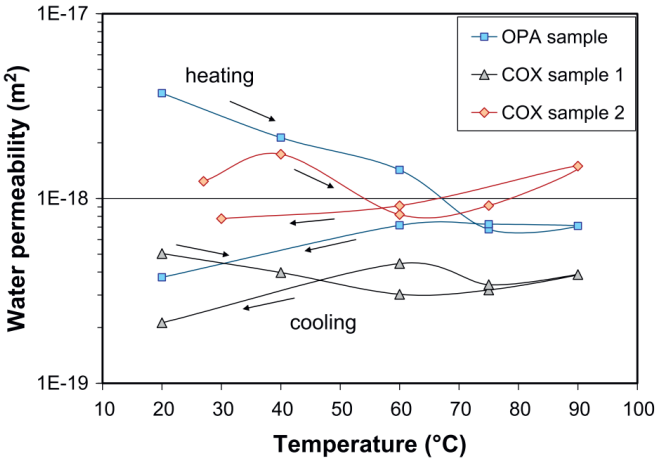

Figure 42. Dependency of water permeability of fractured claystone on temperature ((Zhang 2011).

Various laboratory sealing experiments were carried out on strongly cracked samples of different sizes and shapes from the Callovo-Oxfordian claystone and the Opalinus clay under relevant repository conditions. The sealing behaviour of the fractures was detected by deformation, permeability, and wave velocity measurements, and are summarised as follows, based on the experimental work cited above.

a) The fracture aperture decreases exponentially with increasing normal confining stress.

b) Wetting by water flow through fractures induces swelling and slaking of the clay matrix, filling and clogging of the interstices, and a drastic decrease in permeability.

c) Heating from 20°C to 90°C has no remarkable impact on the water permeability of fractures, while cooling down again decreases the permeability slightly.

d) The thermally induced changes in hydraulic conductivity are mainly attributed to the variations of water viscosity and density.

e) Under the applied THM conditions, the intrinsic permeability of the fractured claystones decreases significantly to the very low levels, which corresponds to intact claystone.

6.7 Long-term deformation at high temperatures

Long-term deformation of a clay host rock is of high importance for assessment of the safety of a repository with regard to the support of the openings, compaction of the EDZ as well as the backfill/seal, and progressive closure of the repository to permanent isolation of the waste in the host rock. This

important issue has been intensively investigated on the COx and Opalinus claystones during the last decade. Both claystones exhibit creep capability or time-dependent deformability under various THM conditions (Gasc-Barbier et al. 2004); (Zhang and Rothfuchs 2004b); (Zhang et al. 2007b); (Gräsle 2009); (Zhang 2015).

The long-term deformation of the claystones is influenced by temperature, which was observed in creep tests under various thermal loads to high temperatures up to 90°C-110°C (Zhang et al. 2017). Indeed, larger creep strains appear at elevated temperature (Belmokhtar et al. 2017a).

As a typical example, Figure 43 shows two creep tests on COx samples during a heating/cooling cycle in the temperature range of 28°C-110°C and 30°C-60°C and under stresses of σ_1/σ_3 =15 MPa/0.5 MPa and 15 MPa/3 MPa, respectively. The samples were highly saturated with water in degrees of 94%-99%. The strain-time curves obtained on each sample show that:

a) each temperature increase led to a radial expansion shortly but a slight compression in axial direction.
b) the axial, radial, and volumetric strains increased quite linearly with time at each elevated temperature below 90°C, suggesting no or less thermal transient creep.
c) at higher temperatures above 90°C, the creep slowed down.
d) cooling down resulted in a radial contraction shortly but negligible axial strain, and almost no further creep continued at the lowered temperatures.

The acceleration of creep at temperatures up to 90°C is probably contributed by the reduction of viscosity and friction resistance of bound water-films between solid particles.

At higher temperatures above 90°C, the undrained conditions could not sustain, allowing the thermally mobilized pore water release to an amount of □ 2% after testing. As a consequence, the pore structure was consolidated, increasing the friction resistance between particles and hence decelerating the creep at the high temperatures.

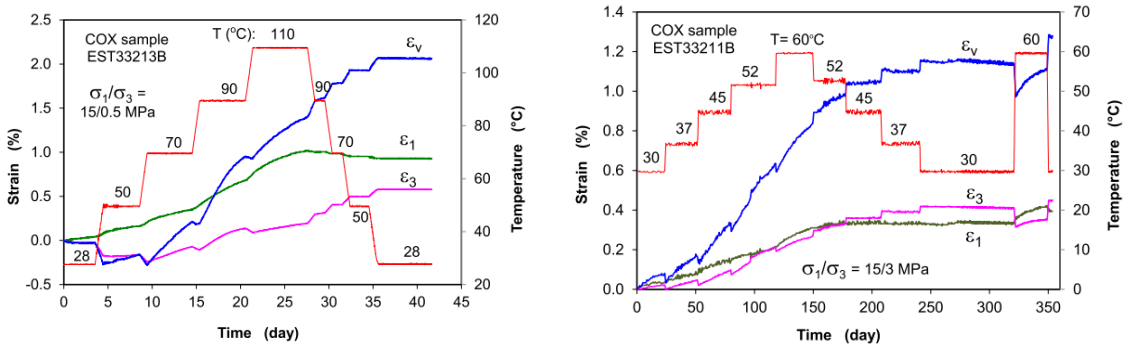

(a) (b)

Figure 43. Creep of COx samples during heating/cooling cycle at different temperatures (Zhang et al. 2017).

The creep rates obtained for the Opalinus claystone are relatively higher due to the high content of clay minerals, compared to those of the COx claystone. As mentioned earlier, the creep under low stresses of $\Delta\sigma$ < 10 MPa varies almost linearly with stress, which is probably controlled by diffusion in bound water-films between solid particles. Beyond that the creep is additionally contributed by microcracking (Figure 44).

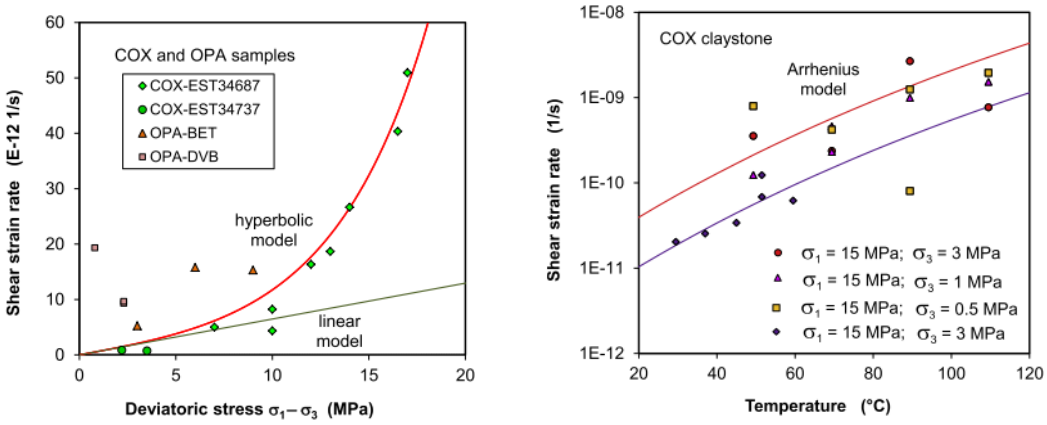

(a) (b)

Figure 44. Stationary shear creep rate of the water-saturated COx claystone as function of deviatoric stress (a) and temperature (b) (Zhang et al. 2017).

An observed time dependent anisotropic compaction under two different temperatures 25°C and 80°C is shown in Figure 45. The figure shows a volumetric creep response under constant isotropic stress, with axial creep strain larger than radial one. Larger creep strains appear at elevated temperature as shown in Figure 45. However, at times larger than 10 days creep rates do not differ too much, with an axial strain rate of $4.8\times10^{-10}s^{-1}$ at 25°C compared to $3.5\times10^{-10}s^{-1}$ at 80°C and a radial one of $1.5\times10^{-10}s^{-1}$ at 25°C compared to $0.9\times10^{-10}s^{-1}$ at 80°C.

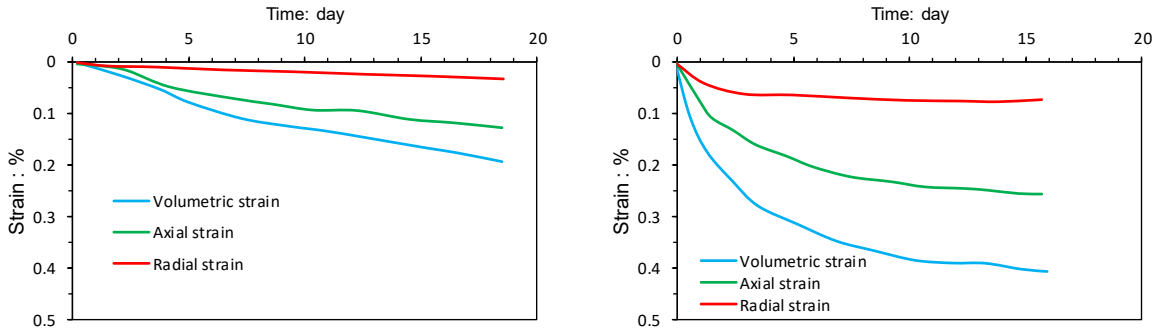

Figure 45. Creep strains: (a) 25°C, (b) 80°C (Belmokhtar et al. 2017b).

5. In-situ THM characterisation

In this section some key features of the response of argillaceous materials to in-situ heating test in three underground laboratories are reviewed. The aim in this section is to use the observations obtained in in-situ heating tests to enhance our understanding of the THM behaviour of argillaceous geomaterials under field conditions. Considering the fact that these materials provide the geological background to many civil engineering projects, interest in these types of material has increased, because they are being considered as potential host geological media for underground repositories of high-level radioactive waste, in recent years (Gens 2004). As discussed above, they exhibit favourable characteristics, such as low permeability, a degree of self-healing capacity when fractured, significant retardation properties for solute transport, and no foreseeable economic value.

Another significant issue is heat-emitting nature of High-level radioactive waste. Therefore, the use of Argillaceous materials in this type of application brings to the fore the thermal response of this type of material and, especially, the interaction of thermal phenomena with hydraulic and mechanical behaviour. The possible use of these types of clay as geological hosts for radioactive waste has prompted the construction of several underground laboratories. They include: the Hades laboratory in Mol (Belgium), excavated in Boom clay; and the Mont Terri laboratory of northern Switzerland, constructed in Opalinus clay and the Meuse/Haute Marne laboratory of Eastern France, sited in a thick stratum of Callovo-Oxfordian claystone. Underground laboratories allow, by the performance of appropriate in situ tests, observation of the clay response in complex situations that mimic some of the conditions likely to be encountered in a deep geological repository. To assess the hydro-mechanical effects of the thermal transient on the host clay in a deep repository, various in situ heating tests have been performed at several underground laboratories (Gens et al. 2007a).

The CACTUS, ATLAS, and CERBERUS tests (Picard et al. 1994); (Bernier and Neerdael 1996); (de Bruyn and Labat 2002)(François et al. 2009b) were performed in the Boom clay at the HADES underground research facility in Mol, Belgium. The HE-B, HE-D and HE-E tests were carried out in the Mont Terri laboratory in Northern Switzerland, which was constructed in Opalinus clay (Gens et al. 2007a). The TER and TED heating test is was carried out in Bure at the Meuse/Haute Marne laboratory located in Eastern France (Gens et al. 2007b)(Conil and Armand 2012), which was constructed in the Callovo-Oxfordian mudstone. Finally, HA-ALC1604 in situ heating test which is currently under way in Bure at the Meuse/Haute Marne laboratory which is constructed in the Callovo-Oxfordian claystone. Observations, interpretation and THM modelling of this test will be given in the later chapters. This section concentrates on the response of Boom clay, Opalinus clay and Callovo-Oxfordian claystone, to thermal loading in the context of the insitu heating tests performed in the different underground laboratory stated above.

7.1 HADES underground research facility

7.1.1 General

The HADES underground research facility is located in Mol, Belgium (Bastiaens and Bernier 2006). It consists of two access shafts and a main gallery with some secondary drifts and shafts (Figure 46). The main gallery has a length of about 200m with an average internal diameter of 4 and is situated at a depth of 223 m. The laboratory has been excavated in Boom clay, a Tertiary plastic clay of modest cementation and relatively low strength. At the underground facility location, the Boom clay lies between 190 m and 290 m below the surface. The Boom clay layer is nearly horizontal, dipping about 1-2% towards the north-east. It is bound on the upper and lower part by pervious materials. A regional geological profile is sketched in Figure 47.

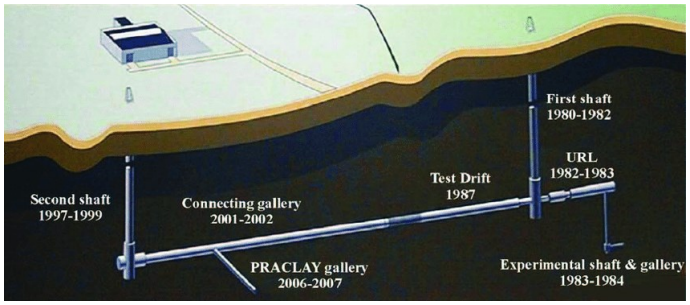

Figure 46. Layout of the HADES underground research facility (Gens 2013).

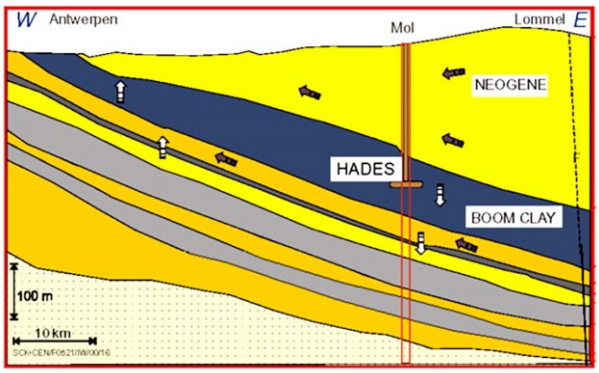

Figure 47. Geological profile showing the location of the HADES laboratory (very distorted scales) (Gens 2013).

7.1.2 Response to underground excavation

The response of Boom clay to deep excavation has been explicitly studied in the CLIPEX experiment (Li et al. 2006). It involved the close observation of the excavation of the 85m-long 4.8m diameter connecting gallery using a comprehensive monitoring system installed prior to the start of the excavation. Open face excavation was adopted using a road header protected by a 2.3 m-long shield. The shield was equipped with a cutting head to achieve a smooth excavation profile. Lining was provided by 40-cm thick unreinforced concrete segments. Excavation rate was of the order of 3 m/day. At the excavation level, vertical stress is 4.5 MPa and the pore water pressure undisturbed by excavation is 2.2 MPa. A value of K_0=0.9 is usually accepted, consistent with the best estimate of overconsolidation ratio of about 2.4 (Horseman et al. 1987). In this case, therefore, initial stress anisotropy is unlikely to be large.

Perhaps the most interesting observations involved the measurements of pore water pressure that exhibited a very characteristic behaviour (Figure 48). Pore pressure increases as the excavation approaches due to the transfer of stress to the ground away from the excavation. At some point, pore pressure drops due to excavation unloading becoming even negative (suction). Pore pressure finally goes to atmospheric when connection is established with the already excavated area. It was also noteworthy that effects of excavation on displacements and pore pressures were felt at very large distances, of the order of 60 m, i.e. more than 12 diameters.

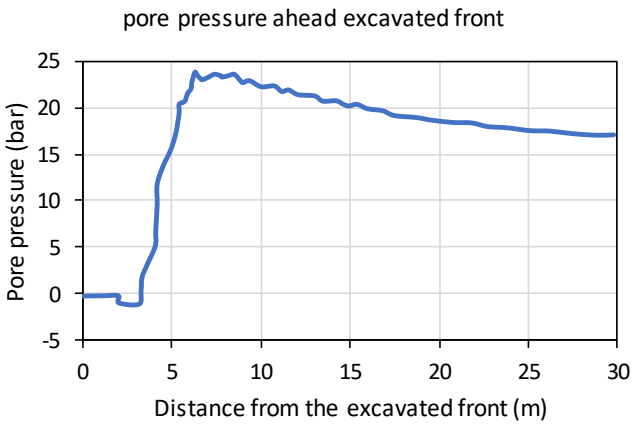

Figure 48. Evolution of pore pressure as a function of the distance to the excavation front (Bernier et al. 2007).

Development of fractures was observed during the excavation. Excavation disturbance is generally reflected in an increase of permeability. This is illustrated in Figure 49 that shows the measured values of permeability against distance to the tunnel wall in two different directions. It can be observed that the increased permeability extends about one diameter. The effect is certainly larger in the vertical direction. Measurements were made one year apart but little change in permeability was recorded. A modest permeability anisotropy is also observed, permeability along bedding is, as expected, the larger one.

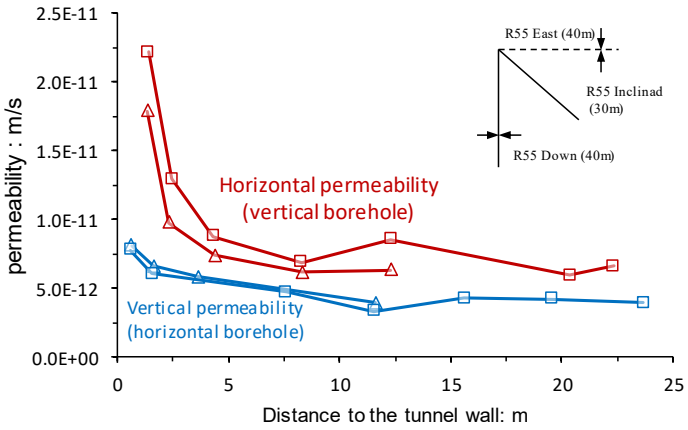

Figure 49. Permeability around the connecting gallery measured in a horizontal and a vertical borehole (Bastiaens et al. 2006).

7.1.3 ATLAS III in situ heating test in boom clay

The original test set-up for ATLAS was performed in 1992 by SCK.CEN within the framework of the European project Interclay II (1990–1994) (Knowles et al. 1996). During the first phase of the heating test programme, later named *ATLAS I*, a constant heat source of 900W was used from July 1993 to June 1996. During the second phase (*ATLAS II*), the power was increased to 1800W and maintained from June 1996 to May 1997. This was followed by shutdown and natural cooling starting from June 1997 on (de Bruyn and Labat 2002)(François et al. 2009b). After the set-up had been extended in 2006,

the heater was switched on again from April 2007 to April 2008 with a stepwise power increase, followed by an instantaneous shutdown. This phase is called ATLAS III (Figure 50).

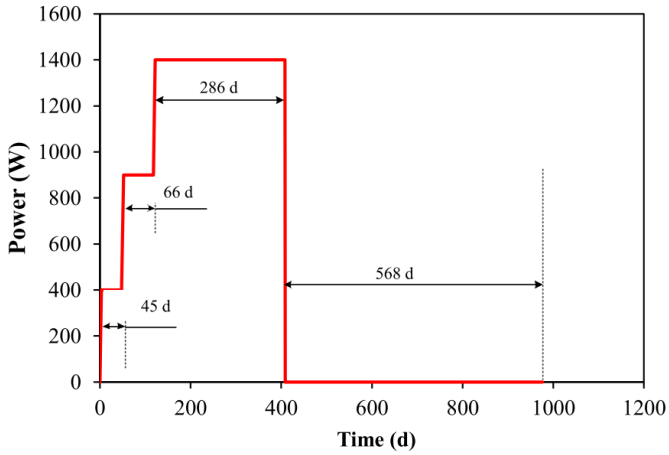

Figure 50. Heating procedure of ATLAS III in situ heating test.

The objectives of ATLAS III were to obtain a more accurate picture of the temperature and pore water pressure by drilling two additional instrumented boreholes, to broaden the THM characterization of the Boom clay at a larger scale and at different temperature levels, to serve as preparation for the Praclay Heater test, to provide a reference for up-scaling the Praclay Heater test and finally to provide data for a modelling benchmark study in the European project TIMODAZ (2006–2010) (TIMODAZ 2007).

The test set-up consists of a central heater borehole and four instrumented observation boreholes. The central heater borehole (AT89E) and three observation boreholes (AT85E, AT93E, and AT98E) are in the same horizontal plane while the fourth observation borehole (AT97E) is slightly inclined towards the heater borehole. The inclination is about 10° down and 10° towards the heater borehole. Figure 51 illustrates the plan view of the ATLAS III test.

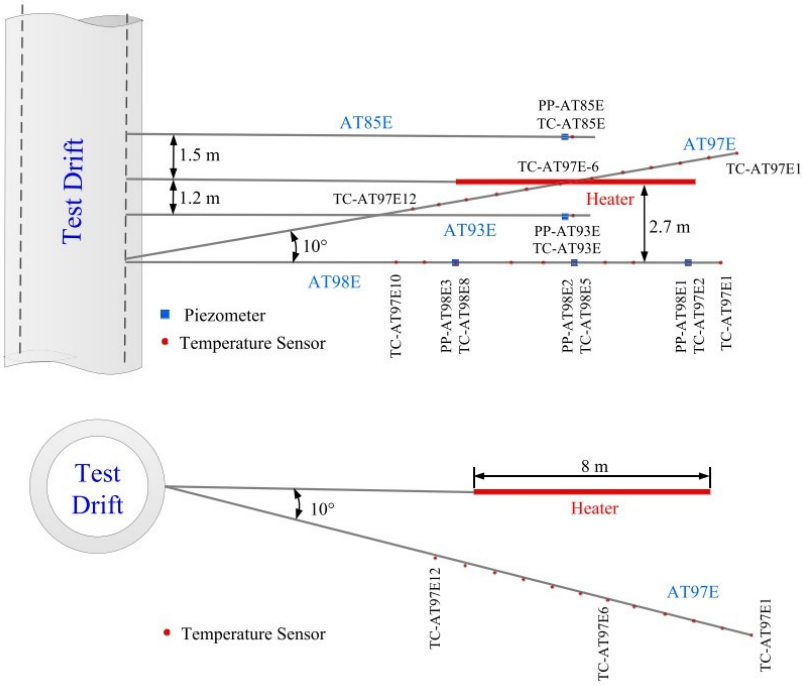

Figure 51. Schematic view with instrumentation of the ATLAS III in situ test (Chen et al. 2017).

Thermal results

The average temperature increases in the boreholes AT85E and AT93E is shown in Figure 52. The temperature increase is larger at AT93E than that at AT85E due to the shorter distance of AT93E to the heater tube (see Figure 51). Maximum temperature increases of 24°C and 22°C are observed by the sensors at AT93E and at AT85E, respectively. The successive heating steps are well visible. A decrease in temperature is only visible 2 days after switching off the heater.

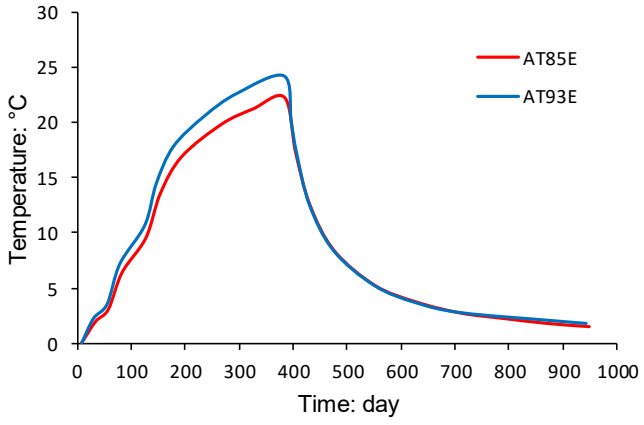

Figure 52. Evolution of temperature change measured in boreholes AT85E and AT93E (modified after (Chen et al. 2011).

Pore pressures

Figure 53 shows the evolution of the por pressure evolution at five piezometer filters located in boreholes AT85E, AT93E and AT98E. The maximum por pressure increases range between 0.5 MPa and 1.0

MPa. Due to the slow drainage towards the underground laboratory, initial pore water pressures range from 1.2 MPa to 1.75 MPa depending on the distance to the Test Drift. At the end of March 2008, a sudden drop of pore pressure was imposed on the piezometer PP-AT85E in order to determine the permeability of the clay host rock near this sensor. It is interesting to observe that at the start of each heating phase, a temporary decrease of the pore pressure occurs in all the piezometers. The opposite phenomenon is observed when switching off the heater.

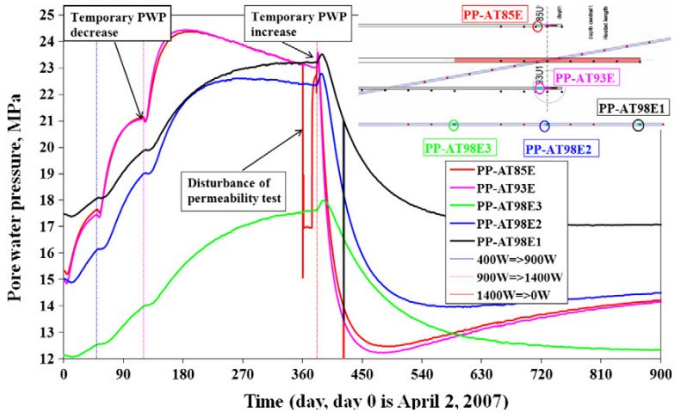

Figure 53. Evolution of pore pressure at five piezometer filters located in boreholes AT85E, AT93E and AT98E (Chen et al. 2011).

THM coupling

Figure 54 present the increases of temperature, pore pressure and average total stress measured in boreholes AT85E and AT93E respectively, and for groups of sensors that are very close to each other. As shown in the Figure 55, After the power is increased, pore pressure decreases immediately, then they start to increase only when the local temperature reacts to the increased power. After the power is switched off, pore pressure increases immediately and then decrease when the local temperatures start to decrease due to the switching off of the power. However, changes of both pore pressure and average total stress measured in AT85E (and AT93E) show similar trends of evolution and magnitude.

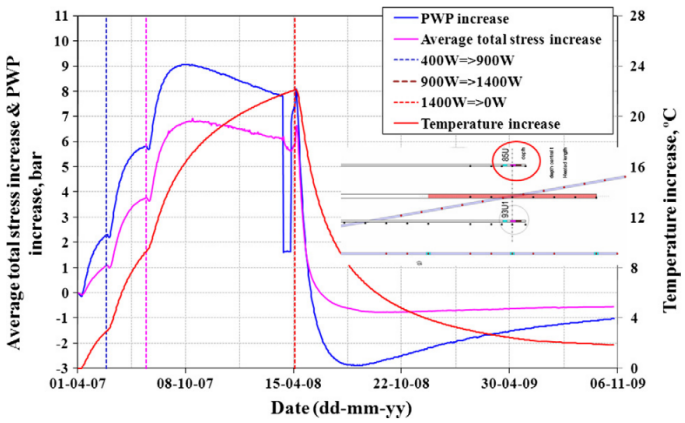

Figure 54. Summary of the increases of average total stress, pore water pressure, and temperature in borehole AT85E, measured close to the mid-plane of the heater ((Chen et al. 2011).

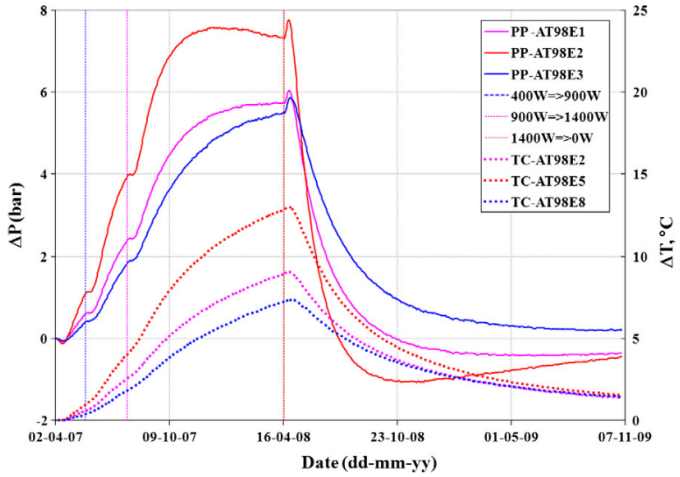

Figure 55. Summary of the increase of pore water pressure and temperature in borehole AT98E ((Chen et al. 2011).

Thermal anisotropy

Borehole AT98E lies in the same horizontal plane as the heater, while borehole AT97E is inclined and passes below the heater. Close to the symmetry plane perpendicular to the heater axis, sensor AT98E5 lies at a horizontal distance of 2.68 m from the centre of the heater while sensor AT97E6 is located 2.75 m from the heater in the vertical direction, so they are located in different directions and with almost the same distance to the heater. Figure 56 shows a maximum temperature difference of 6°C between both sensors. The temperature increase in AT98E5 is about twice the increase observed in AT97E6. Such a difference is a clear evidence of the anisotropic thermal conductivity in the Boom clay.

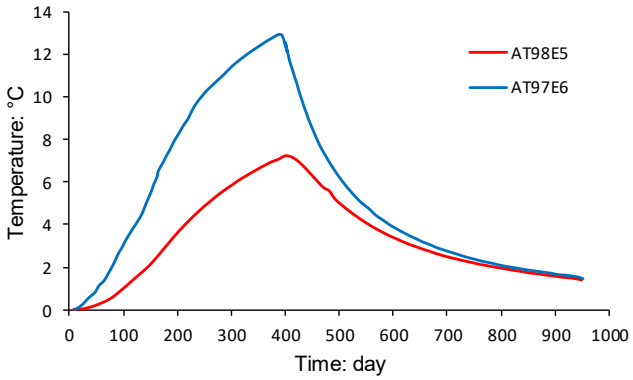

Figure 56. Both measured and computed temperature increase at locations TC-AT98E5 and TC-AT97E6 (modified after (Chen et al. 2011).

The ATLAS III small scale in situ test has been developed to assess the hydro-mechanical effects on the Boom clay of a significant temperature gradient. The test was provided a large set of good quality and well documented data on temperature, pore pressure and total stress, and many interesting observations have been made. The extended measurements of the temperature field provide clear evidence of thermal anisotropy. The test had a simple geometry, depends essentially on a single material (Boom clay), and has well defined boundary conditions, which facilitates the comparison between measurement and numerical modelling.

7.2 Mont Terri rock laboratory

7.2.1 General

The Mont Terri rock laboratory (Thury and Bossart 1999) is located in Northwestern Switzerland near the town of St. Ursanne and has been excavated from an existing reconnaissance/evacuation gallery of a motorway tunnel. The laboratory is situated in an asymmetrical anticline formed during the folding of the Jura mountains as shown in the geological cross- section of Figure 57. It is excavated in Opalinus clay a strongly bedded claystone. Because of tectonic activity, the rock strata dip at an angle of 45° to the southeast. Intense bedding is observed throughout, bedding thickness is generally on the centimetre scale. Opalinus clay at the laboratory site has an overall thickness of around 160 m and the present overburden is 250 m approximately. Three facies are distinguished in the Opalinus clay layer: shaly, sandy and carbonate-rich; most of the laboratory is contained in the shaly facies, the most clayey one.

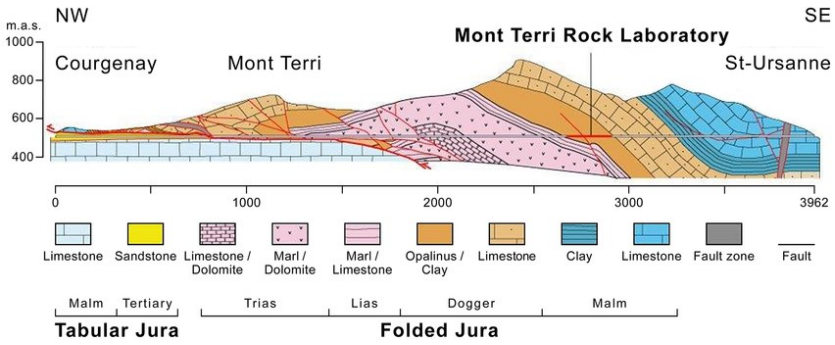

Figure 57. Geological cross-section of the Mont Terri rock laboratory (Freivogel and Huggenberger 2003).

7.2.2 Response to underground excavations

A mine-by test (ED-B test) was carried out in the Mont Terri rock laboratory (Corkum and Martin 2007) taking advantage of the completion of the central part of the New Gallery (Figure 58). The drift is circular, 3.6 m-diameter and the test section is 35 m long at a depth of approximately 270 m. The tunnel was excavated full face with a road header progressing from the NW to towards the SE. A 200 mm-thick steel fibre-reinforced shotcrete, installed about 7m behind the front, was used as support. Most of the instrumentation was installed before the start of the exaction from Niches OP and BF excavated in the reconnaissance gallery. The distance between the two galleries is 24 m approximately.

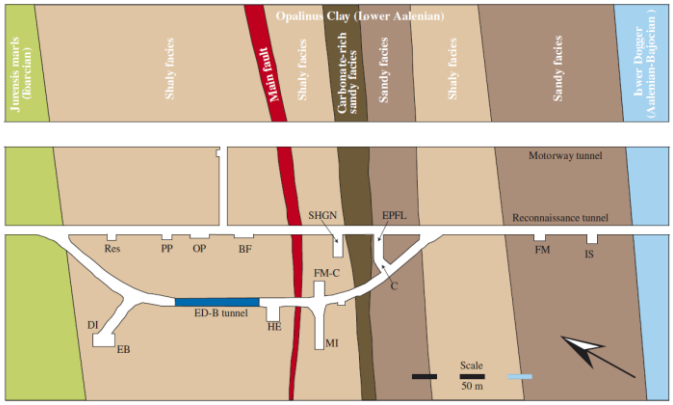

Figure 58. Location of the mine-by test ED-B (Corkum and Martin 2007).

Again, the most relevant information obtained in the mine-by test refers to the development of pore pressures. Figure 59 shows the evolution of pore pressure during the excavation of the New Gallery. A familiar pattern emerges. Long before the arrival of the excavation front, pore pressures rise steadily as excavation proceeds. When the excavation front crosses the measuring section, there is a sharp increase due to the anisotropy of in situ stresses and material stiffness. Afterwards the pore pressure reduces; in the case of the sensor located 50 cm from the tunnel wall, atmospheric pore pressure is measured suggesting a direct connection with the tunnel opening.

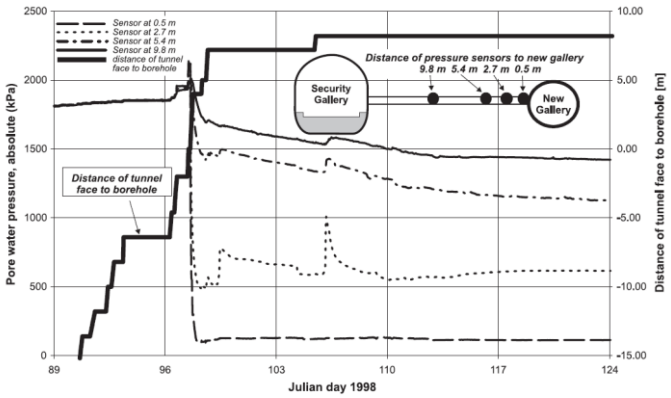

Figure 59. Pore pressure evolution during the excavation of the New Gallery measured in sensors at different distances from the tunnel wall (Bossart et al. 2004).

The pattern of fractures generated in the excavations in the Mont Terri laboratory is quite specific and it is summarised in Figure 60. Laterally, a series of extensional fractures roughly parallel to the tunnel wall generally appear. In contrast, fractures in roof and floor are more related to the deformation of the bedding that is especially intense in this material. Indeed, failure mechanisms clearly controlled by the deformation, detachment and buckling of bedding layers have been observed a number of times. In fact, the same fracture and failure patterns have been found in hollow cylinder tests performed in the laboratory.

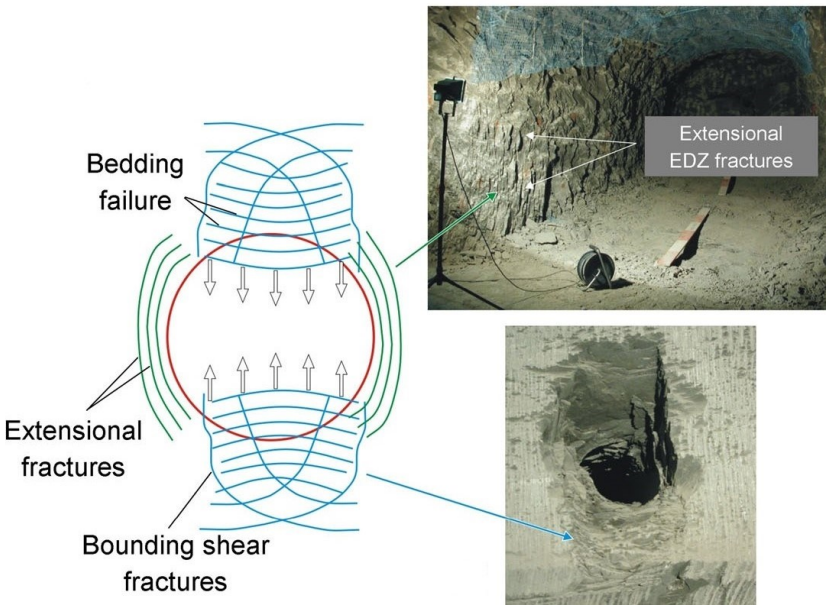

Figure 60. Fracture patterns as observed in the Mont Terri rock laboratory (Blümling et al. 2007a).

The extent and characteristics of the fractured zone in stable openings away from failure has been studied intensively (Bossart et al. 2004); (Bossart et al. 2002). A variety of observation methods have been used. The conceptual model shown in Figure 61 has been derived. The excavation damaged zone comprises two subzones, the inner one where factures are interconnected and an outer one in which

fractures are isolated and less frequent. In the inner zone oxidation phenomena are observed and the hydraulic conductivity may increase up to 2-4 orders of magnitude. However, much of this loss of tightness is subsequently recovered as Opalinus clay has a significant capacity for self-sealing once it be- comes saturated (Bossart et al. 2004).

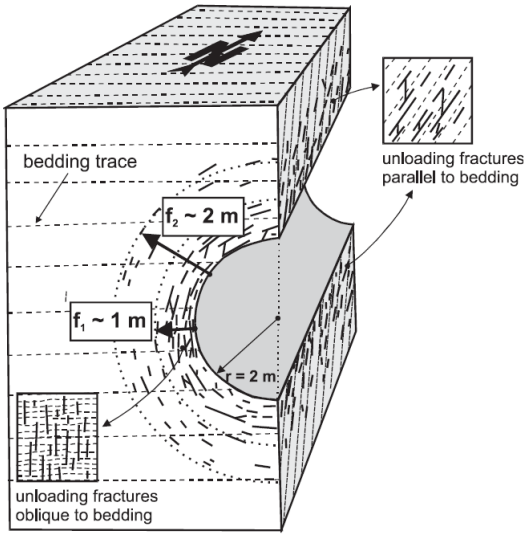

Figure 61. Conceptual model of the excavation damaged zone. f1 indicates the extent of the inner zone and f2 the boundary of the outer zone (Bossart et al. 2004).

7.2.3 HE-D insitu heating test in Opalinus Clay

The three Mont Terri rock laboratory in situ heating tests considered are: HE-B, HE-D and HE-E. They encompass a variety of features concerning the geometrical setting, presence and type of backfill, maximum temperature and heating duration. Figure 62 shows their location in the Mont Terri rock laboratory. Opalinus Clay is intensively bedded; the closely-spaced bedding planes dip at an angle of approximately 45° at the laboratory location. All tests have been performed in the shaly facies of Opalinus Clay.

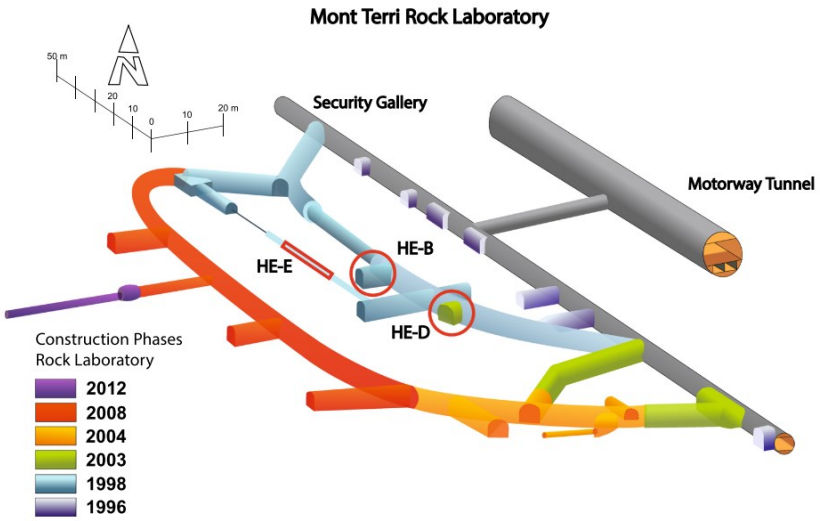

Figure 62. Location of the main heating tests performed in the Mont Terri rock laboratory (Gens et al. 2017).

Figure 63 shows a top view of the HE-D test area. A horizontal test layout was chosen in order to have a largely uniform lithology. Temperatures were measured along two boreholes drilled (D1 and D2) from the niche HE-D. However, perhaps the most relevant observations were those combining measurements of temperatures and pore pressures at the same point in order to relate directly the two variables. This was achieved in borehole D3 and in a series of small diameter boreholes (D7 to D17) drilled from the MI niche. The pore pressure measurements of sensors located below the main borehole were quite successful, but the pore pressure probes located above the main borehole exhibited a rather slow response attributed to difficulties encountered in de-airing the sensor area. Finally, sliding micrometre tubing was installed in boreholes D4 and D5 to measure incremental deformations at 1 m intervals.

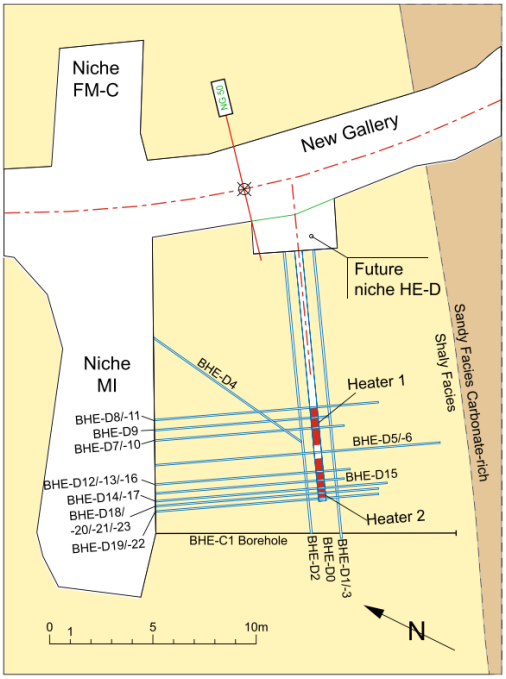

Figure 63. Schematic layout of the in situ test HE-D (Gens et al. 2017).

Approximately 1 month after installation and pressurization, the heaters were switched on with a total power of 650 W (325 W per heater). The heaters were then left under constant power during 90 days. Afterwards the power was increased threefold, to 1950 W (975 W per heater) and maintained at that level for 248 days more. The heating period lasted form March 2004 to February 2005. At the end of the second heating stage, the heaters were switched off and the clay was allowed to cool down. Temperatures, pore pressures and deformations were measured throughout.

Thermal results

Examples of the observations obtained are shown in Figure 64 in terms of evolution of at different distances from the heaters.

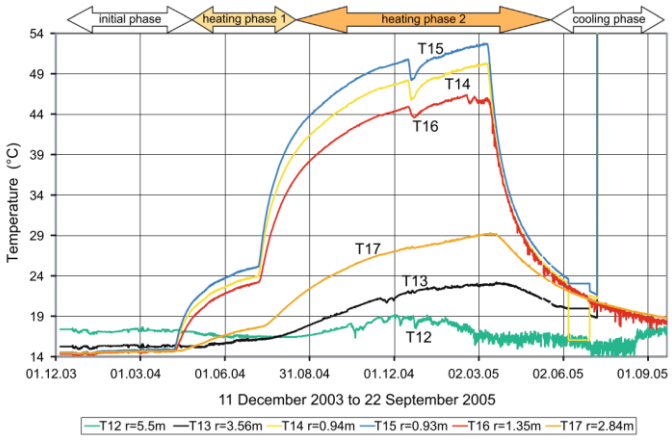

Figure 64. Evolution of temperature at different distances of the heater axis. Experiment HE-D (Gens et al. 2017).

pore pressures

In Opalinus Clay, the main hydraulic phenomenon associated with thermal effects is the generation of pore pressure due to changes of temperature. When Opalinus Clay (and other argillaceous rocks) is subjected to a temperature increase, the pore pressure will also increase due to the fact that the thermal expansion of the water is larger than that of the porous skeleton itself. The low permeability of Opalinus Clay ensures that the resulting excess pore pressure does not dissipate rapidly.

Interesting insights can be obtained examining a typical evolution of temperature and pore pressure as presented in Fig. 16. It was recorded in borehole D3 (Figure 65) with the sensors located 1.1 m away from the axis of the heater in the direction of the bedding planes. It can be observed that pore pressures react immediately to heating, exhibiting a very strong response. Increments of 2.25 MPa are measured at this particular location; this is a magnitude similar to the estimated minor principal stress in the area. It is also interesting to note that the evolutions of temperature and pore pressures do not coincide. Pore pressure reaches a maximum at a particular time and then it decreases in spite of the fact that temperature continues to rise. This is the result of the interplay between the generation of pore pressures due to thermal action and the dissipation of pore pressures due to consolidation. At this particular location, dissipation by liquid-flow overcomes the temperature increase effects in the later stages of the experiment.

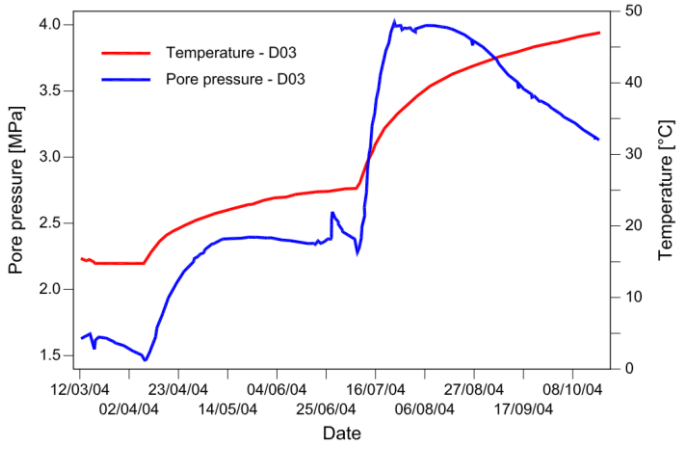

Figure 65. Evolution of temperature and pore pressure in borehole D3 during the HE-D test (Gens et al. 2017).

Thermally induced mechanical effects

Mechanical effects result from the joint action of temperature changes and pore pressure generation and dissipation. They can be perceived from the measurements of relative displacements in boreholes D4 and D5 performed using a sliding micrometer (Figure 66). Borehole D5 was drilled at a direction approximately normal to the main borehole containing the heaters; the deformations measured at

various times are plotted in Fig. 21. It can be observed that in the region around the heaters, extension deformations occur, but they become compressive strains at locations further away from the heater. The volume increases of the clay close to the heater, driven by thermal expansion, produces compression in the outer zones.

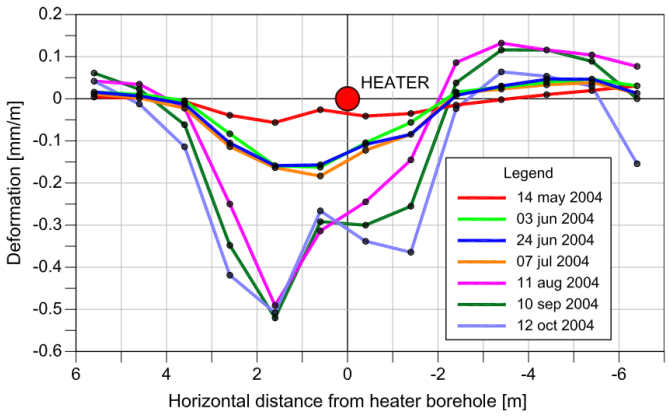

Figure 66 Distributions of deformation measured at different times in borehole D5, drilled approximately perpendicular to the main borehole. HE-D test (Gens et al. 2017).

7.3 Meuse/Haute-Marne underground research laboratory

7.3.1 General

The Meuse/Haute-Marne underground research laboratory is located in Eastern France near the town of Bure (Delay et al. 2007). It consists of surface facilities, two shafts (an access shaft and a ventilation shaft) and a network of drifts, constructed at a depth of 490m, in which the scientific experiments are carried out. It has been excavated in the Callovo-Oxfordian (COx) claystone, an indurated hard clay that forms part of the Jurassic formation of the Parisian Basin. A geological profile is shown in Figure 67. The target horizon is 130 m thick, between elevations 420 and 550 below the surface. Very little tectonic activity has taken place since the mudstone deposition and the bedding planes are practically horizontal throughout.

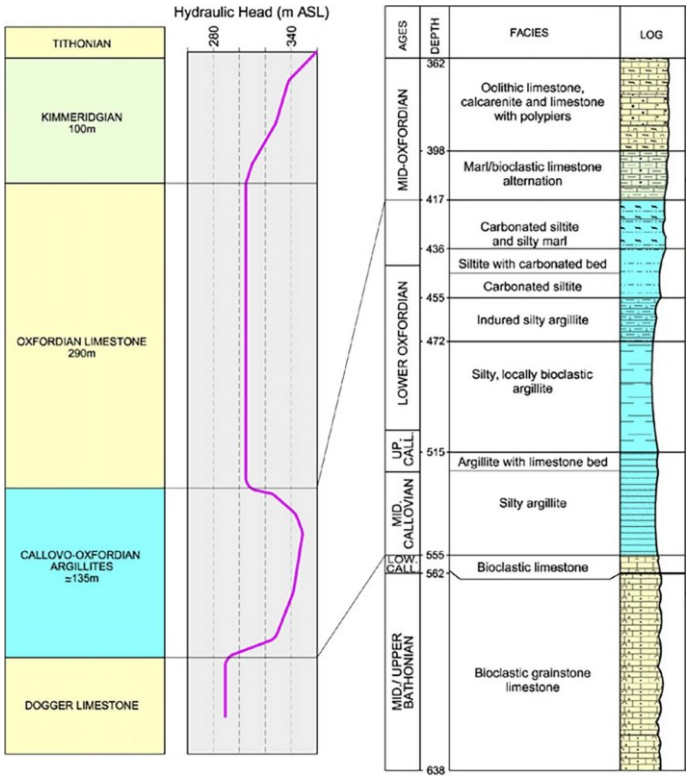

Figure 67. Geological profile at the Meuse/Haute-Marne underground research laboratory (Delay et al. 2007).

7.3.2 Shaft excavation

A mine-by test experiment (REP) was performed during the sinking of the main shaft of the Meuse/Haute-Marne underground laboratory (Figure 68). The shaft had an average diameter of 6.1 m and was excavated by drill-and-blast method. Prior to reaching the test section, excavation was stopped (at elevation -445 m from the surface) and a 40-m long observation niche was constructed. From this niche a series of instrumentation boreholes were drilled. Once observations had stabilized, shaft excavation was resumed. The experiment section was located between elevations -460 and -476 with special attention to the central zone. As discussed earlier, the clay fabric is likely to be isotropic on the horizontal planes. However, the horizontal in situ stresses are not isotropic; there is a major horizontal principal stress (σ_H) oriented in the NW-SE direction estimated to be around 15 MPa. The minor horizontal principal stress (σ_h) is oriented in the NE-SW direction and has a value of 12 MPa, approximately similar to overburden. Initial pore pressure is about 4.2 MPa but it is affected somewhat by drainage towards the shaft and the niche.

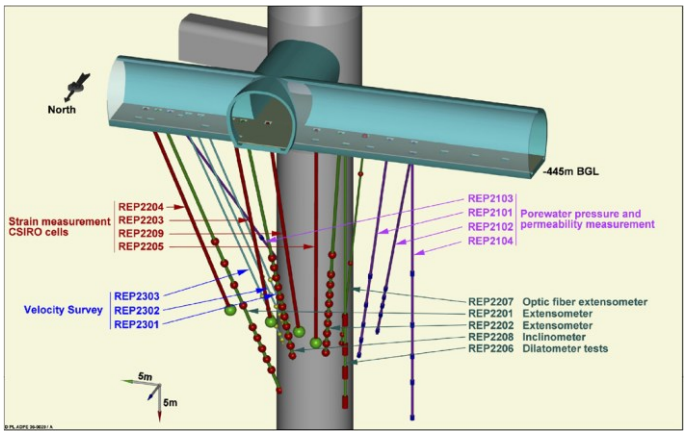

Figure 68. Layout of the REP experiment showing the main shaft, the observation niche and the instrumentation boreholes.

Figure 69 shows the axial displacements in borehole 2202, located in the zone of the major principal horizontal stress, σ_H . It can observe that compression is measured ahead of the excavation but when the excavation front passes a particular measurement location, displacements change to extension. In any case, movements are small, less than 3 mm. In a similar borehole, located in the area of the minor principal horizontal stress, displacements are even smaller.

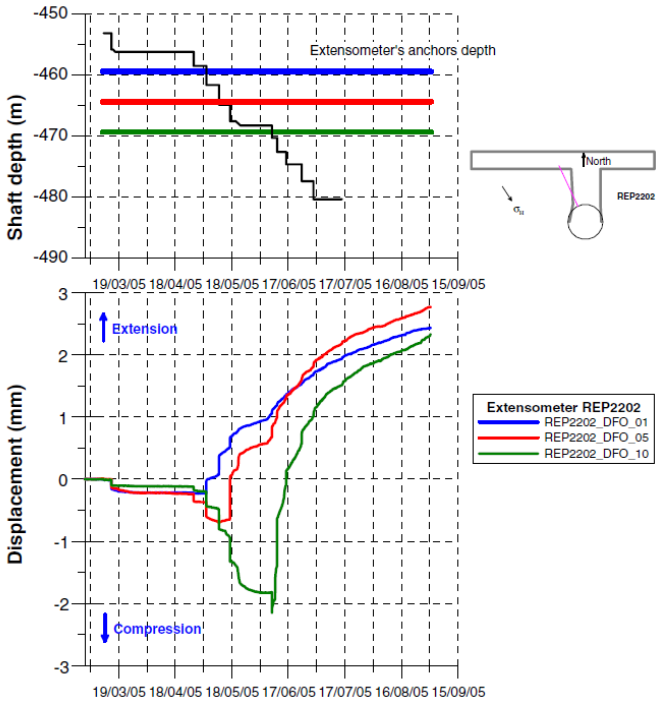

Figure 69. Axial displacements in borehole 2202 (Delay et al. 2007).

More interesting is the evolution of pore pressures as excavation progresses. In Figure 70a, the pore pressures measured in a borehole placed in the zone of the major principal horizontal stress are shown. It can be observed that there is a reduction of pore pressures even before the excavation reaches the measuring point; the reduction becomes much larger as excavation progresses past due to unloading.

In contrast, the pore water measured in the zone of the minor principal stresses (Figure 70b) exhibits an increase prior to the arrival of the excavation front. The different behaviour of the pore pressures in the two zones corresponds precisely with what is predicted if the anisotropy of principal stresses is considered. As the material is presumed basically isotropic in a horizontal plane, this contrast in rock response can be safely attributed to the anisotropy of in-situ stresses. Naturally, once the excavation has progressed beyond the measuring points the two boreholes behave similarly, showing a large reduction in pressures. However, the final pore pressure values still show some differences for points located at similar distances from the shaft wall, measurements in the minor principal stress zone giving larger values.

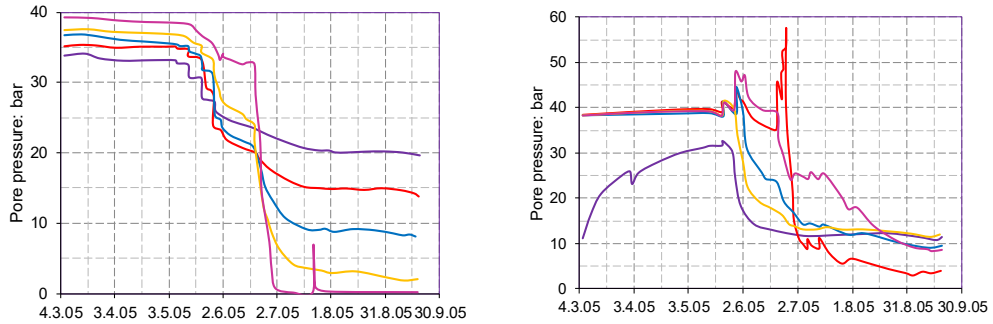

(a) (b)

Figure 70. Pore water pressure measured in (a) borehole 2101 located in the zone of the major principal stress (b) borehole 2102 located in the zone of the minor principal stress (modified from (Armand et al. 2005).

Rock permeabilities were measured before and after excavation. Before excavation, permeability ranged from 9×10^{-14} m/s to 7×10^{-13} m/s. It was found that close to the shaft wall permeability had increased up to an order of magnitude in spite of the small displacements observed. Figure 71 shows the distribution of permeability increase with distance to the shaft wall, the zone extends to 4-5 m, less than one shaft diameter. Measurements continued for 2.5 years after the end of excavation, but permeability remained largely unchanged over this period.

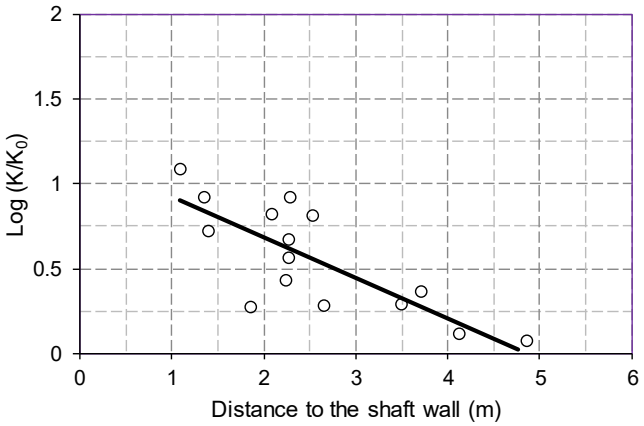

Figure 71. Distribution of permeability after excavation compared to the permeability values before excavation (modified from (Armand et al. 2005).

7.3.3 Excavations of horizontal drifts

Field observations of the effects of the excavation of the horizontal drifts forming the main body of the laboratory have also yielded significant information. Again, only a very limited selection of results is presented here. The tunnels network is located at the main level of the laboratory (depth: 490 m). It can be noted that, on purpose, the drifts are aligned with the principal stress directions. The tunnels have a horseshoe shape and a section of 17m^2 and have been normally excavated with pneumatic hammer. The support generally consists of steel sets, 2.4 m-long rock bolts (about 1 bolt / m2) and shotcrete. Convergence sections have been installed very close to the excavation face.

Figure 72 shows vertical and horizontal convergences measured in a drift with the same orientation as the minor horizontal principal stress whereas Figure 73 presents the same type of data for a drift aligned with the major horizontal principal stress. At this depth, deformations due to excavation are significantly larger than at the level of the REP experiment indicating a weaker, less stiff material. The observations also demonstrate very clearly the effect of the insitu stresses. In the case of drifts aligned with the minor principal stress (Figure 72), the stress state is anisotropic, and the vertical convergence is significantly larger than the horizontal one. When the drift is aligned with the major principal stress, vertical and horizontal convergences are very similar, consistent with a nearly isotropic stress state, as the minor horizontal principal stress and the vertical overburden stress have very similar magnitudes.

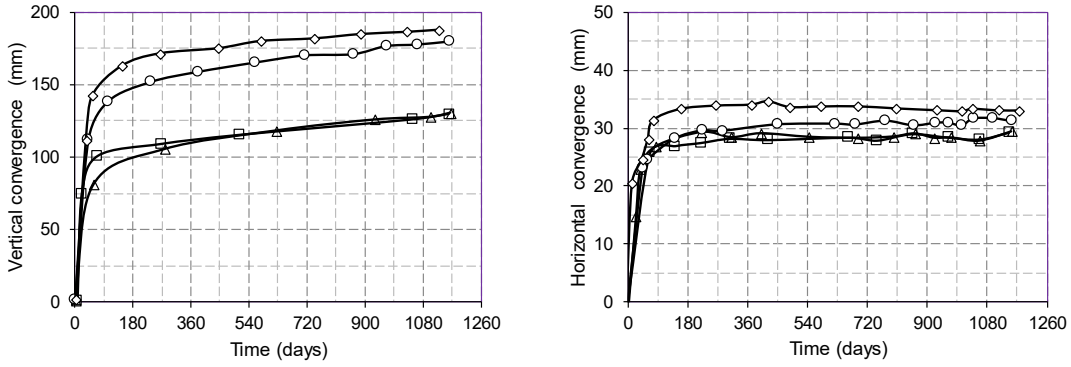

(a) (b)

Figure 72. Observed horizontal and vertical convergence in a drift aligned with the minor horizontal principal stress (modified from (Armand et al. 2005).

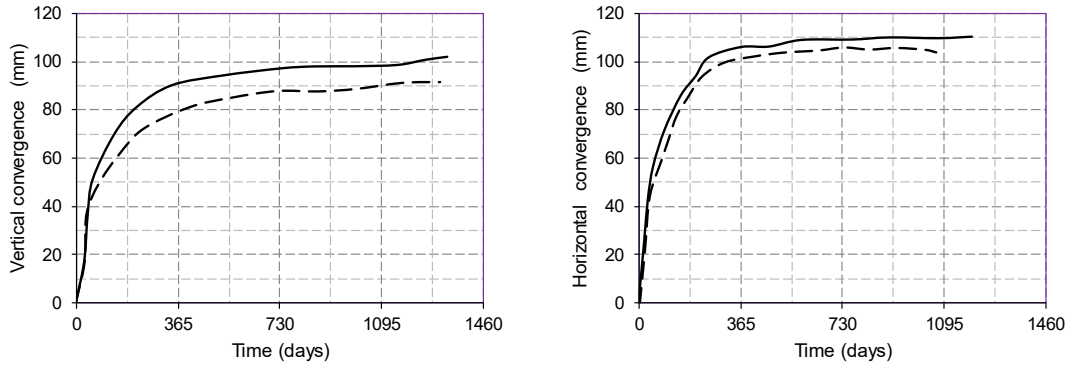

(a) (b)

Figure 73. Observed horizontal and vertical convergence in a drift aligned with the major horizontal principal stress (modified from (Armand et al. 2005).

Moreover, convergences have been measured over a period of over three years to characterize the evolution of tunnel deformations over time (Armand et al., 2005). Observations revealed that there may be behaviour differences in the short term after excavation but, for longer periods, time-dependent deformations settle down to a logarithmic relationship with time. Similar creep rates are observed in the two cases. It may be recalled that a logarithmic long-term development of deformations was also observed in tunnel excavated in Boom clay, a similar behaviour for quite different materials.

Indeed, a number of fracture systems were observed during the excavation of the tunnels. The most characteristic one is the herringbone fractures that form about 1 diameter (4 m) ahead of the excavation front (Figure 74). The system of fractures follows the same herringbone pattern as observed in the horizontal drifts at the HADES underground laboratory in Mol in spite of the very large differences in the type of host material; in one case it is a weak plastic soil-like clay and in the other case it is a strong indurated argillite. It is therefore interesting to note that materials sitting at opposite ends of the spectrum of hard soils-weak rocks exhibit the same pattern of fracturing. In the Meuse/Haute-Marne laboratory,

this system of fractures is generally somewhat more pronounced in the drifts aligned with the major horizontal principal stress direction.

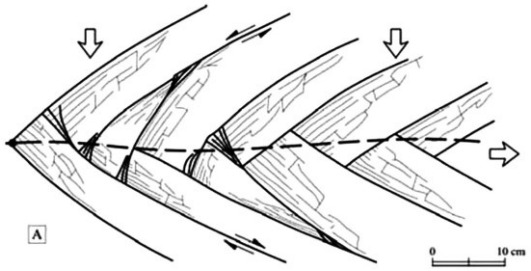

Figure 74. Scheme of the herringbone fractures caused by drift excavation (Armand et al., 2005)

In addition, vertical and oblique fractures are created after the herringbone fractures. The final size of the fractured zone depends on the orientation of the drift as illustrated in Figure 75. As indicated above, the presence of the fracture zones influences very strongly the pattern and distribution of displacements; indeed, a large proportion of the displacements is localised in the fractured zone.

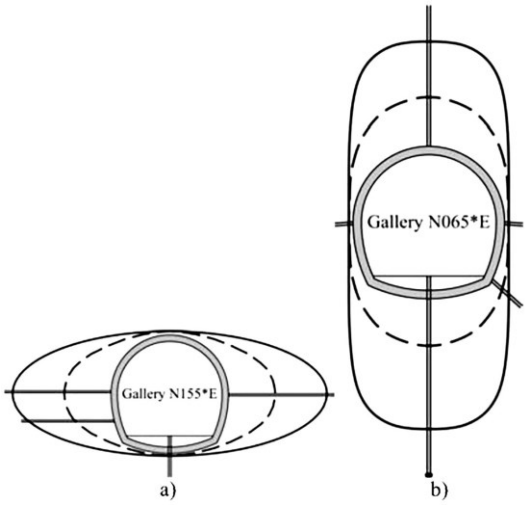

Figure 75. Extension of the fractured zone (Armand et al., 2005). a) Drifts parallel to the major principal horizontal stress, b) Drifts parallel to the minor principal horizontal stress.

7.3.4 TER in situ heating test in COx claystone

The TER experiment has been dedicated to observe and investigate the response of the Callovo-Oxfordian claystone subjected to heating and cooling and to characterize thermal and THM properties of the rock. It consists of heating the clay rock during a long enough period of time in order that a significant change can occur and be measured by different sensors. The TER experiment has been conducted in the Callovo-oxfordian claystone at a depth of 490 m in the M/HM underground research laboratory. It consists of a heater borehole (TER1101) and nine observation boreholes (Figure 76). The heater borehole is drilled horizontally form the TER ‘‘Carrure’’ to the depth of 10 m in the direction of

maximum horizontal stress r_H (in the direction of N65°E). In addition, TER1101 is equipped with a heating element and temperature sensors in order to control the homogeneity of temperature field within the probe (Figure 77). To monitor the impact of heating cycles on the rock, about 50 sensors are implanted in the surrounding observation boreholes.

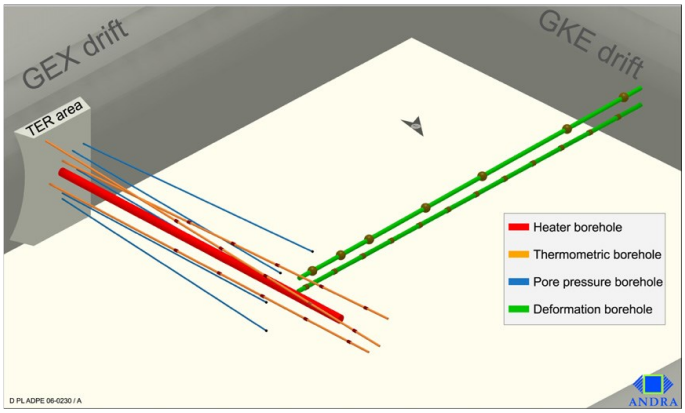

Figure 76. View of the TER experiment in the Meuse Haute Marne underground research laboratory (Bian et al. 2012).

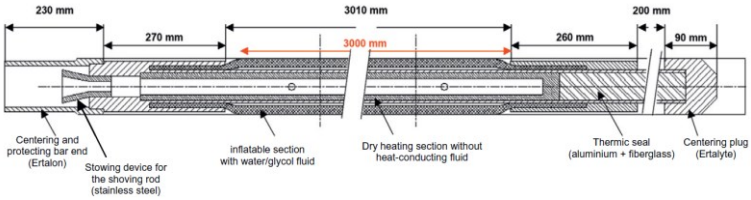

Figure 77. Detailed layout of TER hater device (Bian et al. 2012).

Thermal results

Figure 78 illustrates the measurement results of different sensors located on the heater surface during heating phases and cooling phase. The so-called ‘‘cooling phase’’ is relative to the period when the injected power is switched off. At the beginning of each heating phase, a rapid increase of temperature is observed. Then the temperature stabilizes progressively with the applied constant heater power. Finally, during the cooling phase, due to the switch off of heating power, the temperature drops sharply and tends to recover its initial value. Furthermore, it is noted that at the end of first heating phase, an increase of temperature up to 24°Cis obtained in the heater while a greater variation of 58°C is observed during the second heating phase. This difference is relative to the fact that a greater heating power is applied during the second heating phase.

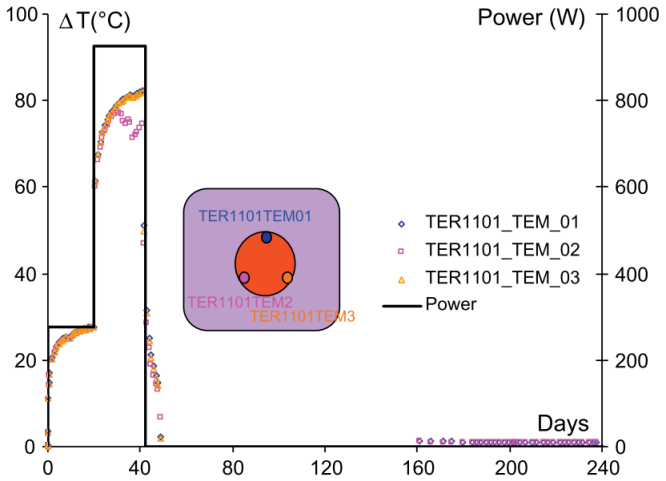

Figure 78. Variation of temperature at the surface of heating borehole TER1101 (Bian et al. 2012).

The comparison of measurement data shows that the temperature evolution depends strongly on the sensor location. distance from the heater and location direction. Two captures (TER1401TEM01 and TER1402TEM01), located in the same direction with respect to the bedding plan, are compared first. It is noted that the bigger temperature is obtained at TER1401TEM01which is close to the heater element with respect to TER1402TEM01 (Figure 79).

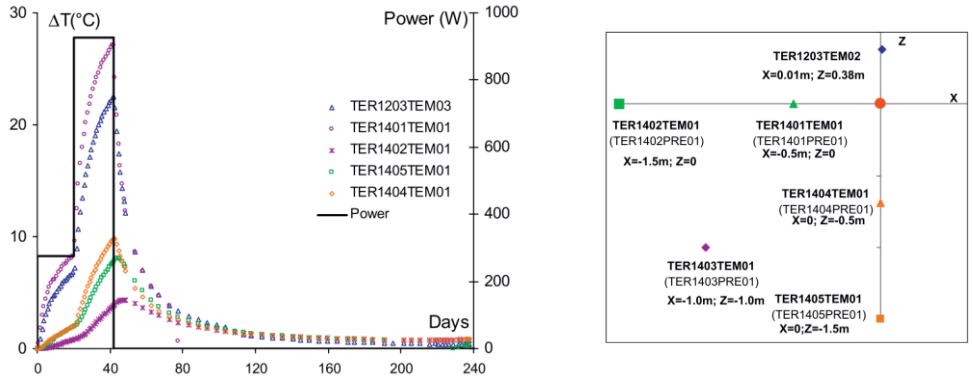

(a) (b)

Figure 79. Variation of temperature in the observation boreholes (Bian et al. 2012).

In conclusion, the maximum temperature and the temperature's increase speed decreases with the distance from the heater. Furthermore, it's interesting to note that, during two heating phases, the temperature increases more strongly in the bedding plan direction (TER1402TEM01). On the other hand, after switching off the heating power, at the measured points located far from the heater, the temperature continues to rise during 5 days in the direction perpendicular to the bedding (TER1405TEM01) while in the direction parallel to the bedding (TER1402TEM01), a short period (≈ 3

days) of temperature increase is observed. However, these experimental results confirm the anisotropy of thermal properties.

pore pressures

The evolution of water pore pressure at different measured points is illustrated in Figure 80 the nearest measure point TER1401PRE01 to the heater is studied (Figure 80). The first heating period creates an important pressure increase up to 1 MPa. The second heating phase induces a rapid augmentation of water pore pressure up to 3 MPa. This overpressure is essentially relative to the difference of thermal expansion between solid matrix and water. Moreover, the very low permeability of claystones cannot provide adequate drainage to dissipate this pressure. After that, with the stabilization of temperature, the generated overpressure is dissipated by advection of water according to the Darcy's law. Consequently, after reaching the maximum level, the pore pressure drops down slowly even when the temperature still increases. In the cooling phase, the contrary phenomenon is observed when the heater power stops working. a sudden drop of pressure is perceived due to the condensation and contraction of pore water. At some measured points (TER1401/1404PRE01), the pressure is significantly lower than its initial value. The under pressure may be relative to the following phenomena: thermal consolidation, microcrack network and permeability. However, hydraulic equilibrium process is very slow due to low permeability of studied material. As the duration of TER experiment is very short, one cannot see the recovery of initial pressure at the end of the experiment.

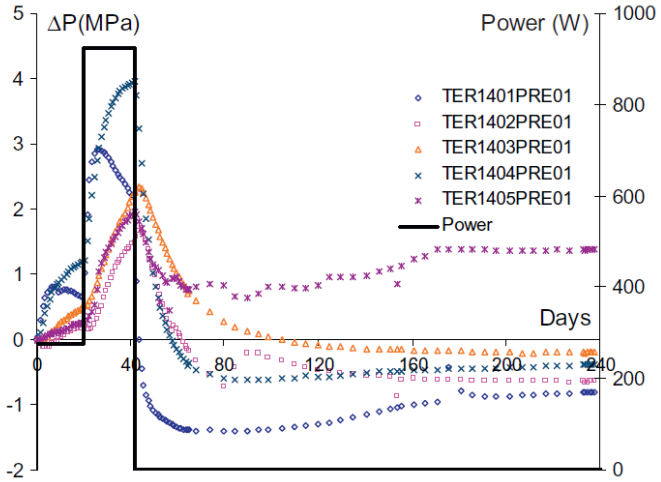

Figure 80. Variation of pore pressure in the observation boreholes (Bian et al. 2012).

Displacement

The displacement is measured in borehole TER1301 which is perpendicular to the heating borehole TER1101. Figure 81 presents the radial deformation evolution at different points in borehole TER1302.

The location of these points is illustrated in Figure 82. For all sensors, an important expansion is observed. This phenomenon can be detected clearly at the sensors in the near field. Due to the start of heating, the sensors are subjected to a phase of dilation and the intervals between the sensors adjoins exhibit an evident expansion of interval due to the expansion of the rock close to the heater. A further rapid increase of deformation can be recognized at the beginning of the second heating phase. During the cooling phase, the rocks contacts gradually and recover progressively the nature state of rock. However, in the far-field, the claystone formation works essentially in compression due to the increasing rock pressure created by the expansion of rock near the heater. Generally, the duration of phase and value of maximum dilation are location dependent.

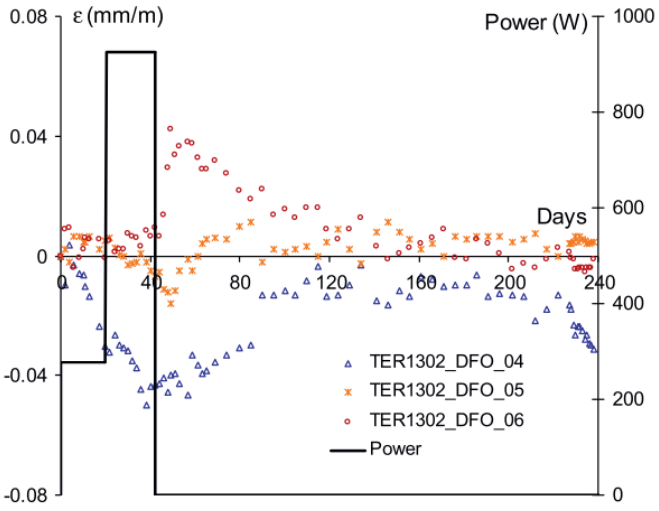

Figure 81. Variation of strain in the observation TER1302 (Bian et al. 2012).

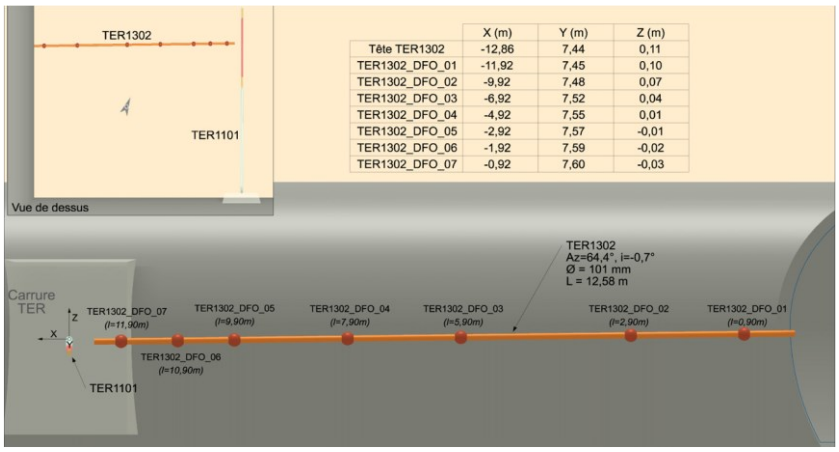

	X (m)	Y (m)	Z (m)
Tête TER1302	-12,86	7,44	0,11
TER1302_DFO_01	-11,92	7,45	0,10
TER1302_DFO_02	-9,92	7,48	0,07
TER1302_DFO_03	-6,92	7,52	0,04
TER1302_DFO_04	-4,92	7,55	0,01
TER1302_DFO_05	-2,92	7,57	-0,01
TER1302_DFO_06	-1,92	7,59	-0,02
TER1302_DFO_07	-0,92	7,60	-0,03

Figure 82. Position of strain sensors in the observation borehole TER1302 (Bian et al. 2012).

7.3.5 ALC1604 in situ heating test in COx claystone

The ALC1604 is an in situ heating test conducted in the Meuse/Haute-Marne (MHM) Underground Research Laboratory (URL) at the main 490m deep-level where the host rock is Callovo-Oxfordian

(COx) claystone (Tourchi et al. 2019a, b, c, 2020, 2021a, b, 2022a, b, 2023; Tourchi 2020; Bumbieler et al. 2021). The experiment aims to reproduce a standard disposal cell for the nuclear waste. It consists of a horizontal microtunnel of approximately 25m in length and 0.7m in diameter. It comprises a cell body, approximately 19m long, for HLW disposal and a 6m-long cell head section (Figure 83a). Both cell body and cell head sections incorporate a non-alloy steel sleeve called Casing and Insert, respectively (Figure 83b,c). The cell head is separated from the cell body by a metal radiation protection plug. The far end of the cell is closed off by a plate, also made of non-alloy steel. The diameter of the Casing is smaller than that of the Insert, and the Casing can slide through and retrievability of the waste is possible. Five heaters (H1-H5), each 3m long and 0.5m in diameter, have been installed contiguously in the body section, as indicated in Figure 83a. The ALC1604 cell microtunnel was excavated from the GAN gallery at an approximate rate of 0.3-0.5m/h; the excavation was completed in 7 days. As indicated in Figure 84, the cell is excavated in the direction of the major principal horizontal stress. This orientation has important implications for the hydro-mechanical response of the rock around the excavations. The THM behaviour of the COx claystone during the test has been monitored through nine boreholes drilled from the GAN gallery and the NRD niche (Figure 84) which comprises.

After a short two-week trial step at low power (33 W/m), the main heating phase was started with a constant 220 W/m power along the 15m occupied by the heater elements. This power was calculated so that a temperature of approximately 90°C would be reached in the casing after two years. After a heating period of about six years, a staged coiling phase is currently ongoing. Some of the most important features that makes this experiment different from previous ones are the large length of the heated zone, the presence of a steel sleeve around the heaters and the presence of a gap between the sleeve and the rock.

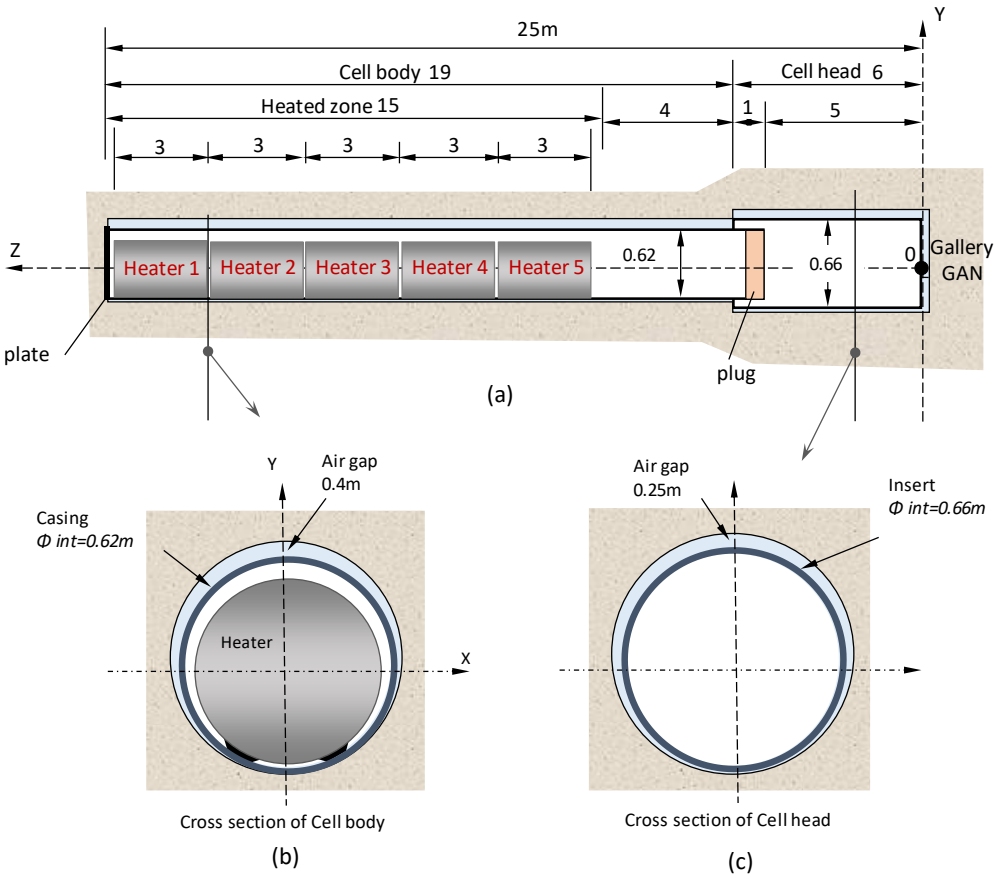

Figure 83. Layout of ALC1604 in situ test. a) Longitudinal view, b) cross sections of cell body, c) cross section of the cell head (Tourchi et al. 2021a).

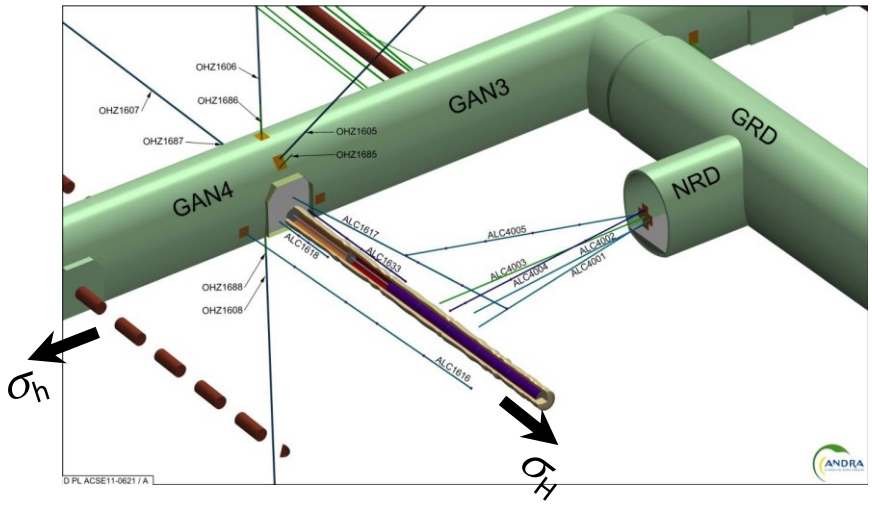

Figure 84. Schematic layout of ALC1604 in situ test. Locations of observation boreholes drilled from niche NRD and gallery GAN (Armand et al. 2017)

Pore pressure response to a thermal load

In COx claystone, the main hydraulic phenomenon associated with thermal effects is the generation of pore pressure due to changes of temperature. When COx claystone (and other argillaceous rocks) is subjected to a temperature increase, the pore pressure will also increase due to the fact that the thermal

expansion of the water is larger than that of the porous skeleton itself. The low permeability of COx claystone ensures that the resulting excess pore pressure does not dissipate rapidly. Nevertheless, the predictions of pore pressures evolution of the host rock (COx claystone) during excavation is of great importance. An important concern in the experiment is a good understanding of the pore pressure response due to excavation operations too.

As shown below, hydro-mechanical coupling, and particularly the configuration and extent of the EDZ, play a significant role in the pore pressure response. Figure 85 shows the variation with time of pore pressures, measured with capacitive sensors in section 17.5m deep (z=17.5m). The same graph is shown in Figure 85b, but with an emphasis on the first days. Water pressure raises at those locations as the excavation front approaches the measurement points up to a value of about 8 MPa, i.e. 3.3 MPa above the initial value. After that, pressure drops rapidly to 2MPa as soon as the excavation front passes the corresponding measuring points. However, in the zone above the tunnel crown, pressures decrease which is linked to the geometry of the damaged zone around the cell so that is more pronounced horizontally and the EDZ barely grows in this direction. In addition, permeability remains almost constant, by the implemented formulation. Figure 85 shows the evolution of pore pressures at the borehole ALC1617 that is located in the vertical plane of the tunnel (above the tunnel crown), 3.2 m away from the wall outside the EDZ. There is a slight increase of pore pressures as the excavation front approaches the measurement points, which was captured by the analysis.

Interesting insights can be obtained examining a typical evolution of temperature and pore pressure as presented in Figure 85. As expected, temperature increases during the thermal load trigger a significant upsurge of pore pressures. It is noticeable that the pore pressure responds to the temperature rise immediately, and the higher the temperature change, the stronger the response. The maximum pore pressure increase, in this case, is 7.5 MPa, a significant magnitude. It can also be observed that the pore pressure evolution does not precisely match that of temperature; at some time, the pore pressure stops rising, even though temperatures increase further. Dissipation by liquid flow overcomes the thermal effect. This phenomenon is especially noticeable at two points located in the bedding plane (ALC1616 and ALC4001). Although in the 140 days after the beginning of the heating, the overpressure peak was observed on the horizontal plane of the tunnel, this peak was not actually achieved in the vertical plane above the curve of the tunnel in over 800 days. The difference in time taken to reach the

overpressure peak in the vertical and horizontal planes can be explained by the rock's anisotropic thermal and hydraulic properties (Figure 85).

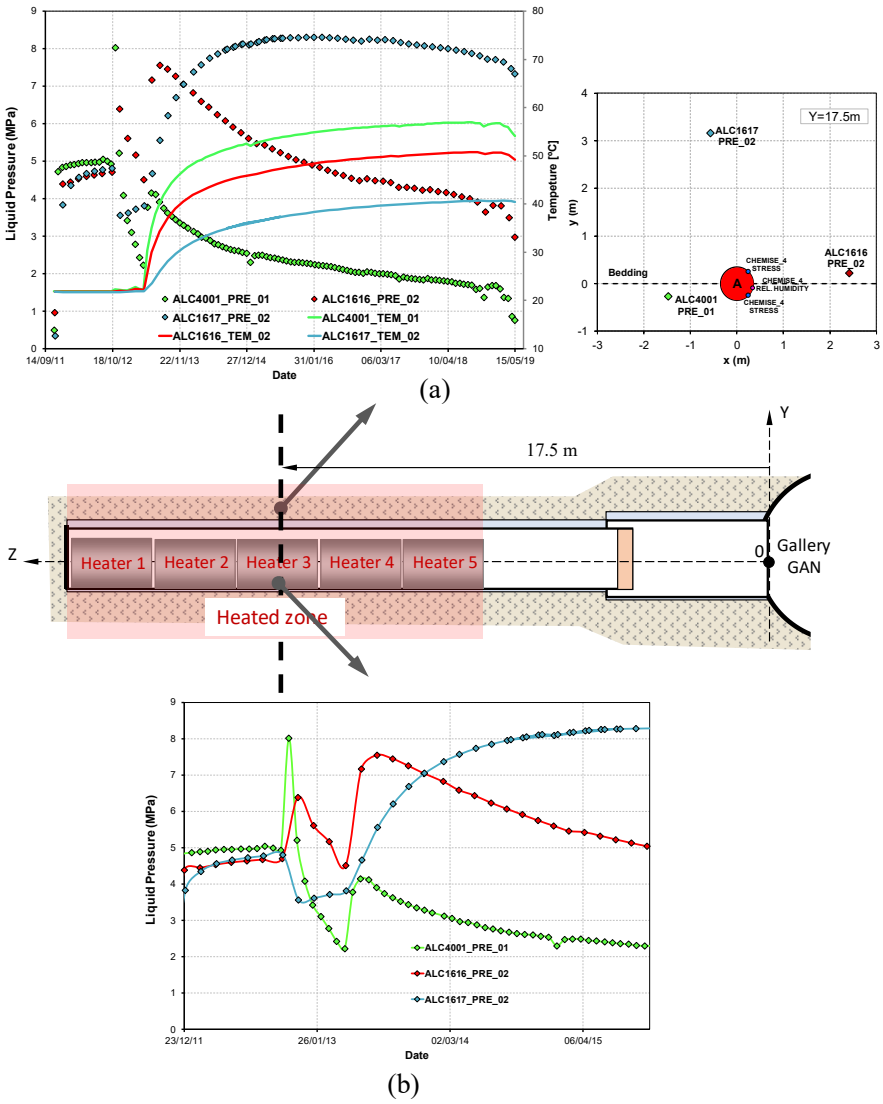

Figure 85. Pore pressure and temperature evolution measured in sensors ALC1616_PRE_02, ALC1617_PRE_02 and ALC4001_PRE_01 located on the same section as the heaters (17.5 m deep from the gallery) (Tourchi 2020).

Excavation damaged zone

Field observations have revealed that excavation operations induce damage and fracturing around the MHM URL galleries (Armand et al. 2014), creating an excavation damaged zone (EDZ), where significant changes in flow and transport properties take place (Tsang et al. 2005). Significant efforts have been made to simulate these experimental excavations (Seyedi and Gens 2017) and to gain insights into the design of the actual repository. The EDZ is identified as one of the critical issues affecting the long-term behaviour of the tunnel near-field (Blümling et al. 2007). The observed configuration of the EDZ depends on the orientation of the excavation with respect to the anisotropic in-

situ stress state. As stated above, the ALC1604 cell is parallel to the major horizontal stress σH and has a nearly isotropic stress state in the plane normal to the tunnel axis. Despite that, the EDZ extends further in the horizontal direction (Figure 86), suggesting strong anisotropic characteristics of the rock mass. Figure 86 shows the distribution of fractures around a similar micro-tunnel (ALC3005) excavated in COx claystone parallel to ALC1604 cell.

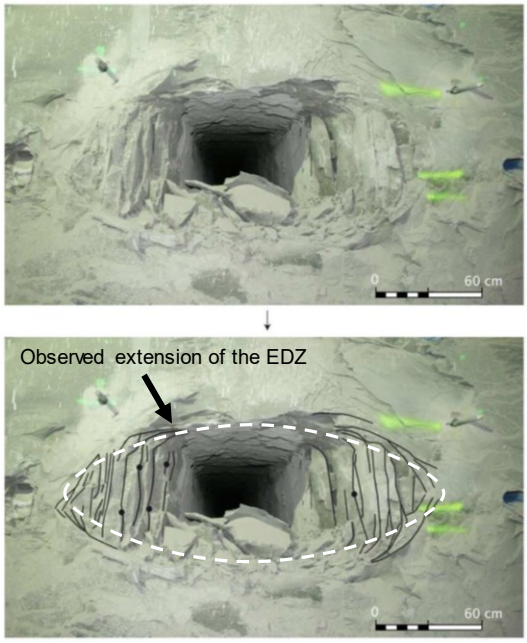

Figure 86. Extension of the damaged zone around an HLW cell parallel to major horizontal stress, showing the elliptical distribution of fractures around the opening, with a larger extension in the horizontal direction (Armand et al. 2014).

7.4 Summary of In-situ THM characterisation

The observations of the response of argillaceous rocks to deep underground excavations and in-situ heating tests in three different laboratories have provided important information concerning the thermo-hydro-mechanical behaviour of these materials.

It has been observed that the short-term hydromechanical response is strongly affected by stiffness and in situ stress anisotropy. It has also been noted that the hydromechanical response is detected at large distances from the excavation front and that the displacements close to the tunnel are mainly controlled by fractures. Indeed, development of very systematic fracture systems has been observed even for quite different materials and depths. Fracturing is mainly governed by stress redistribution and material strength, the method of excavation and support has only limited influence. In some cases (such as in the Opalinus clay at Mont Terri), fracturing is fully controlled by the presence of strong structural features. Finally, very long-term observations indicate that the delayed development of displacements (under contained conditions) follows closely a semi-log relationship with time.

The understanding of the behaviour of Opalinus Clay, Boom clay and COx claystone under thermal loading has been much advanced by the performance and study of a number of in situ heating tests: ATLAS III, HE-D, TER and ALC1604 experiments. Those tests cover a wide range of test layouts and conditions. In spite of this, the observed behaviour of those materials is quite similar in the three cases. Although the temperatures applied by the heaters are rather high, the temperature increases in the materials have been generally moderate because of the rapid thermal attenuation with distance. In spite of those modest increases, the generation of pore pressures has been very significant in all cases. The mechanism underlying the generation of pore pressures is well understood; it arises from the combination of the effects of differential rock/water thermal dilation and of pore pressure dissipation, controlled by rock permeability.

There is less information on thermal effects on mechanical variables. However, insitu tests indicated that deformations and displacements are small but more modest effects result from the coupling of hydraulic phenomena to mechanical behaviour. The dissipation of pore pressures induces additional displacements and strains that, due to the high argillaceous rock's stiffness, are smaller than thermally-induced deformations. In principle, mechanical damage could impact the hydraulic observations if a zone of higher permeability develops due to material damage. However, no such thermally induced damaged zone has been observed; in fact, hydraulic measurements carried out in a different test, revealed that heating might be beneficial with respect to rock damage as the intrinsic permeability reduced significantly after an increase of temperature. And finally, there is no perceptible coupling from hydraulic and mechanical phenomena to thermal behaviour. Practically all heat transport is by conduction and the thermal conductivity of the material does not change as deformations are small the material remains saturated throughout. In addition, mechanical energy dissipation is negligible in a non-isothermal case.

6. Concluding remarks

In spite of the large variability of composition, grading and geological history of argillaceous rocks, there exists a common core of geological processes and framework interpretations that provides a unified scheme for the understanding of the thermo-hydro-mechanical behaviour of these materials. Naturally, there are a number of exceptions to the general trends that require appropriate modifications of the conceptual frameworks. Indeed, a proper understanding of non-standard behaviour benefits from the existence of an established framework that can be used as benchmark.

A number of factors and features of hydromechanical behaviour have been reviewed including response under compressive loading, brittleness and progressive failure, anisotropy, permeability and hydromechanical coupling. It has been argued that anisotropy is a basic feature in these materials that must be considered in order to achieve a proper understanding of their engineering response in geotechnical problems. Permeability is always low in argillaceous materials and requires especial techniques for their determination. Permeability values are more closely related to pore size distribution than to overall porosity. The role, value and determination of Biot's coefficient in indurated materials still require considerable further research. Brittleness is a widespread feature of the strength of these materials in conventional geotechnical situations. Strength loss usually occurs in two stages corresponding basically to two mechanisms: loss of bonding and particle realignment. Brittleness leads to the occurrence of progressive failure and to difficulties in determining the operational strength in engineering problems. It is unlikely that a general rule to estimate operational strength can be found and, at present, numerical analysis appears as an increasingly effective way to tackle this type of problems.

Moreover, a number of factors and features of thermal behaviour have been reviewed including elastic response, volume change behaviour, strength, thermal pressurization, effect of temperature on permeability, self-sealing and long-term deformation at high temperatures. The effect of temperature increase on the elastic properties of the COx claystone is not yet clearly demonstrated. Further tests are needed to verify the existence of a potential critical temperature from which there is a significant decrease of elastic modulus for the COx claystone.

A thermo-plastic contraction is observed in normally consolidated clays and an elasto (expansion) plastic (contraction) response is observed in overconsolidated clays, depending on the OCR in Boom clay. Opalinus clay characterized by a linear thermo-elastic expansion that is typical of overconsolidated samples (Boom clay), followed by a plastic contraction. The peculiarities of the mechanical response of COx claystone to heating established in early experiments consist in a thermoplastic contraction, as opposed to the thermoelastic expansion of heavily overconsolidated Boon clay and Opalinus clay. Since these initial developments, additional experimental evidence has been added later, which have determined thermal expansion behaviour of the claystones by heating which was consistent with the in-situ observations during heating experiments. In spite of conflicting report of thermal dependency of

strength in argillaceous materials, experimental studies on Opalinus Clay, Boom clay and COx claystone evidence a more ductile response and smaller shear strengths at elevated temperatures.

Thermal pressurization was investigated in detail, showing a decrease in thermal pressurization coefficient with increased temperature. Undrained heating tests indeed appeared as quite complex with the combined effect of thermal pore pressure build- up with the corresponding effective stress decrease that mobilises some changes in compression-swelling coefficients with both temperature and stress changes. Good understanding of thermal pressurization is necessary to better assess the stability of galleries during the thermal phase.

Early experiments have revealed that hydraulic conductivity of argillaceous rocks increases with temperature. Later has been found a linear relationship between porosity and permeability which is independent of temperature. More recently, investigations showed that the permeability is not totally independent of temperature and slightly increases with temperature. Excellent self-sealing properties of the argillaceous materials have been reported in the literature. Experimental data showed that the self-sealing properties of the Boom Clay, the Opalinus clay and COx claystone are not affected by temperature elevation. The long-term deformation of the claystones is influenced by temperature, which was observed in creep tests under various thermal loads to high temperatures up to 90°C-110°C. Indeed, larger creep strains appear at elevated temperature.

Future studies

- Thermal conductivity as well as its anisotropy.
- variation in hydraulic conductivity with temperature.
- Variation of the thermal conductivity with temperature as well as the saturation.
- Modification of the stiffness (Young's modulus) and strength (internal friction angle and cohesion) induced by temperature.
- Temperature effects on the evolution of EDZ as well as on the sealing/healing process of EDZ.
- Possibility and pattern of the additional damage/failure induced by temperature : more laboratory tests under well controlled boundary conditions.
- Creep rates (viscosity related parameters) as well as its/their dependence on the temperature.

References

Akagi H, Komiya K (1995) Constant rate of strain consolidation properties of clayey soil at high temperature. In: Proc. Int. Symp. Compression and Consolidation of Clayey Soils--IS--Hiroshima. pp 3–8

Alkhalifah T (1997) Velocity analysis using nonhyperbolic moveout in transversely isotropic media. Geophysics 62:1839–1854

Amadei B (1996) Importance of anisotropy when estimating and measuring in situ stresses in rock. In: International Journal of Rock Mechanics and Mining Sciences & Geomechanics Abstracts. pp 293–325

Amorosi A, Rampello S (2007) An experimental investigation into the mechanical behaviour of a structured stiff clay. Géotechnique 57:153–166

Anandarajah A (2000) On influence of fabric anisotropy on the stress--strain behavior of clays. Comput Geotech 27:1–17

Andra (2005) Dossier 2005, Référentiel du site Meuse/Haute-Marne. Report CRPADS040022B. Châtenay-Malabry: ANDRA

Armand G, Bumbieler F, Conil N, et al (2017) Main outcomes from in situ thermo-hydro-mechanical experiments programme to demonstrate feasibility of radioactive high-level waste disposal in the Callovo-Oxfordian claystone. Journal of Rock Mechanics and Geotechnical Engineering 9:415–427. https://doi.org/10.1016/j.jrmge.2017.03.004

Armand G, Leveau F, Nussbaum C, et al (2014) Geometry and properties of the excavation-induced fractures at the meuse/haute-marne URL drifts. Rock Mech Rock Eng 47:21–41. https://doi.org/10.1007/s00603-012-0339-6

Armand G, Su K, Wileveau Y, Delay J (2005) Expérimentation REP Résultats des mesures après la phase de fonçage du puits entre les cotes-454 m et-480 m. ANDRA report DRPADPE050855A, Paris, France

Baldi G, Hueckel T, Pellegrini R (1988) Thermal volume changes of the mineral--water system in low-porosity clay soils. Canadian geotechnical journal 25:807–825

Banks DC, Strohm WE, De Angulo M, Lutton RJ (1975) Study of clay slopes along the Panama canal, Report No3, Engineering analyses of slides and strength properties of clay shales along the Gaillard Cut

Bass JD (1995) Elasticity of minerals, glasses, and melts. Mineral physics and crystallography: A handbook of physical constants 2:45–63

Bastiaens W, Bernier F (2006) 25 years of underground engineering in a plastic clay formation: the HADES underground research laboratory. In: Geotechnical aspects of underground construction in soft ground. Proceedings of the 5th international conference of TC 28 of the ISSMGE, the Netherlands, 15-17 june 2005. pp 795–801

Bastiaens W, Bernier F, Li XL (2006) An overview of long-term HM measurements around HADES URF. In: Proceedings of EUROCK. pp 9–12

Bauer C, Pouya A, Ghoreychi M (1997) Propriétés thermo-mécaniques des argilites silto-carbonatées de l'est. Andra report BRP0G3S97-001

Belanteur N, Tacherifet S, Pakzad M (1997) Etude des comportements mécanique, thermo-mécanique et hydro-mécanique des argiles gonflantes et non gonflantes fortement compactées. Revue française de géotechnique 31–50

Belmokhtar M, Delage P, Ghabezloo S, Conil N (2017a) Thermal Behaviour and Creep of the Callovo-Oxfordian Claystone. In: Poromechanics 2017 - Proceedings of the 6th Biot Conference on Poromechanics

Belmokhtar M, Delage P, Ghabezloo S, Conil N (2018) Drained Triaxial Tests in Low-Permeability Shales: Application to the Callovo-Oxfordian Claystone. Rock Mech Rock Eng 51:1979–1993. https://doi.org/10.1007/s00603-018-1442-0

Belmokhtar M, Delage P, Ghabezloo S, Conil N (2017b) Thermal Volume Changes and Creep in the Callovo-Oxfordian Claystone. Rock Mech Rock Eng 50:2297–2309. https://doi.org/10.1007/s00603-017-1238-7

Bernier F, Li XL, Bastiaens W (2007) Twenty-five years' geotechnical observation and testing in the Tertiary Boom Clay formation. Géotechnique 57:229–237

Bernier F, Neerdael B (1996) Overview of in-situ thermomechanical experiments in clay: Concept, results and interpretation. Eng Geol 41:51–64. https://doi.org/10.1016/0013-7952(95)00032-1
Bhandari AR, Flemings PB, Polito PJ, et al (2015) Anisotropy and stress dependence of permeability in the Barnett shale. Transp Porous Media 108:393–411
Bian HB, Jia Y, Armand G, et al (2012) 3D numerical modelling thermo-hydromechanical behaviour of underground storages in clay rock. Tunnelling and Underground Space Technology 30:93–109. https://doi.org/10.1016/j.tust.2012.02.011
Biot MA, Willis DG (1957) The elastic coefficients of the theory of consolidation: Journal of Applied Mechanics
Blümling P, Bernier F, Lebon P, Derek Martin C (2007a) The excavation damaged zone in clay formations time-dependent behaviour and influence on performance assessment. Physics and Chemistry of the Earth 32:588–599. https://doi.org/10.1016/j.pce.2006.04.034
Blümling P, Bernier F, Lebon P, Martin CD (2007b) The excavation damaged zone in clay formations time-dependent behaviour and influence on performance assessment. Physics and Chemistry of the Earth, Parts A/B/C 32:588–599
Bock H (2001) Mont Terri Project. RA experiment: Rock mechanics analyses and synthesis; data report on rock mechanics. Mont Terri Consortium
Bossart P, Meier PM, Moeri A, et al (2002) Geological and hydraulic characterisation of the excavation disturbed zone in the Opalinus Clay of the Mont Terri Rock Laboratory. Eng Geol 66:19–38. https://doi.org/10.1016/S0013-7952(01)00140-5
Bossart P, Trick T, Meier PM, Mayor J-C (2004) Structural and hydrogeological characterisation of the excavation-disturbed zone in the Opalinus Clay (Mont Terri Project, Switzerland). Appl Clay Sci 26:429–448
Boudali M, Leroueil S, Srinivasa Murthy BR (1994) Viscous hebaviour of natural clays. In: International conference on soil mechanics and foundation engineering. pp 411–416
Brace WF (1980) Permeability of crystalline and argillaceous rocks. In: International Journal of Rock Mechanics and Mining Sciences & Geomechanics Abstracts. pp 241–251
Bruyn D (1999) Influence d'une élévation de température sur le comportement physique et mécanique de l'argile de Boom dans le cadre de la problématique de galeries d'enfouissement de déchets radioactifs. UCL-Université Catholique de Louvain
Bumbieler F, Plua C, Tourchi S, et al (2021) Feasibility of constructing a full-scale radioactive high-level waste disposal cell and characterization of its thermo-hydro-mechanical behavior. International Journal of Rock Mechanics and Mining Sciences 137:104555. https://doi.org/10.1016/j.ijrmms.2020.104555
Burland JB (1990) On the compressibility and shear strength of natural clays. Géotechnique 40:329–378. https://doi.org/10.1680/geot.1990.40.3.329
Campanella, Mitchell JK (1968) Influence of temperature variations on soil behavior
Carcione JM (2000) A model for seismic velocity and attenuation in petroleum source rocksAn Acoustic Model for Petroleum Source Rocks. Geophysics 65:1080–1092
Cekerevac C, Laloui L (2004) Experimental study of thermal effects on the mechanical behaviour of a clay. J Numer Anal Meth Geomech 28:209–228. https://doi.org/10.1002/nag.332
Chen GJ, Sillen X, Verstricht J, Li XL (2011) ATLAS III in situ heating test in boom clay: Field data, observation and interpretation. Comput Geotech 38:683–696. https://doi.org/10.1016/j.compgeo.2011.04.001
Chen WZ, Ma YS, Yu HD, et al (2017) Effects of temperature and thermally-induced microstructure change on hydraulic conductivity of Boom Clay. Journal of Rock Mechanics and Geotechnical Engineering. https://doi.org/10.1016/j.jrmge.2017.03.006
Cho J-W, Kim H, Jeon S, Min K-B (2012) Deformation and strength anisotropy of Asan gneiss, Boryeong shale, and Yeoncheon schist. International journal of rock mechanics and mining sciences (1997) 50:158–169
Clayton CRI (1997) General Report, Session 2: The mechanical properties and behaviour of hard soils and soft rocks. Geotechnical Engineering of Hard Soils and Soft Rocks 3:1839–1877

Conil N, Armand G (2012) IN SITU HEATING TEST IN CALLOVO-OXFORDIAN CLAYSTONE :
Coop MR, Cotecchia F (1995) The compression of sediments at the archaeological site of Sibari. In: Proc. 11th Eur. Conf. Soil Mech. Found. Engng, Copenhagen. pp 19–26
Corkum AG, Martin CD (2007) Modelling a mine-by test at the Mont Terri rock laboratory, Switzerland. International Journal of Rock Mechanics and Mining Sciences 44:846–859
Cotecchia F, Chandler RJ (2000) A general framework for the mechanical behaviour of clays. Géotechnique 50:431–447
Coussy O (2004) Poromechanics. John Wiley & Sons
Crilly T (1996) Unload-reload tests on saturated illite specimens at elevated temperature
Cui YJ, Sultan N, Delage P (2000) A thermomechanical model for saturated clays. Canadian Geotechnical Journal 37:607–620
Cui Y-J, Terpereau J-M, Marcial D, et al (2004) A geological and geotechnical characterisation of the loess of Northern France. In: Advances in geotechnical engineering: The Skempton conference: Proceedings of a three day conference on advances in geotechnical engineering, organised by the Institution of Civil Engineers and held at the Royal Geographical Society, London, UK, on 29--31. pp 417–428
de Bruyn D, Labat S (2002) The second phase of ATLAS: The continuation of a running THM test in the HADES underground research facility at Mol. Eng Geol 64:309–316. https://doi.org/10.1016/S0013-7952(01)00109-0
Delage P (2013a) On the thermal impact on the excavation damaged zone around deep radioactive waste disposal. Journal of Rock Mechanics and Geotechnical Engineering 5:179–190. https://doi.org/10.1016/j.jrmge.2013.04.002
Delage P (2013b) On the thermal impact on the excavation damaged zone around deep radioactive waste disposal. Journal of Rock Mechanics and Geotechnical Engineering 5:179–190. https://doi.org/10.1016/j.jrmge.2013.04.002
Delage P, Sultan N, Cui YJ (2000) On the thermal consolidation of Boom clay. Canadian Geotechnical Journal 37:343–354
Delay J, Vinsot A, Krieguer J-M, et al (2007) Making of the underground scientific experimental programme at the Meuse/Haute-Marne underground research laboratory, North Eastern France. Physics and Chemistry of the Earth, Parts A/B/C 32:2–18
Demars KR, Charles RD (1982) Soil volume changes induced by temperature cycling. Canadian geotechnical journal 19:188–194
Despax D (1976) Influence de la température sur les propriétés mécaniques des argiles saturées. Ph. D. thesis, Ecole Centrale de Paris, Paris, France
Donath F (1964) Strength variation and deformational behavior in anisotropic rock. State of Stress in the Earth's Crust 281:
Eriksson LG (1989) Temperature effects on consolidation properties of sulphide clays. In: International Conference on Soil Mechanics and Foundation Engineering: 13/08/1989-18/08/1989. pp 2087–2090
Fei Y (1995) Thermal expansion. Mineral physics and crystallography: a handbook of physical constants 2:29–44
Fox PJ, Edil TB (1996) Effects of stress and temperature on secondary compression of peat. Canadian Geotechnical Journal 33:405–415
François B, Laloui L, Laurent C (2009a) Thermo-hydro-mechanical simulation of ATLAS in situ large scale test in Boom Clay. Comput Geotech 36:626–640. https://doi.org/10.1016/j.compgeo.2008.09.004
François B, Laloui L, Laurent C (2009b) Thermo-hydro-mechanical simulation of ATLAS in situ large scale test in Boom Clay. Comput Geotech 36:626–640. https://doi.org/10.1016/j.compgeo.2008.09.004
Franklin JA, Gruspier JE (1983) Evaluation of shales for construction projects-an ontario shale rating system
Freivogel M, Huggenberger (2003) Freivogel M, Huggenberger P. Modellierung bilanzierter Profile im Gebiet Mont Terri–La Croix (Kanton Jura). Mont Terri Project–Geology,

paleohydrogeology and stress field of the Mont Terri region. Federal Office for Water and Geology Rep. 4:7–44
Garitte B, Gens A, Vaunat J, Armand G (2014) Thermal conductivity of argillaceous rocks: determination methodology using in situ heating tests. Rock Mech Rock Eng 47:111–129
Gasc-Barbier M, Chanchole S, Bérest P (2004) Creep behavior of Bure clayey rock. Appl Clay Sci 26:449–458
Gens A (2010) Soil-environment interactions in geotechnical engineering. Geotechnique 60:3–74. https://doi.org/10.1680/geot.9.P.109
Gens A (2011) On the hydromechanical behaviour of argillaceous hard soils-weak rocks (Keynote Lecture). In: Geotechnics of Hard Soils – Weak Rocks, Proceedings of the 15th European Conference on Soil Mechanics and Geotechnical Engineering. Thomas Telford, London, pp 71–118
Gens A (2013) On the hydromechanical behaviour of argillaceous hard soils-weak rocks
Gens A (2004) The role of Geotechnical Engineering for nuclear energy utilisation
Gens A, Garitte B, Olivella S, Vaunat J (2009a) Applications of multiphysical geomechanics in underground nuclear waste storage. Revue européenne de génie civil 13:937–962. https://doi.org/10.3166/regc.13.937-962
Gens A, Sánchez M, Guimarães LDN, et al (2009b) A full-scale in situ heating test for high-level nuclear waste disposal: observations, analysis and interpretation. Géotechnique 59:377–399. https://doi.org/10.1680/geot.2009.59.4.377
Gens A, Sánchez M, Guimarães LDN, et al (2009c) A full-scale in situ heating test for high-level nuclear waste disposal: Observations, analysis and interpretation. Geotechnique 59:377–399. https://doi.org/10.1680/geot.2009.59.4.377
Gens A, Vaunat J, Garitte B, Wileveau Y (2007a) In situ behaviour of a stiff layered clay subject to thermal loading: observations and interpretation. Géotechnique 57:207–228. https://doi.org/10.1680/geot.2007.57.2.207
Gens A, Vaunat J, Garitte B, Wileveau Y (2007b) In situ behaviour of a stiff layered clay subject to thermal loading: Observations and interpretation. Stiff Sedimentary Clays: Genesis and Engineering Behaviour - Geotechnique Symposium in Print 2007 123–144. https://doi.org/10.1680/geot.2007.57.2.207
Gens A, Wieczorek K, Gaus I, et al (2017) Performance of the Opalinus Clay under thermal loading: experimental results from Mont Terri rock laboratory (Switzerland). Swiss J Geosci 110:269–286. https://doi.org/10.1007/s00015-016-0258-8
Ghabezloo S, Sulem J (2010) Effect of the volume of the drainage system on the measurement of undrained thermo-poro-elastic parameters. International Journal of Rock Mechanics and Mining Sciences 47:60–68
Graham J, Tanaka N, Crilly T, Alfaro M (2001) Modified Cam-Clay modelling of temperature effects in clays. Canadian Geotechnical Journal 38:608–621. https://doi.org/10.1139/t00-125
Gräsle W (2009) Long-term behaviour of Opalinus clay--a new experimental approach involving undrained and drained triaxial creep tests. In: Proceedings of the European Commission TIMODAZ-THERESA International Conference, Luxembourg. pp 343–347
Habibagahi K (1973) Temperature Effect on Consolidation Behavior of Overconsolidated Soils. In: Proceedings, 8th International Conference on Soil Mechanics and Foundation Engineering. pp 159–163
Habibagahi K (1976) Temperature effects on primary consolidation. Page Behaviour of a Malaysian Residual Granite Soil as a Sand-Silt-Clay Composite Soil 7:95
Hawkins AB (2000a) General report: The nature of hard rocks/soft soils. In: The geotechnics of hard soils-soft rocks. pp 1391–1402
Hawkins AB (2000b) General report: The nature of hard rocks/soft soils. In: The geotechnics of hard soils-soft rocks. pp 1391–1402
Heitz J-F, Hicher P-Y (2002) The mechanical behaviour of argillaceous rocks--Some questions from laboratory experiments. In: Proc. Int. Symp. Hydromechanical and Thermohydromechanical Behaviour of Deep Argillaceous Rock. pp 99–108

Hornby BE (1998) Experimental laboratory determination of the dynamic elastic properties of wet, drained shales. J Geophys Res Solid Earth 103:29945–29964
Horseman ST, Winter MG, Enwistle DC (1987) Geotechnical characterization of Boom clay in relation to the disposal of radioactive waste
Houston SL, Houston WN, Williams ND (1985) Thermo-mechanical behavior of seafloor sediments. Journal of Geotechnical Engineering 111:1249–1263
Hu DW, Zhang F, Shao JF (2014) Experimental study of poromechanical behavior of saturated claystone under triaxial compression. Acta Geotech 9:207–214. https://doi.org/10.1007/s11440-013-0259-y
Hueckel T, Baldi G (1991) Thermoplasticity of Saturated Clays: Experimental Constitutive Study. Journal of Geotechnical and Geoenvironmental Engineering ASCE 116:1778–1796
Hueckel T, Borsetto M (1990) Thermoplasticity of saturated soils and shales: Constitutive equations. Journal of Geotechnical Engineering 116:1765–1777. https://doi.org/10.1061/(ASCE)0733-9410(1990)116:12(1765)
Hueckel T, Francois B, Laloui L (2009) Explaining thermal failure in saturated clays. Geotechnique 59:197–212. https://doi.org/10.1680/geot.2009.59.3.197
Hvorslev MJ (1937) Über die Festigkeitseigenschaften gestörter bindiger Böden: With an abstract in English. Danmarks naturvidenskabelige samfund, i kommission has GEC Gad
IAEA (2003) The Long Term Storage of Radioactive Waste: Safety and Sustainability. Vienna, Austria: IAEA
Jardine RJ, Gens A, Hight DW, Coop MR (2004a) Developments in understanding soil behaviour. In: Advances in geotechnical engineering: The Skempton conference: Proceedings of a three day conference on advances in geotechnical engineering, organised by the Institution of Civil Engineers and held at the Royal Geographical Society, London, UK, on 29--31. pp 103–206
Jardine RJ, Gens A, Hight DW, Coop MR (2004b) Developments in understanding soil behaviour, Advances in Geotechnical Engineering, The Skempton Conference
Kavvadas MJ (1999) Experiences from the construction of the Athens Metro project. In: Twelfth European Conference on Soil Mechanics and Geotechnical Engineering (Proceedings) The Netherlands Society of Soil Mechanics and Geotechnical Engineering; Ministry of Transport, Public Works and Water Management; AP van den Berg Machinefabriek; Fugr
Khemissa M (1998) Mesure de la perméabilité des argiles sous contrainte et température. Revue française de Géotechnique 11–22
Kim JS, Kwon SK, Sanchez M, Cho GC (2011) Geological storage of high level nuclear waste. KSCE Journal of Civil Engineering 15:721–737. https://doi.org/10.1007/s12205-011-0012-8
Knowles NC, Jeffries RM, Come B (1996) Benchmarking the thermomechanical behaviour of clays—a progress report—the CEC interclay project. Eng Geol 41:65–71
Kuntiwattanakul P, Towhata I, Ohishi K, Seko I (1995) Temperature effects on undrained shear characteristics of clay. Soils and Foundations 35:147–162
Kwon O, Kronenberg AK, Gangi AF, et al (2004) Permeability of illite-bearing shale: 1. Anisotropy and effects of clay content and loading. J Geophys Res Solid Earth 109:
Lachenbruch AH (1980) Frictional heating, fluid pressure, and the resistance to fault motion. J Geophys Res Solid Earth 85:6097–6112
Ladd CC, Varallyay J (1965) The influence of stress system on the behavior of saturated clays during undrained shear
Lemueil S, Vaughan PR (1990) The general and congruent effects of structure in natural soils and weak rocks. Geotechnique 40:467–488
Leroueil S, Vaughan PR (1991) Discussion: The general and congruent effects of structure in natural soils and weak rocks. Géotechnique 41:281–284
Li X, Yu H-S (2009) Influence of loading direction on the behavior of anisotropic granular materials. Int J Eng Sci 47:1284–1296
Li XL, Bastiaens W, Bernier F (2006) The hydromechanical behaviour of the Boom Clay observed during excavation of the connecting gallery at Mol site. Proceedings of

EUROCK2006-Multiphysics Coupling and Long Term Behaviour in Rock Mechanics, Liege, Belgium 467–472
Lima A, Romero E, Gens A, et al (2010) Heating pulse tests under constant volume on Boom clay. Journal of rock mechanics and geotechnical engineering 2:124–128
Liu Z, Shao J, Xie S, et al (2019) Mechanical Behavior of Claystone in Lateral Decompression Test and Thermal Effect. Rock Mech Rock Eng 52:321–334. https://doi.org/10.1007/s00603-018-1573-3
Mánica MA (2018) Analysis of underground excavations in argillaceous hard soils - weak rocks
Masri M, Sibai M, Shao JF, Mainguy M (2014) Experimental investigation of the effect of temperature on the mechanical behavior of Tournemire shale. International Journal of Rock Mechanics and Mining Sciences 70:185–191. https://doi.org/10.1016/j.ijrmms.2014.05.007
McLamore R, Gray KE (1967) The mechanical behavior of anisotropic sedimentary rocks
McTigue DF (1986) Thermoelastic response of fluid-saturated porous rock. J Geophys Res Solid Earth 91:9533–9542
Menaceur H, Delage P, Tang AM, Conil N (2015a) The thermo-mechanical behaviour of the Callovo-Oxfordian claystone. International Journal of Rock Mechanics and Mining Sciences 78:290–303. https://doi.org/10.1016/j.ijrmms.2015.07.002
Menaceur H, Delage P, Tang AM, Conil N (2015b) The thermo-mechanical behaviour of the Callovo-Oxfordian claystone. International Journal of Rock Mechanics and Mining Sciences 78:290–303. https://doi.org/10.1016/j.ijrmms.2015.07.002
Mesri G, Shahien M (2003) Residual shear strength mobilized in first-time slope failures. Journal of Geotechnical and Geoenvironmental Engineering 129:12–31
Mohajerani M (2011) Etude expérimentale du comportement thermo-hydro-mécanique de l'argilite du Callovo-Oxfordien
Mohajerani M, Delage P, Sulem J, et al (2014) The thermal volume changes of the callovo-oxfordian claystone. Rock Mech Rock Eng 47:131–142. https://doi.org/10.1007/s00603-013-0369-8
Mohajerani M, Delage P, Sulem J, et al (2012) A laboratory investigation of thermally induced pore pressures in the Callovo-Oxfordian claystone. International Journal of Rock Mechanics and Mining Sciences 52:112–121
Monfared M, Sulem J, Delage P, Mohajerani M (2012) On the THM behaviour of a sheared Boom clay sample: Application to the behaviour and sealing properties of the EDZ. Eng Geol 124:47–58. https://doi.org/10.1016/j.enggeo.2011.10.002
Morin R, Silva AJ (1984) The effects of high pressure and high temperature on some physical properties of ocean sediments. J Geophys Res Solid Earth 89:511–526
Muñoz J, Alonso EE, Lloret a. (2009) Thermo-hydraulic characterisation of soft rock by means of heating pulse tests. Géotechnique 59:293–306. https://doi.org/10.1680/geot.2009.59.4.293
Naumann M, Hunsche U, Schulze O (2007) Experimental investigations on anisotropy in dilatancy, failure and creep of Opalinus Clay. Physics and Chemistry of the Earth, Parts A/B/C 32:889–895
Neuzil CE (1994) How permeable are clays and shales? Water Resour Res 30:145–150
Niandou H, Shao JF, Henry JP, Fourmaintraux D (1997) Laboratory investigation of the mechanical behaviour of Tournemire shale. International Journal of Rock Mechanics and Mining Sciences 34:3–16
Nygård R, Gutierrez M, Bratli RK, Høeg K (2006) Brittle--ductile transition, shear failure and leakage in shales and mudrocks. Mar Pet Geol 23:201–212
Palciauskas V V, Domenico PA (1982) Characterization of drained and undrained response of thermally loaded repository rocks. Water Resour Res 18:281–290
Pettijohn FJ (1957) Sedimentary Rocks. 3 Indian edition
Picard JM, Bazargan B, Rousset G (1994) Essai thermohydro- mecanique dans une argile profonde: Essai CACTUS. Luxembourg: CEC
Plum robert l., Esrig melvin I (1969) Some temperature effects on soil compressibility and pore water pressure. Special Report 231

Rice JR (2006) Heating and weakening of faults during earthquake slip. J Geophys Res Solid Earth 111:
Robinet J-C, Rahbaoui A, Plas F, Lebon P (1996) A constitutive thermomechanical model for saturated clays. Eng Geol 41:145–169
Salager S (2008) Expertise sur les mesures sur échantillons d'argilites du coefficient de dilatation thermique, du module et du coefficient de Biot
Sayers CM (2013) The effect of anisotropy on the Young's moduli and Poisson's ratios of shales. Geophys Prospect 61:416–426
Seyedi DM, Gens A (2017) Numerical analysis of the hydromechanical response of Callovo-Oxfordian claystone to deep excavations. Comput Geotech 85:275–276. https://doi.org/10.1016/j.compgeo.2017.03.006
Simpson B (1979) Design Parameters for stiff clays general report. In: 7th European Conference On Soil Mechanics and Foundation Engineering. Brighton, pp 91–125
Skempton AW (1964) Long-term stability of clay slopes, Geo-technique
Skempton AW (1954) The pore-pressure coefficients A and B. Geotechnique 4:143–147
Skempton AW (1969) The consolidation of clays by gravitational compaction. Quarterly Journal of the Geological Society 125:373–411
Skempton AW (1970) The consolidation of clays by gravitational compaction. Quarterly Journal of the Geological Society 125:373–411
Spang B (2002) Excel add-in for properties of water and steam in SI-units. Water97_v13 xla Hamburg
Sulem J, Lazar P, Vardoulakis I (2007) Thermo-poro-mechanical properties of clayey gouge and application to rapid fault shearing. Int J Numer Anal Methods Geomech 31:523–540
Sulem J, Vardoulakis I, Ouffroukh H, et al (2004) Experimental characterization of the thermo-poro-mechanical properties of the Aegion fault gouge. Comptes Rendus Geoscience 336:455–466
Sultan N (1997) Etude du comportement thermo-mécanique de l'argile de Boom: expériences et modélisation. THESE DE DOCTORAT PRESENTEE A L'ECOLE NATIONALE DES PONTS ET CHAUSSEES-SPECIALITE: GEOTECHNIQUE
Sultan N, Delage P, Cui YJ (2002) Temperature effects on the volume change behaviour of Boom clay. Eng Geol 64:135–145. https://doi.org/10.1016/S0013-7952(01)00143-0
Tanaka N (1995) Thermal elastic plastic behaviour and modelling of saturated clay [Ph. D. Thesis][D]. Winnipeg, Man: University of Manitoba
Terzaghi K, Peck RB, Mesri G (1996) Soil mechanics in engineering practice. John Wiley & Sons
Thury M, Bossart P (1999) The Mont Terri rock laboratory, a new international research project in a Mesozoic shale formation, in Switzerland. Eng Geol 52:347–359
Tidfors M, Sällfors G (1989) Temperature effect on preconsolidation pressure. Geotechnical Testing Journal 12:93–97
Tiedemann B (1937) Uber die Schubfestigkeit bindiger boden. Bautechnik 15:433–435
TIMODAZ (2007) Thermal impact on the damaged zone around a radioactive waste disposal in clay host rocks. Deliverable 2. State of the art on THMC. Euratom European Project.
Tourchi S (2020) THM analysis of argillaceous rocks with application to nuclear waste underground storage. Doctor of Philosophy, BarcelonaTech (UPC)
Tourchi S, Gens A, Vaunat J, et al (2020) A thermomechanical model for argillaceous rocks. In: {E3S} {Web} of {Conferences}. EDP Sciences, p 13014
Tourchi S, Gens A, Vaunat J, Scaringi G (2022a) Thermo-hydro-mechanical modeling of clayey geological medium: {Theoretical} framework and numerical study. Copernicus Meetings
Tourchi S, Malcom MAM, Vaunat J, Gens A (2022b) A thermomechanical model for argillaceous hard soils - weak rocks: application to {THM} simulation of deep excavations in claystone. EarthArXiv. https://doi.org/10.31223/X5JH29
Tourchi S, Mánica M, Gens A, Vaunat J (2023) Thermo-hydro-mechanical simulation of deep excavations in claystone. In: {NUMGE} 2023. Imperial College London, London, UK

Tourchi S, Vaunat J, Gens A, et al (2021a) A full-scale in situ heating test in Callovo-Oxfordian claystone: observations, analysis and interpretation. Comput Geotech 133:. https://doi.org/10.1016/j.compgeo.2021.104045
Tourchi S, Vaunat J, Gens A (2019a) THM modelling of the ALC1604 experiment. Final report. Barcelona
Tourchi S, Vaunat J, Gens A, et al (2019b) Coupled thm analysis of long-term anisotropic convergence in the full-scale micro tunnel excavated in the callovo-oxfordian argillite. In: VIII International Conference on Computational Methods for Coupled Problems in Science and Engineering. Barcelona, pp 292–299
Tourchi S, Vaunat J, Gens A, et al (2021b) A full-scale in situ heating test in {Callovo}-{Oxfordian} claystone: observations, analysis and interpretation. Comput Geotech 133:104045. https://doi.org/10.1016/j.compgeo.2021.104045
Tourchi S, Vaunat J, Gens A, et al (2019c) Thermo-Hydro-Mechanical simulation of a full-scale steel-lined micro-tunnel excavated in the Callovo-Oxfordian Argillite. In: XIV International Conference on Computational Plasticity. Fundamentals and Applications COMPLAS 2019. Barcelona, pp 544–552
Towhata I, Kuntiwattanaku P, Seko I, Ohishi K (1993) Volume change of clays induced by heating as observed in consolidation tests. Soils and Foundations 33:170–183
Tsang CF, Bernier F, Davies C (2005) Geohydromechanical processes in the Excavation Damaged Zone in crystalline rock, rock salt, and indurated and plastic clays - In the context of radioactive waste disposal. International Journal of Rock Mechanics and Mining Sciences 42:109–125. https://doi.org/10.1016/j.ijrmms.2004.08.003
Valès F, Minh DN, Gharbi H, Rejeb A (2004) Experimental study of the influence of the degree of saturation on physical and mechanical properties in Tournemire shale (France). Appl Clay Sci 26:197–207
Vardoulakis I (2002) Dynamic thermo-poro-mechanical analysis of catastrophic landslides. Geotechnique 52:157–171
Vernik L, Liu X (1997) Velocity anisotropy in shales: A petrophysical study. Geophysics 62:521–532
Wang Z (2002a) Seismic anisotropy in sedimentary rocks, part 2: Laboratory data: Geophysics
Wang Z (2002b) Seismic anisotropy in sedimentary rocks, part 1: A single-plug laboratory method. Geophysics 67:1415–1422
Yu L, Weetjens E, Sillen X, et al (2014) Consequences of the thermal transient on the evolution of the damaged zone around a repository for heat-emitting high-level radioactive waste in a clay formation: a performance assessment perspective. Rock Mech Rock Eng 47:3–19
Zhang C, Rothfuchs T (2004a) Experimental study of the hydro-mechanical behaviour of the Callovo-Oxfordian argillite. Appl Clay Sci 26:325–336
Zhang C, Rothfuchs T (2004b) Experimental study of the hydro-mechanical behaviour of the Callovo-Oxfordian argillite. Appl Clay Sci 26:325–336. https://doi.org/10.1016/j.clay.2003.12.025
Zhang CL (2015) Deformation of clay rock under THM conditions. Geomech Tunn 8: 426--435
Zhang CL (2018) Thermo-hydro-mechanical behavior of clay rock for deep geological disposal of high-level radioactive waste. Journal of Rock Mechanics and Geotechnical Engineering 10:992–1008. https://doi.org/10.1016/j.jrmge.2018.03.006
Zhang CL (2011) Experimental evidence for self-sealing of fractures in claystone. Physics and Chemistry of the Earth 36:1972–1980. https://doi.org/10.1016/j.pce.2011.07.030
Zhang CL, Conil N, Armand G (2017) Thermal effects on clay rocks for deep disposal of high-level radioactive waste. Journal of Rock Mechanics and Geotechnical Engineering 1–16. https://doi.org/10.1016/j.jrmge.2016.08.006
Zhang CL, Rothfuchs T, Su K, Hoteit N (2007a) Experimental study of the thermo-hydro-mechanical behaviour of indurated clays. Physics and Chemistry of the Earth 32:957–965. https://doi.org/10.1016/j.pce.2006.04.038
Zhang CL, Rothfuchs T, Su K, Hoteit N (2007b) Experimental study of the thermo-hydro-mechanical behaviour of indurated clays. Physics and Chemistry of the Earth 32:957–965. https://doi.org/10.1016/j.pce.2006.04.038

Zhang F, Hu DW, Xie SY, Shao JF (2014) Influences of temperature and water content on mechanical property of argillite. European Journal of Environmental and Civil Engineering 18:173–189. https://doi.org/10.1080/19648189.2013.852485
Zhu W, Wong T (1997) The transition from brittle faulting to cataclastic flow: Permeability evolution. J Geophys Res Solid Earth 102:3027–3041